الجمهورية الجزائرية الديمقراطية الشعبية

République Algérienne Démocratique et Populaire

Ministère de L'Enseignement Supérieur et de la Recherche Scientifique

UNIVERSITÉ SETIF1 FERHAT ABBAS

FACULTÉ DE TECHNOLOGIE

THESE

Présentée au Département de Génie Des Procédés

Pour l'obtention du diplôme de

DOCTORAT

Option : Génie Chimique

Par

DJAMA Chaker

THÈME

Elimination du bleu de méthylène par bioadsorption et processus Fenton à base de $NiFe_2O_4/CuO$

Soutenue le 17/11/2024 devant le Jury :

BAITICHE Milad	**Professeur**	**Univ. Sétif 1**	**Présidente**
BOUGUETTOUCHA Abdallah	**Professeur**	**Univ. Sétif 1**	**Directeur de Thèse**
AMRANE Abdeltif	**Professeur**	**Univ. Rennes1**	**Co-Directeur de Thèse**
BARKAT Djamal	**Professeur**	**Univ. Biskra**	**Examinateur**
OMARI Mahmoud	**Professeur**	**Univ. Biskra**	**Examinateur**
CHEBLI Derradji	**Professeur**	**Univ. Sétif 1**	**Invité**

Table of contents

Chapter I: Bibliography

Acknowledgement

Above all, thanks to Allah for directing me and giving me the health, patience, courage, and ability to undertake this work.

I heartily thank my guidance, Professor BOUGUETTOUCHA Abdallah, whose encouragement, advice, and support helped me complete my doctoral study with a joyful ending.

I am grateful to my co-director, AMRANE Abdelatif for his ideas and suggestions to improve my work.

Special thanks to Professor Professor CHEBLI Derradji, with whom I worked and received fantastic ideas and guidance from his experiences.

I would like to show my gratitude to Professor Tahraoui Hichem, who always helped me when I approached him for aid.

A big thank you to my best friend, Mr. DOUDOU Ilyes. For accompanying me throughout my academic and life journey, I will never forget his generous aid.

I am immensely grateful to my parents, brothers, and sisters for their everlasting love and sacrifices in enabling me to succeed in my education and research career. They constantly encouraged me to reach my dreams and worked diligently to help me achieve them.

I would also like to thank all the juries for coming to participate in my defense and for their helpful and valuable ideas and conversations on my thesis. Finally,

I would like to thank all my family members, friends, and everyone who supported and encouraged me to complete this thesis.

Nomenclature

Cs	Cynara Scolymus
PACK	Acorus calamus
C_0	initial concentration of MB ($mg•L^{-1}$)
C_e	final concentration of MB in the solution
C_t	concentration of MB at time t ($mg•L^{-1}$)
C	the intercept of Intraparticle diffusion function
$C_{1/2}$	the concentration at half–saturation ($mg•L^{-1}$)
C_1	concentrations at half saturation for the first active site ($mg•L^{-1}$)
C_2	concentrations at half saturation for the second active site ($mg•L^{-1}$)
E_{DR}	biosorption energy ($KJ•mol^{-1}$)
E_{int}	System internal energy ($J•mol^{-1}$)
F_t	fraction of MB adsorbed at time t
G	Gibbs free enthalpy ($J•mol^{-1}$)
h	Planck constant ($J•s^{-1}$)
K_B	Boltzmann constant (J•K)
k_1	equilibrium rate constant of PFO equation ($L•min^{-1}$)
k_2	equilibrium rate constant of PSO equation ($L•min^{-1}$)
K_{DR}	activity coefficient of Dubinin–Radushkevich isotherm ($mol^2•KJ^{-2}$)
K_F	Freundlich constant (g•L•mg)
k_{id}	the rate constant of intraparticle diffusion($mg•g^{-1}•min^{-0.5}$)
K_L	Langmuir constant ($L•mg^{-1}$)
k_n	equilibrium rate constant of PNO equation ($L•min^{-1}$)
k_R	Redlich–Peterson (R–P) constant ($L•g^{-1}$)
K_s	Sips constant ($L•mg^{-1}$)
m	mass of the mixture (g)
ms	the exponent of the Sips model
MB	methylene blue
n	number of ions per site
n_1	number of ions per site for the first sites receptor
n_2	number of ions per site for the second sites receptor
nf	Freundlich (R–P) constant

Nomenclature

no	biosorption reaction order
N	number of experimental points performed
N_m	sites receptor density($mg \cdot g^{-1}$)
PFO	pseudo-first-order
PSO	pseudo-second-order
PNO	pseudo-nth-order
Q_e	amount of dye adsorbed at equilibrium ($mg \cdot g^{-1}$)
Q_t	quantity adsorbed at time t ($mg \cdot g^{-1}$)
Q_m	monolayer capacity of the adsorbent ($mg \cdot g^{-1}$)
Qi.mod	model's adsorbate adsorption capacity ($mg \cdot g^{-1}$)
Qi.exp	experimental adsorption capacity ($mg \cdot g^{-1}$)
S_a	Entropy ($J \cdot mol \cdot K^{-1}$)
t	time (min)
T	temperature (K)
V	volume of the mixture (L)
Z_v	Translation partition function per unit volume
Z_{gtr}	translation partition function
α_R	constant of the Redlich–Peterson isotherm ($L \cdot mg \cdot g^{-1}$)
β_R	constant of the Redlich–Peterson isotherm
β_t	mathematical function of F_t
ε	constant related to the adsorption energy for Dubinin–Radushkevich isotherm

Lists of Figures

Chapter *I*

Chapter *I I*

Chapter *I I I*

Chapter *I I I I*

Figure 3. (c) $NiFe_2O_4$, CuO, $NiFe_2O_4$-CuO+H_2O_2(30mM) ; (d) $NiFe_2O_4$, CuO, $NiFe_2O_4$-CuO+H_2O_2(80mM) ; (e) $NiFe_2O_4$, CuO, $NiFe_2O_4$-CuO+H_2O_2(130mM) ; (f)CuO, $NiFe_2O_4$-CuO+H_2O_2(30, 80, 130mM).

Lists of Figures

List of tables

Chapter *I*

Chapter *I I*

Chapter *I I I*

Chapter *I I I I*

General Introduction

Water is a vital resource for all organisms inhabiting the Earth, including humans, animals, plants, and microorganisms. Water is utilized for various purposes, ranging from fundamental ones like drinking and farming to more sophisticated applications in diverse industries. Due to its uneven distribution worldwide, it poses significant political, economic, and geopolitical challenges [1]. When utilized in various sectors or for household purposes, its emissions are unregulated [2].

The primary contaminants in water primarily originate from human activities, which can be categorized as local, punctual, accidental, diffuse, chronic, genetic, voluntary, involuntary, etc. These activities include the release of chemicals, radioactive materials, metals, hydrocarbons, pesticides, chemical fertilizers, phytosanitary products, detergents, organic materials, as well as medicinal and cosmetic substances [3]. Urban areas contribute significantly to water pollution due to the discharge of pollutants from residential areas and human activities. Certain pollutants, such as phenols and their derivatives, dyes**,** and their degradation by-products, are known to have carcinogenic and mutagenic effects. They can also disturb the hormonal system and induce endocrine disruption [4].

The contaminants can be classified into three primary categories: inorganic, organometallic, and organic [5].

- Inorganic or mineral pollutants refer to heavy metals and metalloids, including elements such as Chromium (Cr), Arsenic (As), Iron (Fe), Cadmium (Cd), Lead (Pb), Manganese (Mn), Selenium (Se), and others. They can also include anionic compounds such as nitrates, fluorides, cyanides, and so on [6].
- Organometallic pollutants consist of complex compounds in which a metal ion is chemically bonded to an organic group, such as methylmercury. The primary families include organotins, **organomagnesium**, **organolithium**, organocoppers**,** cuprates, **organozinc,** and organomercurials [7].
- Organic pollutants such as chlorophenols and dyes have very diverse effects which rely on their type [8].

The pollution of aquatic habitats by organic substances, particularly synthetic dyes, is a severe challenge for the environment and human health. In particular, azo dyes and their derivative compounds cause severe toxicity with carcinogenic and genotoxic effects on aquatic life.

Additionally, these contaminants are often not biodegradable. Daily, vast quantities of wastewater containing colors and pigments from many industrial operations (paper, textiles, food goods, etc.) are released into nature. As a result, these molecules find their way to water resources, surface or underground, due to the ineffectiveness of standard wastewater treatment processes [9].

Although each method has advantages and challenges, adsorption and POAs remain the most used techniques in recent years due to their exceptional economic and environmental efficiency and profitability [10]. These techniques can remove a wide range of persistent micropollutants, such as synthetic dyes. One of the key advantages of the adsorption process is the versatility of selecting the precursor. It can be utilized as an adsorbent or as a foundation for creating an adsorbent. Based on the published research, a wide variety of adsorbents have been utilized, such as activated carbon, clays, biosorbents, and zeolites [11]. Among the POAs, homogeneous and heterogeneous Fenton processes appear to be practical, cost-effective, and easy to use, either on their own (using only the oxidant and catalyst) or modified (strengthening the process with an irradiation source such as UV light or microwaves) [12].

And so on; From this perspective, the essential purpose of this thesis involves two parts:

- ✓ the first is to valorize local by-products through the development of innovative low-cost adsorbent materials generated from agricultural and food waste for the elimination of synthetic dyes, including in particular methylene blue in this work, the prepared adsorbents must be subjected to certain specific characteristics, such as that are available and easy to find, are non-toxic, and do not affect the operators' health, with controllable preparation stages, a low-cost product, with high efficiency for water discoloration, and, Easy to regenerate after an adsorption phase, etc.
- ✓ The second objective is that $NiFe_2O_4$ can be combined with CuO as a new multi-component nanocomposite material ($CuO\text{-}NiFe_2O_4$), which will be designed to catalyze H_2O_2, aiming to improve the decomposition efficiency of the latter under neutral conditions as a Fenton process for the degradation of the same synthetic methylene blue dyes used in the adsorption operation.

For the adsorption part, we are interested in the valorization of two local by-products, Acorus calamus and Cynara scolymus. The adsorbents developed will be tested for their capacity in powder form. and the results obtained during this PhD thesis will be presented under articles forms in the fourth following chapters.

In the introductory chapter, a bibliographic search will be carried out to properly establish the problem of this thesis. In this area, we will first cover general information on the numerous types of dyes, their classification based on various parameters, as well as the dangers associated with their use. Research on the various methods of water decolorization will then be discussed, with particular attention dedicated to the adsorption and Fenton process. Additionally, we will give and discuss various sources of low-cost adsorbents (natural, industrial, and agricultural residues), and a general overview of nanoparticle materials based on transition metal oxide.

The second and third chapters of this thesis will concentrate on applying the indicated precursors. The first chapter proposes chemically processing the Acorus calamus using sulfuric acid and then activating it with potassium permanganate to create a product suitable for water treatment, while the second chapter considers applying Cynara scolymus as a direct powder. In addition, the third chapter will use five physical statistical models, whereas the second will only use three.

In the fourth chapter, CuO-$NiFe_2O_4$ nanoparticles have been produced with the hydrothermal technique and employed for the H_2O_2 activation for the removal of methylene bleu.

It should be emphasized that numerous characterization techniques will be applied to study the properties of the created materials, such as Fourier transform infrared spectroscopy (FTIR), scanning electron microscopy (SEM), X-ray diffraction (XRD), as well as thermogravimetric analysis (TGA). At the same time, their performance will be examined using the adsorption of methylene blue, which works as a model with numerous characteristics that can influence its adsorption, such as the beginning concentration of the dye, the contact time, the pH, temperature, and ionic strength.

This work closes with a broad conclusion which highlights the key conclusions gained during this study.

Reference

[1] L.S. Silva, L.C.B. Lima, F.J.L. Ferreira, M.S. Silva, J.A. Osajima, R.D.S. Bezerra, E.C. Silva Filho, Sorption of the anionic reactive red RB dye in cellulose: Assessment of kinetic, thermodynamic, and equilibrium data, Open Chem. 1 (2015).

[2] A.A. Oladipo, M. Gazi, Enhanced removal of crystal violet by low cost alginate/acid activated bentonite composite beads: Optimization and modelling using non-linear regression technique, J. Water Process Eng. (2014). https://doi.org/10.1016/j.jwpe.2014.04.007.

[3] C. Djama, A. Bouguettoucha, D. Chebli, A. Amrane, H. Tahraoui, J. Zhang, L. Mouni, Experimental and Theoretical Study of Methylene Blue Adsorption on a New Raw Material, Cynara scolymus—A Statistical Physics Assessment, Sustainability 15 (2023) 10364.

[4] C. Laoubi, H. Nacer, La dégradation du bleu de méthylène par la photocatalyse hétérogène (tiO2/ultraviolet), (2017).

[5] A.C. Khorasani, S.A. Shojaosadati, Magnetic pectin-Chlorella vulgaris biosorbent for the adsorption of dyes, J. Environ. Chem. Eng. 7 (2019) 103062.

[6] M.K. Seliem, M. Mobarak, Cr (VI) uptake by a new adsorbent of CTAB–modified carbonized coal: experimental and advanced statistical physics studies, J. Mol. Liq. 294 (2019) 111676.

[7] J. Feng, R. Liu, P. Chen, S. Yuan, D. Zhao, J. Zhang, Z. Zheng, Degradation of aqueous 3,4-dichloroaniline by a novel dielectric barrier discharge plasma reactor, Environ. Sci. Pollut. Res. 22 (2015) 4447–4459. https://doi.org/10.1007/s11356-014-3690-1.

[8] R.M. Klipper, H. Hoffmann, T. Augustin, The Removal of Divalent Anions and Cations from Feed Brine for Chloralkali-Electrolysis Cells by Utilization of Ion Exchange Technology, in: Ion Exch. Adv., Springer, 1992: pp. 414–419.

[9] F. Bonvin, L. Jost, L. Randin, E. Bonvin, T. Kohn, Super-fine powdered activated carbon (SPAC) for efficient removal of micropollutants from wastewater treatment plant effluent, Water Res. 90 (2016) 90–99.

[10] X. Peng, J. Qu, S. Tian, Y. Ding, X. Hai, B. Jiang, M. Wu, J. Qiu, Green fabrication of magnetic recoverable graphene/MnFe 2 O 4 hybrids for efficient decomposition of

methylene blue and the Mn/Fe redox synergetic mechanism, RSC Adv. 6 (2016) 104549–104555.

[11] R. Dhinesh Kumar, R. Thangappan, R. Jayavel, Facile preparation of LaFeO 3/rGO nanocomposites with enhanced visible light photocatalytic activity, J. Inorg. Organomet. Polym. Mater. 27 (2017) 892–900.

[12] A. Haleem, A. Shafiq, S.-Q. Chen, M. Nazar, A comprehensive review on adsorption, photocatalytic and chemical degradation of dyes and nitro-compounds over different kinds of porous and composite materials, Molecules 28 (2023) 1081.

Chapitre I :

Bibliography

1 Introduction

In this chapter, we will conduct a literature search to better comprehend the challenges of this thesis. This section initially includes general information on the numerous types of dyes, their classification according to various parameters, and the dangers associated with their use. Subsequently, research into the many methods of water decolorization is discussed, of which the adsorption and Fenton approaches are the most in-depth. In addition, numerous sources of low-cost adsorbents (natural, industrial, and agricultural residues) are provided and explored, as well as comparative tables of different powder precursors used in the literature and their adsorption effectiveness with various contaminants.

2 synthetic dyes?

Colors, which are unsaturated aromatic chemicals, have special qualities such as color intensity, solubility, and fastness. Dyes are coloring particles that are distinguishable from each other by their chemical composition and that can be used to impart tints and tones to materials [1]. It is usual for natural dyes to be manufactured on a small scale from naturally available materials such as insects or plants. The English chemist, William Perkins, unintentionally discovered synthetic colors [2].

3 Dyes categorization

There are several classifications for commercial dyes. It can be categorized using any combination of structure, color, and application methods. Since the chemical structure system's color nomenclature is so complicated [3], it is typically preferable to classify materials according to their applications. The classification of dyes based on their chemical makeup is shown in Table 1. Table 2 shows the purposeful distribution of dyes [4]. Apart from the previously discussed aspects, dyes are categorized as cationic (which includes all basic dyes), anionic (which includes direct, acidic, and reactive dyes), and nonionic (which includes dispersed dyes) depending on the charge of their particles upon dissolution in an aqueous application medium. Many industries utilize dyes, including textiles, paper, printing, carpets, plastics, food, and cosmetics. Because these dyes are frequently disposed of in rivers and lakes since they are also present permanently in industrial waste [5].

Table 1: Classification of dyes according to their chemical composition [6].

Dyes class	description	Example
Azo	It is composed of one or more azo groups -N=N-, which are the dyes most widely employed in the textile business	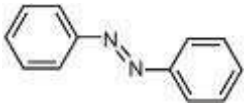
Anthraquinone	It is mainly composed of anthraquinone molecules.	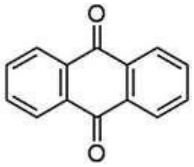
Indigoid	These dyes make it possible to achieve a variety of tints, ranging from orange to turquoise	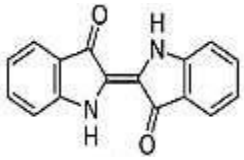
Phthalocyanine	These are complex structures that are based on a central metal atom (for example (Fe, Cu, Pb, Co, Mg)	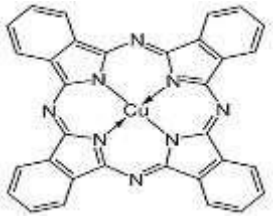
Xanthene	Compounds in this group are extremely fluorescent. Fluorescein is the most distinguishing component	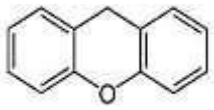
Nitro and nitroso dyes.	These dyes consist of a nitro group (-NO2) associated with an amine or hydroxyl group.	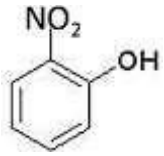

Table 2: Classification of dyes based on their applications [2].

Dyes class	Application
Acid	leather, Wool, silk, inks, nylon, and paper
Dispersive	Polyamide, acrylic polyester, acetate, and plastics
Basic	Inks, treated nylon paper, polyacrylonitrile, and polyester
Sulfurous	Cotton and viscose polyamides and polyesters rarely silk
Reactive	Wool, silk, cotton, and nylon
Direct	Nylon, leather, rayon, paper, and cotton
Vat	Wool and Cotton.
Mordant	Wool, silk
Pigments	Used in printing processes

4 Azo dyes

Azo dyes have one or more azo groups in their molecular structure (-N = N-). Most dyes now used are in this category, which comprises more than 50% of global dye production. Different types of azo dyes exist, such as basic, acidic, direct and reactive, dispersion, and mordant dyes [7]. The reactivity of azo dyes is regulated by many circumstances. The type of the substituent in the molecular structure is the first element. They are acidic (if the functional groups are protonated), basic (deprotonated with a pair of free electrons on the nitrogen), or non-ionic depending on the pH. Additionally, additional components influence the basicity of dyes; for example, the presence of acceptor substituents in aromatic rings such as –Cl or –NO2 groups diminishes the basicity of amino groups. If they contain extra acidic groups (hydroxyl, carboxyl, or sulfonyl groups), azo dyes may also display amphoteric characteristics [8]. In the textile industry, these dyes are used to give color to polyester, nylon, cellulose diacetate, triacetate, and acrylic fibers. They are also found as additives in petroleum-based products and the coloring of leather, paints, plastics, papers, wood, oils, cosmetics, pharmaceuticals, metals, and meals.

5 evaluation of health concerns connected with dyes

The study of the dangers for the coloring business is still in the development phase, and the features of individual exposure to dyes are generally unknown. The presence of dye precursors has been linked to bladder cancer [9]. Textile dyes that include aromatic amines can cause damage to the DNA of cells, raising the risk of cancer. This is why several nations have implemented guidelines for dyeing textiles. When azo dye is applied regularly, long-term exposure results in a substantial quantity of absorbed amines that surpass the practically acceptable dosage limit. Indeed, the colors used in textiles constitute a major health concern. For example, the dye Acid Black 210 is used in dyeing cotton, leather, and wool. However, according to a guideline from the Dutch Health Council, this dye is a human carcinogen that can cause skin harm when inhaled or applied to the skin. Additionally, the use of food coloring is closely associated with allergies, hyperactivity, irritability, and aggression, where many people have had allergic reactions after eating and indications of irritation. cutaneous have been observed [10].

5.1 Dyes-related allergies:

Since 1868, there have been documented instances of allergic reactions to natural dyes used in garments. In 1884, following the commercialization of new synthetic colors, there were numerous complaints of severe skin rashes related to wearing underpants. Nylon stockings were marketed in the United States in 1940. Shortly after their introduction, incidents of dermatitis related to nylon stockings were discovered; this ailment was first described as “nylon allergy." However, a subsequent study found that the dermatitis was caused by dyes and not nylon. According to Dobkevitch and Baer 24, eczema has been linked to cross-sensitivity between the dispersion of yellow azo dye and the para-amino chemical p-phenylenediamine in nylon fabrics. In addition, incidences of allergic contact dermatitis (ADC) have been documented. They were detected in 1985 because they wore dark clothing, largely due to a contact reaction to other dyes (blue 06, blue 124, etc.) [11].

5.2 Aquatic ecosystem toxicity

The color can influence the concentration and toxicity of heavy metals in fish. In addition to all marine species, dyes represent major environmental difficulties since they enhance the toxicity of aquatic life, disrupt the self-purification process, and alter the ecosystem's beauty. The fundamental problem is that most synthetic colors resist light and oxidation. In this way, the absorption of colors and pigments into garbage causes communal pollution, which impacts the

aquatic ecosystem and the aesthetics of the environment. This is why dyes should be of considerable concern, as they can cause various environmental hazards [12].

5.3 Various procedures for removing watercolor

Dye wastewater treatment methods, including fungal and bacterial decolorization methods, can be divided into biological, chemical, and physical technologies. These methods have advantages and drawbacks but are often limited due to high costs and disposal issues in the textile and paper industries [13]. Due to the complex nature of effluents, there is currently no single process capable of providing adequate treatment. In practice, a combination of different processes is often used to achieve the desired water quality most economically [14].

Biological treatment is often the most economical alternative compared to other physical and chemical processes [15]. Biodegradation methods such as fungal decolorization, microbial degradation, microbial biomass adsorption, and bioremediation systems are commonly used to treat industrial effluents. However, their application is often restricted due to technical constraints, such as large land areas, sensitivity to diurnal variation, and the toxicity of some chemicals [16].

Chemical methods include coagulation or flocculation combined with flotation and filtration, precipitation-flocculation with Fe (II)/Ca $(OH)_2$, electroflotation, electrokinetic coagulation, conventional oxidation methods with oxidizing agents (ozone), irradiation, or electrochemical processes. These chemical techniques are often expensive [17], and the accumulation of concentrated sludge creates disposal problems. Advanced oxidation processes, based on the generation of powerful oxidizing agents such as hydroxyl radicals, have been applied with success for pollutant degradation but are costly and commercially unattractive [18].

Physical methods, such as membrane-filtration processes and adsorption techniques, have a limited lifetime before membrane fouling occurs. Liquid-phase adsorption is one of the most popular methods for removing pollutants from wastewater due to its high-quality treated effluent and its superiority over other techniques for water re-use in terms of initial cost, flexibility, simplicity of design, ease of operation, and insensitivity to toxic pollutants. Adsorption also does not result in the formation of harmful substances [18].

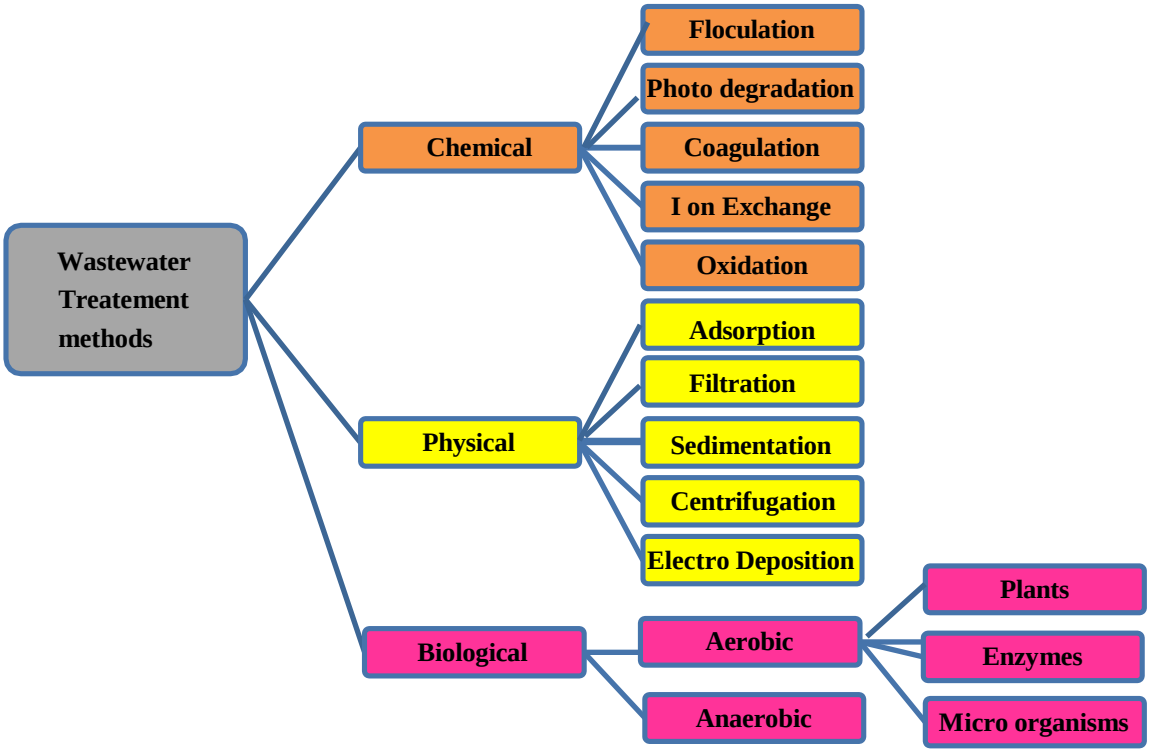

Figure 1. The methods most frequently employed to treat wastewater.

6 Adsorption technique

The term adsorption was first coined by Du Bois-Reymond, but Kayser first published it in 1881 to distinguish between gas condensation on the surface and gas adsorption. Adsorption is a surface phenomenon during which molecules of a fluid (gas or liquid), termed adsorbate, connect to the surface of a solid, called an adsorbent. By the surface of the solid, we mean the external and internal surfaces created by the network of pores and cavities inside the adsorbent [19].

6.1 Adsorption types

Gas-solid adsorption takes place at constant pressure and temperature from a thermodynamic point of view and is generally accompanied by a reduction in enthalpy in the form of heat release (the adsorption energy), whose order of magnitude makes it possible to distinguish between two completely different forms of adsorption.

6.1.1 Physical Adsorption

It is a physical type of adsorption that occurs when the forces that fix the adsorbate in a mono- or multimolecular layer on the adsorbent's surface are of the same order as the van der Waals forces. This type of adsorption is characterized by [20]:

- Rapidity in achieving equilibrium (depending on temperature, concentration, and pressure) between the adsorbed and fluid phases. If, sometimes, equilibrium is only established after a more or less considerable time, it is accepted that this originates from the fact that surface adsorption is accompanied by additional phenomena: dissolution of the gas in the solids and capillary condensation in the pores and capillaries of the solid. It is sometimes referred to as 'sorption'‘;
- A reduction in adsorption capacity with increasing temperature; a heat of adsorption substantially of the same order as the heat of liquefaction of the adsorbed gas;
- Relatively easy reversibility and lack of specificity [21].

6.1.2 Chemical Adsorption

It is chemical-type adsorption that occurs when chemical bonding forces (much stronger than van der Waals forces) share or transfer electrons. As a result, there are ruptures and the formation of chemical bonds on the surface between the reagent and the adsorbent's active sites [22].

Chemisorption is characterized by:

- A slow equilibrium must be reached between the adsorbed phase and the flowing medium.
- Heat generated during adsorption comparable to those of reactions (from 40 to 100 kJ/mole) roughly 10 times physical adsorption.
- A non-reversibility.

When conditions are right, chemical adsorption can often overlap with physical adsorption [23].

6.2 Principal adsorbents

Strictly speaking, all solids are adsorbents. However, only adsorbents with a suitable specific surface area (surface area per unit mass) can be of practical interest. The most prevalent industrial adsorbents are activated carbons, zeolites, silica gels, and activated aluminas.

6.2.1 Activated carbons

Activated carbons, derived from various carbonaceous materials such as wood, coal, coconut, and petroleum residues, are widely used industrially as adsorbents. These carbons consist of elementary graphite microcrystallites with a wide range of pores, ranging from micropores to mesopores and macropores, formed through controlled carbonization processes [24].

6.2.2 Mineral adsorbents

Mineral adsorbents can exist naturally or synthesized [25].

- Clays are aluminosilicates. These are natural materials, which are activated to have better adsorbent capabilities.
- Zeolites are porous aluminosilicates formed from SiO_4 and AlO_4 chains. They have ionic structures because of the aluminum atoms, which require an exchangeable cation to compensate for negative charges. Cations obstruct micropores and interact with adsorbed molecules, affecting adsorption properties. Modifications can enhance their suitability for specific applications.
- Activated aluminas, produced through flash thermolysis of aluminum trihydroxide ($Al(OH)_3$), are porous, moderately polar, and highly hydrophilic adsorbents used for drying due to their amorphous structure.
- Les gels de silice (SiO_2, nH_2O) peuvent être obtenus par précipitation de silice en faisant réagir une solution de silicate de sodium avec un acide minéral. Le gel obtenu est ensuite lavé, séché et activé [26].

6.3 Adsorbents made from food and agricultural waste.

Much effort has been made to develop affordable and easily accessible adsorbents to remove organic pollutants, including constituent residues. Most agricultural residues, such as fruits and vegetable peels, are left without use [27], which makes them very promising as adsorbents due to their physicochemical characteristics and affordability [28]. Adsorbents from food scraps play an essential role in water treatment due to their ability to eliminate various organic contaminations. Furthermore, with an increase in population, the demand and consumption of food and fruits amounts to billions of tons per year; this involves significant production of fruit waste such as peels, leaves, stems, seeds, shells, etc. [29]. In this way, by carrying out a mild treatment, they can be used as adsorbents at a lower cost. In recent years, many scientists have focused on exploring novel adsorbents based on natural materials which are alternatives to those used.

Table 3: Some agricultural waste utilized as a precursor for the manufacture of adsorbents.

Precursor	Prepared adsorbent	Pollutant	Adsorbed amount (mg/g)	Reference
Stipa Tenassicima	Raw	Congo red	7.93	[30]
Pomegranate	Raw	Cd (Ⅱ)	132.5	[31]
Corncob husk	Biochar	As (III)	50	[32]
Jackfruit peel	Biochar	Phosphate	7.95	[33]
Tea leaves	Activated carbon	Rhodamine B	757.6	[34]
Banana peels	Chemically modified	Mn (II)	5.73	[35]
Date stones	Activated carbon	Malachite green	98	[36]
Pistachio shells	Raw	Basic Blue 41	21.8	[37]
Cones of pinus	Raw	Congo Red	102.8	[38]

6.4 Factors influencing the adsorption phenomena

The adsorption balance between an adsorbent and an adsorbate is determined by several parameters, the most important of which are listed below:

6.4.1 Effect of concentration

The dye's adsorption capacity can also be altered by its starting concentration. If the dye concentration is insufficient, the dye adsorption may fail to reach the saturation phase, and the adsorbent may be wasted. The dye's adsorption capacity increases with the initial concentration until the free active sites on the adsorbent's surface are saturated [39].

6.4.2 Effect of pH

Solution pH often plays a key role in the adsorption of organic dyes, which might help understand the adsorption mechanism. For example, when fixing dyes by electrostatic contact, the pH of the dye solution plays an essential role in their adsorption. Maximum dye removal occurs at the pH where the adsorbent has the greatest affinity for the dye molecules; the latter can be detected using the isoelectric point. Thus, cationic dyes are attracted to negatively charged adsorbents, while anionic dyes are attracted to positively charged adsorbents. Furthermore, in other mechanisms (Van der Waal force, hydrogen bonding, or hydrophobic-

hydrophobic interactions), the initial pH may not be as important, and adsorption may occur across a larger pH range [40].

6.4.3 Effect of the specific surface

The specific surface area is a crucial measure of the adsorbent's sorption capacity. It denotes the accessible surface area concerning the adsorbent's unit weight. However, this specific surface area only represents a minimal portion of the total surface area available for adsorption. This total surface area can be increased by grinding the solid mass, which further multiplies its total porosity [41].

6.4.4 Effect of the temperature

Adsorption is an endothermic or exothermic event, depending on the adsorbent material and the type of molecules adsorbed. Numerous adsorption enthalpy values are provided in the literature, which attests to the variety of thermodynamic processes.

6.4.5 Effect of ionic force

Ionic strength plays a vital function in regulating adsorption processes. Hydrophobic and electrostatic interactions, hydrogen bonds, and surface functional group interactions between adsorbents and dyes are the key drivers of dye adsorption [42]. However, ionic strength has a complex and poorly understood effect on dye adsorption, as it can alter electrostatic and hydrophobic interactions. Generally, ionic strength was closer to the real environment [43].

6.4.6 Effect of Contact Time

As the contact time rises, the dye removal rate increases to a certain amount. However, any further increase in contact time will not affect adsorption due to the buildup of dye at the accessible adsorption site on the adsorbent surface. At this point, the amount of free dye and the amount of adsorbed dye are in dynamic equilibrium. The equilibrium time is the time required to reach this phase, and the dye's adsorption capacity corresponds to the maximum adsorption capacity [44].

7 Advanced oxidation processes (AOPs)

AOPs were first developed in the 1980s for the treatment of drinking water and were subsequently widely employed for the treatment of different wastewater. AOPs largely rely on highly reactive oxygen species (ROS) created by photocatalysis, electrochemistry, or peroxides, which can activate the oxidation reaction in water to break down micropollutants and kill microorganisms. For chemical oxidation-based AOPs, ozone (O_3), hydrogen peroxide (H_2O_2), and persulfate (PS) are the most often employed oxidant precursors. Various oxidant activation

methods, including heat, ultraviolet, alkali, transition metals, and carbonaceous materials, have been utilized to create ROS more efficiently. AOPs can be classified into two categories: homogeneous and heterogeneous.

7.1 Homogeneous AOPs

homogeneous AOPs use O_3, H_2O_2, and persulfate, including peroxydisulfate (PDS, $S^2O_8^{2-}$) and peroxymonosulfate (PMS, HSO_5 -).

7.2 Ozone-based AOPs

With a high redox potential (E0 = 2.1 V), ozone is a powerful oxidant capable of oxidizing inorganic and organic compounds, as well as inactivating pathogens and ARB&Gs found in water. Contaminants can be ozonated in two ways: by direct reactivity by the O_3 molecule, which reacts predominantly with the ionized and dissociated form of organic molecules, and by indirect oxidation by the hydroxy radical (•OH), which is created from the O_3 (Eq. (1)) to initiate indiscriminate oxidation [45,46].

$$3O_3 + H_2O \rightarrow 2 \bullet \mathrm{OH} + 4O_2 \quad (1)$$

7.3 UV/ H_2O_2 and UV/PS

Conventional UV lamps' use of mercury has been widely employed for urban wastewater treatment, which can successfully prevent cell replication by destroying their DNA. The application of light-emitting diodes (LEDs) makes UV-C LEDs particularly promising for water disinfection since they are significantly cheaper, smaller, lighter, and less fragile than typical mercury vapor lamps. Single UV may efficiently degrade some organic pollutants but at large doses (> 10, 000 mJ/cm2), such as the high abatement efficiency (>85%) of sulfonamides, quinolones, NDMA, herbicides, and pesticides from water. However, it displayed low removal capability for most CECs [47,48].

7.4 Photo Fenton and Fenton-like AOPs

Unlike activation strategies by energy supply (such as UV), transition metal ions, such as ferrous ions (Fe^{2+}), have the benefits of reduced energy use and greater activity. According to the classic Fenton reaction, the activation of H_2O_2 is explained by dissolving Fe^{2+} in a solution to create •OH (Eq. (2)). Activation of PMS and PDS by Fe^{2+} is also effective [49].

$$F_e^{2+} + H_2H_2 \rightarrow F_e^{3+} + OH^- + \bullet \mathrm{OH} \quad (2)$$

7.5 Heterogeneous Fenton-like process

The heterogeneous Fenton-like system appeared to eliminate or reduce the disadvantages that accompany the application of the homogeneous system mentioned above. Several researchers report quite a bit of work concerning the elimination of a wide range of micropollutants by the heterogeneous Fenton-like process using materials based on transition metals such as iron and copper [50,51].

The capacity of different iron-based minerals to degrade organic pollutants in the presence of H_2O_2 or other oxidants has been relatively well studied in recent years. Among these compounds, we can cite magnetite (Fe_3O_4: a mixture of Fe^{2+} and Fe^{3+}), hematite (Fe_2O_3), goethite (FeOOH), zero-valent iron Fe0, and composites containing iron, for example iron-graphene.

The catalytic reaction in the presence of iron minerals is strongly influenced by the pH of the medium. In particular, the dissolution of iron oxides at acidic pH can lead to homogeneous Fenton-type reactions and affect the stability and durability of the catalysts.

Copper and copper-containing materials are the most studied catalysts after iron in the discipline of green chemistry, because of their possibility of application in the heterogeneous Fenton process in a wide pH range, and therefore, avoiding one of the major disadvantages of the Fenton system (the pH limit).

Among the materials that appear as excellent catalysts in the oxidation processes of micropollutants, specifically the heterogeneous Fenton process, we cite lamellar double hydroxides and their derivatives.

8 Reference

[1] V. Katheresan, J. Kansedo, S.Y. Lau, Efficiency of various recent wastewater dye removal methods: A review, J. Environ. Chem. Eng. 6 (2018) 4676–4697.

[2] S.V.H. Madiraju, Color removal and treatment of dye and sugar waste water using low cost adsorbents, (2018).

[3] M.K. Purkait, S. DasGupta, S. De, Adsorption of eosin dye on activated carbon and its surfactant based desorption, J. Environ. Manage. 76 (2005) 135–142.

[4] V.K. Gupta, Application of low-cost adsorbents for dye removal–a review, J. Environ. Manage. 90 (2009) 2313–2342.

[5] K. GracePavithra, V. Jaikumar, P.S. Kumar, P. SundarRajan, A review on cleaner strategies for chromium industrial wastewater: present research and future perspective, J. Clean. Prod. 228 (2019) 580–593.

[6] S. Markandeya, S.P. Shukla, D. Mohan, Toxicity of disperse dyes and its removal from wastewater using various adsorbents: a review, Res. J. Environ. Toxicol 11 (2017) 72–89.

[7] C.R.L. de Souza, P. Peralta-Zamora, Degradation of reactive dyes by the metallic iron/hydrogen peroxide system, Quim. Nova 28 (2005) 226–228.

[8] M. Mobarak, E.A. Mohamed, A.Q. Selim, L. Sellaoui, A. Ben Lamine, A. Erto, A. Bonilla-Petriciolet, M.K. Seliem, Synthèse et caractérisation de matériaux magnétiques pour l'adsorption de polluants présents dans les eaux, Chem. Eng. J. 369 (2019) 333–343.

[9] K.G. Pavithra, V. Jaikumar, Removal of colorants from wastewater: A review on sources and treatment strategies, J. Ind. Eng. Chem. 75 (2019) 1–19.

[10] R. Orrego, G. Moraga-Cid, M. González, R. Barra, A. Valenzuela, A. Burgos, J.F. Gavilán, Reproductive, physiological, and biochemical responses in juvenile female rainbow trout (Oncorhynchus mykiss) exposed to sediment from pulp and paper mill industrial discharge areas, Environ. Toxicol. Chem. An Int. J. 24 (2005) 1935–1943.

[11] K. Hunger, R. Hamprecht, P. Miederer, C. Heid, A. Engel, K. Kunde, W. Mennicke, J. Griffiths, Dye classes for principal applications, Ind. Dye. Chem. Prop. Appl. (2002) 113–338.

[12] A.A. Oladipo, M. Gazi, Enhanced removal of crystal violet by low cost alginate/acid activated bentonite composite beads: Optimization and modelling using non-linear regression technique, J. Water Process Eng. (2014).

https://doi.org/10.1016/j.jwpe.2014.04.007.

[13] C.I. Pearce, J.R. Lloyd, J.T. Guthrie, The removal of colour from textile wastewater using whole bacterial cells: a review, Dye. Pigment. 58 (2003) 179–196.

[14] G. McMullan, C. Meehan, A. Conneely, N. Kirby, T. Robinson, P. Nigam, I. Banat, R. Marchant, W.F. Smyth, Microbial decolourisation and degradation of textile dyes, Appl. Microbiol. Biotechnol. 56 (2001) 81–87.

[15] Y. Fu, T. Viraraghavan, Fungal decolorization of dye wastewaters: a review, Bioresour. Technol. 79 (2001) 251–262.

[16] A. Stolz, Basic and applied aspects in the microbial degradation of azo dyes, Appl. Microbiol. Biotechnol. 56 (2001) 69–80.

[17] M.F.R. Pereira, S.F. Soares, J.J.M. Órfão, J.L. Figueiredo, Adsorption of dyes on activated carbons: influence of surface chemical groups, Carbon N. Y. 41 (2003) 811–821.

[18] A. Marco, S. Esplugas, G. Saum, How and why combine chemical and biological processes for wastewater treatment, Water Sci. Technol. 35 (1997) 321–327.

[19] A. Dąbrowski, Adsorption—from theory to practice, Adv. Colloid Interface Sci. 93 (2001) 135–224.

[20] F.L. Slejko, Adsorption technology: a step-by-step approach to process evaluation and application, (1985).

[21] S. Brunauer, L.S. Deming, W.E. Deming, E. Teller, On a theory of the van der Waals adsorption of gases, J. Am. Chem. Soc. 62 (1940) 1723–1732.

[22] C.H. Giles, D. Smith, A. Huitson, A general treatment and classification of the solute adsorption isotherm. I. Theoretical, J. Colloid Interface Sci. 47 (1974) 755–765.

[23] K.Y. Foo, B.H. Hameed, Insights into the modeling of adsorption isotherm systems, Chem. Eng. J. 156 (2010) 2–10.

[24] I. Koomen, S.P. McGram, K.E. Giller, Effects of cadmium on the biota: influence of environmental, Soil Biol. Biochem. 22 (1990) 871–873.

[25] H. Babich, G. Stotzky, Effects of cadmium on the biota: influence of environmental factors, Adv. Appl. Microbiol. 23 (1978) 55–117.

[26] J.T. Trevors, G.W. Stratton, G.M. Gadd, Cadmium transport, resistance, and toxicity in bacteria, algae, and fungi, Can. J. Microbiol. 32 (1986) 447–464.

[27] S. Basu, G. Ghosh, S. Saha, Adsorption characteristics of phosphoric acid induced activation of bio-carbon: Equilibrium, kinetics, thermodynamics and batch adsorber design, Process Saf. Environ. Prot. 117 (2018) 125–142.

[28] C. Paduraru, L. Tofan, C. Teodosiu, I. Bunia, N. Tudorachi, O. Toma, Biosorption of zinc (II) on rapeseed waste: equilibrium studies and thermogravimetric investigations, Process Saf. Environ. Prot. 94 (2015) 18–28.

[29] J. Guo, A.C. Lua, Textural and chemical properties of adsorbent prepared from palm shell by phosphoric acid activation, Mater. Chem. Phys. 80 (2003) 114–119.

[30] D. Chebli, A. Bouguettoucha, T. Mekhalef, S. Nacef, A. Amrane, Valorization of an agricultural waste, Stipa tenassicima fibers, by biosorption of an anionic azo dye, Congo red, Desalin. Water Treat. 54 (2015) 245–254.

[31] M.K. Seliem, M. Mobarak, A.Q. Selim, E.A. Mohamed, R.A. Halfaya, H.K. Gomaa, I. Anastopoulos, D.A. Giannakoudakis, E.C. Lima, A. Bonilla-Petriciolet, A novel multifunctional adsorbent of pomegranate peel extract and activated anthracite for Mn (VII) and Cr (VI) uptake from solutions: Experiments and theoretical treatment, J. Mol. Liq. 311 (2020) 113169.

[32] J.I.Z. Montero, A.S.C. Monteiro, E.S.J. Gontijo, C.C. Bueno, M.A. de Moraes, A.H. Rosa, High efficiency removal of As (III) from waters using a new and friendly adsorbent based on sugarcane bagasse and corncob husk Fe-coated biochars, Ecotoxicol. Environ. Saf. 162 (2018) 616–624.

[33] A. Nayak, B. Bhushan, V. Gupta, S. Kotnala, Fabrication of microwave assisted biogenic magnetite-biochar nanocomposite: A green adsorbent from jackfruit peel for removal and recovery of nutrients in water sample, J. Ind. Eng. Chem. 100 (2021) 134–148.

[34] M. Goswami, P. Phukan, Enhanced adsorption of cationic dyes using sulfonic acid modified activated carbon, J. Environ. Chem. Eng. 5 (2017) 3508–3517.

[35] A. Ali, Removal of Mn (II) from water using chemically modified banana peels as efficient adsorbent, Environ. Nanotechnology, Monit. Manag. 7 (2017) 57–63.

[36] M. Hijab, P. Parthasarathy, H.R. Mackey, T. Al-Ansari, G. McKay, Minimizing adsorbent requirements using multi-stage batch adsorption for malachite green removal using microwave date-stone activated carbons, Chem. Eng. Process. Intensif. 167 (2021) 108318.

[37] İ. Şentürk, M. Alzein, Adsorptive removal of basic blue 41 using pistachio shell adsorbent-Performance in batch and column system, Sustain. Chem. Pharm. 16 (2020) 100254.

[38] A. Bouguettoucha, D. Chebli, T. Mekhalef, A. Noui, A. Amrane, The use of a forest waste biomass, cone of Pinus brutia for the removal of an anionic azo dye Congo red from aqueous medium, Desalin. Water Treat. 55 (2015) 1956–1965.

[39] V. Riihimäki, Cadmium. Occurrence and effects, Work. Environ. Health 9 (1972) 91–101.

[40] N. Kannan, G. Rengasamy, Comparison of cadmium ion adsorption on various activated carbons, Water. Air. Soil Pollut. 163 (2005) 185–201.

[41] A.K. Meena, K. Kadirvelu, G.K. Mishra, C. Rajagopal, P.N. Nagar, Adsorptive removal of heavy metals from aqueous solution by treated sawdust (Acacia arabica), J. Hazard. Mater. 150 (2008) 604–611.

[42] Y. Hu, T. Guo, X. Ye, Q. Li, M. Guo, H. Liu, Z. Wu, Dye adsorption by resins: effect of ionic strength on hydrophobic and electrostatic interactions, Chem. Eng. J. 228 (2013) 392–397.

[43] Q. Li, Q.-Y. Yue, H.-J. Sun, Y. Su, B.-Y. Gao, A comparative study on the properties, mechanisms and process designs for the adsorption of non-ionic or anionic dyes onto cationic-polymer/bentonite, J. Environ. Manage. 91 (2010) 1601–1611.

[44] M.A.M. Razi, M.N.A.M. Hishammudin, R. Hamdan, Factor affecting textile dye removal using adsorbent from activated carbon: A review, in: MATEC Web Conf., EDP Sciences, 2017: p. 6015.

[45] Y. Deng, R. Zhao, Advanced oxidation processes (AOPs) in wastewater treatment, Curr. Pollut. Reports 1 (2015) 167–176.

[46] X. Duan, H. Sun, Z. Shao, S. Wang, Nonradical reactions in environmental remediation processes: Uncertainty and challenges, Appl. Catal. B Environ. 224 (2018) 973–982.

[47] Y. Lee, D. Gerrity, M. Lee, S. Gamage, A. Pisarenko, R.A. Trenholm, S. Canonica, S.A. Snyder, U. Von Gunten, Organic contaminant abatement in reclaimed water by UV/H2O2 and a combined process consisting of O3/H2O2 followed by UV/H2O2: prediction of abatement efficiency, energy consumption, and byproduct formation, Environ. Sci. Technol. 50 (2016) 3809–3819.

[48] J. Wang, S. Wang, Activation of persulfate (PS) and peroxymonosulfate (PMS) and application for the degradation of emerging contaminants, Chem. Eng. J. 334 (2018) 1502–1517.

[49] H.J.H. Fenton, LXXIII.—Oxidation of tartaric acid in presence of iron, J. Chem. Soc. Trans. 65 (1894) 899–910.

[50] Y. Wang, H. Zhao, G. Zhao, Iron-copper bimetallic nanoparticles embedded within ordered mesoporous carbon as effective and stable heterogeneous Fenton catalyst for the degradation of organic contaminants, Appl. Catal. B Environ. 164 (2015) 396–406.

[51] J. Mao, X. Quan, J. Wang, C. Gao, S. Chen, H. Yu, Y. Zhang, Enhanced heterogeneous Fenton-like activity by Cu-doped BiFeO 3 perovskite for degradation of organic pollutants, Front. Environ. Sci. Eng. 12 (2018) 1–10.

Chapter II:

Statistical physics modeling of azo dyes biosorption onto a modified powder of Acorus calamus in a batch reactor

Chapter II: Statistical physics modeling of azo dyes biosorption onto a modified powder of Acorus calamus in a batch reactor.

1. Introduction

Water is the main raw material on our planet, for humans, animals, plants, and microorganisms. Virtually all the vital phenomena of the biosphere are related to the availability of water. Water pollution affecting rivers, seas, groundwater, and lakes is the result of the wastewater arising from many industrial discharges repeatedly contaminated with diverse organic, inorganic, and volatile compounds, such as benzene, toluene, phenol, heavy metals, suspended solids, etc[1]. This causes a degradation of the ecosystem. Among the industries that use water in large quantities are the tanning and textile industries, where it is used primarily for dyeing and finishing. These industries are one of the main sources of huge pollution problems in the world due to their water polluted with toxic dyes, even in small amounts. 100,000 varieties of textile dyes with annual production estimated at 7.105 metric tons are available on the world market; 30% of these dyes are used at more than 1000 tonnes per year, and 90% of textile products are used at 100 tonnes per year or less [2, 3].2 to 20% of textile dyes are diversified in liquid effluents during the dyeing process and can cause serious problems because their presence in water, even in very small amounts, is very visible and indisputable[4, 5]. Industrial treatment waste containing this type of dye has a great interest. A vast variety of biological, chemical, and physical techniques has been developed and tested in the treatment of effluents filled with dyes, such as flocculation, precipitation, ion exchange, membrane filtration, irradiation, and ozonation. However, the use of these processes is very costly and contributes to the creation of vast volumes of sludge[2, 6]. Adsorption remains one of the most favorable methods for removing dyes, due to its simplicity of realization.[7, 8].

The principle of the adsorption treatment is to trap the dyes with a solid material called adsorbent. There are several solid materials in the literature (biosorbents, clays, zeolites, and activated carbon ...) that can be used in water-bleaching processes. In recent years, Research has focused on the use of cost-effective adsorbents, available locally, biodegradable absorbent made from natural sources[9]. In this regard, biosorbents synthesized from lignocellulosic residues have been widely used as an adsorbent to treat colored effluents, because of their very large porous structure, large surface area, and high adsorption capacity. Among these adsorbents, we can mention among others:datekernels[10],appleskin[11]olivekernels(10), peachkernels[13], corncobs[14], coffeebeans[15], andcoffeegrounds[16, 17], Tea waste[18], bagasse[19], coconutshell[20], and apricot kernels[21]fungi[22], algae[23],chitosan[24]bacteria[25], and in recen ttimes, Ash of Cassia Fistula seeds[26], rice husk[27] , coconut shell and coal ash[28], Stipa tenassicima fibers[29], cones

of Pinusbrutia[30], wild carob[31], LDHs[32], and acid treated Cupressus semperirens cones pomegranate peel [33], and more recently,pectin from orange industry residues[34], polyacrylamide-diatomite (PAA-D)[35], Fe_3O_4[36], chitosan vermiculite beads[37], Pseudoevernia furfuracea[8], Orange Peel traited with H_3PO_4[38], particle Ziziphus jujuba stones (BZJS1)[39].

Methylene blue is the most frequently used dye in cotton dyeing, wool, and silk. It causes difficulty breathing when there is an inhalation, a burning sensation if swallowed by mouth, causes nausea [5]**.** In the present study, we were interested in the removal of methylene blue (BM) dye using a new inexpensive and naturally abundant material *Acorus collected* from the Sahara of Algeria which is considered to be a potential material for adsorption of cationic dyes. Moreover and to our knowledge, no work has been reported in the literature on the use of this material for the elimination of dyes, it was first treated with H_2SO_4 and then activated with $KMnO_4$. The new material is called PACK and subsequently shows its efficiency in the treatment of polluted water. Various experimental parameters were analyzed such as pH, contact time, effect of mass, and effect of initial dye concentration. The effect of temperature on the adsorption of the dye was also studied and the thermodynamic parameters were determined.

2. Materials and methods

2.1. Materials

The Acorus calamus collected from the Sahara of Algeria is used as biosorbent support in this work. The following chemical products were used, Methylene Blue (MB), H_2SO_4 (65%), $KMnO_4$, and humic acid. All of the chemicals mentioned are collected from Sigma-Aldrich

2.2. Preparation of dye solutions and concentration determination

Methylene Blue (MB), a typical cationic dye was selected as an adsorbent. Its chemical structure and some of its properties are presented in Fig 1 and Table 1. It was obtained from ACROS with 99.99% purity**.**

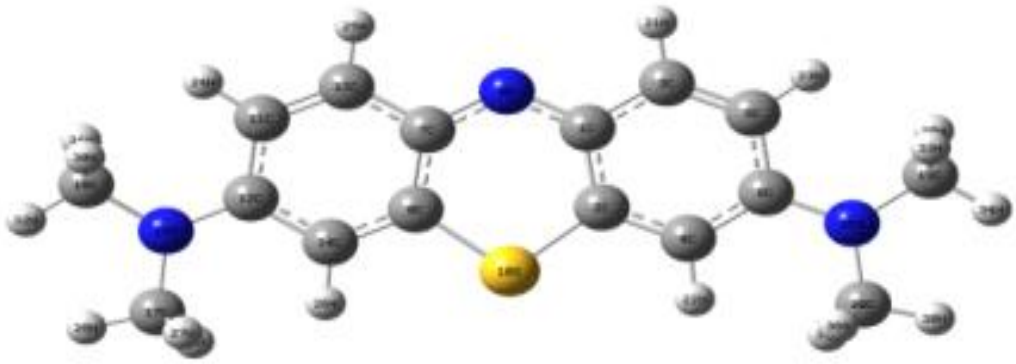

Figure 1. Chemical structure of the methylene blue.

Working solutions were prepared by dilution of the stock solution with distilled water to yield the appropriate concentrations. The pH of the solutions was changed by adding either 0.1 M HCl or 0.1 M NaOH solutions. Before use, all bottles and glassware were beforehand cleaned and then rinsed with distilled water and oven-dried at 60°C. There residual dye concentrations were assessed by an SP-8001 UV/vis Spectrophotometer of Axiom (Germany, Shimadzu).

Table 1: Chemical properties of Methylene Blue.

Dye	Classification	λ_{max} (nm)	Empirical formula	Formula weight (g. mol^{-1})	Solubility in water
Methylene Blue	Cationic dye	664	$C_{16}H_{18}N_3ClS$	320	>50g. L^{-1}

2.3. Preparation of the adsorbent

Aquatic reeds of Sahara (Algeria) were dried at a temperature of about 40°C. This quantity was sieved and crushed to obtain small grains, generally less than 2 mm. First treatment was carried out with a mixture of sulfuric acid (65%) and the aquatic reeds powder with a ratio of (1g(powder): 20ml(H_2SO_4)), the reaction mixture was stirred at a temperature of 70 °C for 5 hours. The powder was filtered and washed several times with distilled water until purification and then dried in an oven overnight at 80 °C. The resulting product was treated again with $KMnO_4$ (1M) with a ratio of (1g (powders) / 10 ml ($KMnO_4$)) at room temperature for 24 hours. The powders obtained are washed until purification and then dried in an oven overnight at 80 °Cand by following the grinding and storage step in desiccators for future use. The obtained product, namely powder of *Acorus Calamus* $KMnO_4$-activated, was abbreviated as PACK.

2.4. Characterization of the adsorbent

2.4.1. Infrared spectroscopy (IRTF)

FTIR analysis enables us to determine the functional surface groups of our materials. This analysis was conducted on a Spectrum Two-type infrared spectroscopy apparatus using the technique of high-pressure KBr granules, the analysis was done over a wavelength range of 400-4000 cm^{-1}.

2.4.2. The Point of Zero Charge of PACK

The pHpzc (pH of the zero or no charge point) refers to the pH value at which the net charge on the adsorbent surface is null. This parameter is very important in adsorption phenomena, especially when electrostatic forces are involved in the mechanisms. A quick and simple protocol to determine the pHpzc consists of placing ml of the distilled water in closed vials and adjusting the pH of each (values between 2 and 12) by addition of NaOH (0.1M) or HCl (0.1M)solution.25 mg of PACK material was added to each vial. The Suspension was agitated at room temperature for around 24 hours, and then the final pH was determined.

2.4.3. Scanning electron microscopy (SEM)

Scanning electron microscopy (SEM) of PACK biosorbent before biosorption was visualized using Hitachi S-3000 N SEM at 10 kV and various magnifications, 500 and 20,000. From the SEM, it is possible to see the topography surface of our material.

2.5. Adsorption studies

2.5.1. Adsorption kinetics

The effect of the contact time on the adsorption of methylene blue (MB) on the material considered in this study at the natural pH, of 6.5. Experiments were performed, adding a given amount of biosorbent (50 mg) in 200 ml of dye solutions of known concentrations (100 and 150 mg/L) in two conical flasks (500 ml) with continuous stirring (250 rpm) at 25 ± 2°C. After withdrawing samples at fixed time intervals and centrifugation, the supernatants were analyzed for residual MB. The amount of dye adsorbed Q_t (mg/g) at time t, was calculated according to Eq. 1.

$$Q_t = \frac{(C_0 - C_t)V}{m} \quad (1)$$

Where C_0 and C_t (mg/L) are the dye concentrations in the solution at the beginning and after time t, V (L) and m (g) are respectively the volume of the solution and the mass of dry biosorbent.

2.5.2. Kinetics modeling

Kinetics provides information on the adsorption process and the type of solute migration from the liquid phase to the solid phase. For this purpose, some models were considered to fit experimental data, the pseudo-first-order, pseudo-second-order (PSO) (PFO)[40, 41], and pseudo-nthorder (PNO)[42, 43], Table 2 describes the models' formulas and their parameters.

Table 2: Adsorption kinetics models used in this work and their parameters.

Kinetics models	Equation	Parameters
Pseudo-first order	$Q_t = Q_e\left(1 - e^{-k_1 t}\right)$	Q_e (mg g^{-1}) and Q_t (mg g^{-1}) refer to the amount of dye adsorbed at equilibrium and at time t (min) respectively. k_1(L min^{-1}) is the equilibrium rate constant of the pseudo-first-order equation
Pseudo-second order	$Q_t = \frac{k_2 Q_e^{\,2} t}{1 + k_2 Q_e t}$	k_2(L min^{-1}) is the equilibrium rate constant of the pseudo-second-order equation
Pseudo-nthorder	$Q_t = Q_e - [(n-1)k_n t + Q_e^{(n-1)}]^{\frac{1}{1-n}}$	k_n is a constant and n is the biosorption reaction order

2.5.3. Adsorption isotherms

The adsorption isotherm is a representative characteristic of the thermodynamic equilibrium between the adsorbent and the adsorbate [29]. It is very useful for understanding the adsorption mechanism; it gives information about the affinity, the binding energy between the adsorbate and the adsorbent, and about the adsorption capacity. A series of Erlenmeyer flasks (50 ml) placed on a multi-station magnetic stirrer shaken at 250 rpm and loaded with 50 ml of MB with different concentrations (in the range 50 to 1100 mg L^{-1}).25 mg of the PACK material was added to each Erlenmeyer; the mixture was stirred for 24 hours, and the process was repeated for two temperatures 20 and 30 °C. Adsorption capacity Q_e (mg.g^{-1}) was calculated based on Eq. (2).

$$Qe = \frac{(C_0 - C_e)V}{m} \quad (2)$$

Where C_0 and C_t (mg/L) are the dye concentrations in the solution at the beginning and after time t respectively, V (L) is the solution volume, and m (g) is the dry adsorbent mass.

2.5.4. Isotherm modeling

Mathematical modeling of isotherms provides a relationship between solute concentration in solution and adsorbed quantity per unit mass of adsorbent[44]. The two most commonly used two-parameter models are the Langmuir Freundlich and Dubinin Radushkevich (D-R) models. However, to go a little further in the understanding of adsorption mechanisms, three-parameter models like the Sips model and the Redlich-Petrson model were also considered. Table 3 describes these isotherm models and their parameters.

Table 3: Adsorption isotherm models adopted in this work and their parameters.

Isotherm	Equation	Parameters
Langmuir	$\frac{Q_e}{Q_m} = \frac{K_L C_e}{1+K_L C_e}$	Q_e (mg g^{-1}) is the amount of MB adsorbed per unit mass of adsorbent C_e. (mg L^{-1})the equilibrium dye concentration in solution Q_m(mg g^{-1}) is the monolayer capacity of the adsorbent K_L the Langmuir constant
Freundlich	$Q_e = K_F C_e^{1/n}$	K_F and n^{-1} are empirical constants indicative of sorption capacity and sorption intensity. respectively
Sips	$\frac{Q_e}{Q_m} = \frac{(K_S C_e)^m}{1+(K_S C_e)^m}$	K_s (L mg^{-1}) the Sips constant m the exponent of the Sips model
Redlich-Peterson	$Q_e = \frac{k_R C_e}{1+\alpha_R C_e^{\beta_R}}$	k_R(L g^{-1}) is the Redlich–Peterson (R-P) isotherm constant α_R (L mg^{-1})is also having a constant unit of $\beta_R$is an exponent
Dubinin-Radushkevich	$Qe = Q_{DR}\exp(-k_{DR}\varepsilon^2)$	Q_{DR} is the capacity of the adsorbent (mg/g) K_{DR} is the activity coefficient (mol^2 KJ^2) E_{DR} The biosorption energy (kJ mol^{-1}), ($E_{DR}=(2K_{DR})^{-0.5}$) ε stands for constant related to the biosorption energy(ε = RTln (1 +1/Ce))

2.6. Statistical physics

In an attempt to understand the adsorption phenomenon using statistical physics processing, the following hypotheses were assumed. It was considered that a variable amount of solute molecules were adsorbed on interstitial Nm sites imposed on the adsorbent (unit mass). Solute molecule (A) adsorption reaction at an interstitial site (S) must include a stoichiometric coefficient n according to the following reaction[45]:

$$nA + S \leftrightarrow A_nS \quad (3)$$

Depending on the value of n, two different ways of adsorption of the solute on the adsorbent can be distinguished. If n is less than 1, only a fraction of solute molecules are adsorbed; it consists in multi-anchorage adsorption. In the second case, if n is greater than 1, it is an interstitial site filled with more than one molecule; this case corresponds to multi-molecular adsorption[46].

Statistical physical simulation is used in this study to explain the adsorption of MB in the PACK material. For a system placed under specified physical conditions, we used the large canonical partition function z_{gc} which describes the microscopic state:

$$z_{gc} = \sum_{N_i}^{\cdot} e^{-\beta(-\varepsilon-\mu)N_i} \quad (4)$$

Where Ni is the receptor site occupation state, μ is the chemical potential, εi is the receptor site adsorption energy, and **β** is defined as 1/kBT (where T is the absolute temperature and kB is the Boltzmann constant).

The MB adsorption isotherms are simulated by three different models of statistical physics, monolayer single-energy, monolayer two-energy, and double-layer two-energy models[45].

The three models are summarized in the following table (Table 4).

Table 4: Grand canonical partition function and equation of the three models of statistical physics

Model	Grand canonical partition function	Equation
1	$z_{gc} = \sum_{N_i=0.1}^{\cdot} 1 + e^{\beta(\varepsilon+\mu)N_i}$	$\mathrm{Qe} = \frac{\mathrm{n.Nm}}{1+\left(\frac{\mathrm{C}_{1/2}}{\mathrm{Ce}}\right)^{\mathrm{n}}}$
2	$z_{gc} = \left(1 + e^{\beta(\varepsilon_1+\mu)}\right)^{N_{1m}} + \left(1 + e^{\beta(\varepsilon_1+\mu)}\right)^{N_{2m}}$	$\mathrm{Qe} = \frac{\mathrm{n1.Nm1.}}{1+\left(\frac{\mathrm{C1}}{\mathrm{Ce}}\right)^{\mathrm{n1}}} + \frac{\mathrm{n2.Nm2}}{1+\left(\frac{\mathrm{C2}}{\mathrm{Ce}}\right)^{\mathrm{n2}}}$
3	$z_{gc} = \sum_{1} 1 + e^{\beta(\varepsilon+\mu)} + e^{2\beta(\varepsilon+\mu)N_m}$	$Qe = n.N_M.\frac{\left(\frac{C}{C1}\right)^n + 2.\left(\frac{C}{C2}\right)^{2n}}{1+\left(\frac{C}{C1}\right)^n + 2.\left(\frac{C}{C2}\right)^{2n}}$

In model 1, it is assumed that the adsorption of the dye takes place by a monolayer single-energy model[47]. The receptor sites can interact with several dye molecules. The quantity adsorbed Q_e as a function of C_e is given by Eq.3 in the Table 4[48].

Where the parameter n represents the number of MB molecules captured per active site of PACK, the density of the adsorbent receptor sites is Nm and the concentration at half-saturation is $C_{1/2}$.

In model 2, monolayer two-energy, the adsorption of MB is assumed on two different sites of PACK with two different energies, E1 for the first site and E2 for the second site. The receptor sites can interact with a variable number of MB molecules, n1 with the first site (type one) and n2 with the second site (type two). The evolution of Q_e as a function of C_e is given by Eq. 4 in Table 4. Where Nm1 and Nm2 are the first and the second type densities of adsorbent receptor sites respectively, C_1 and C_2 are the concentration at half-saturation of the first and of the second receptor site.

For model 3, it is a double-layer two-energy, E_1 for the first layer and E_2 for the second layer, with mention of the second layer having less energy than the first[49]. From this, the quantity Q_e adsorbed as a function of C_e is given by Eq.5 in Table 4[50].

Where C_1 and C_2 are the concentrations of the first and second layers at half-saturation, respectively.

2.7. Statistical assessment of equilibrium parameters

Evaluation of nonlinear adsorption isotherms by the error function (F_{error}) represented by Eq.5 was conducted. This function allows to compare the experimental data point by point with those obtained by the adjusted model. Models with a low F_{error} value are the most appropriate for describing the experimental behavior:

$$F_{error} = \sqrt{\sum_{1}^{P}\left(\frac{1}{P-1}\right).\left(\frac{Q_{i,mod} - Q_{i,exp}}{Q_{i,exp}}\right)} \quad (5)$$

Where $Q_{i,mod}$ is the adsorption capacity by the adsorbent provided by the model; $Q_{i,exp}$ is the experimental adsorption capacity, and P is the number of experimental points performed[51].

2.8. Parameters governing adsorption phenomena

2.8.1. The effect of initial pH on adsorption of MB on PACK

The pH is a very important factor in the adsorption phenomenon. The surface charge and the distribution of ions of the material may change significantly with pH. The effect of pH on the adsorption of MB on PACK has been studied at different initial pH (in the range 3 to 12). The Solutions were adjusted with HCl (1 M) and NaOH (1 M) to the desired values. The initial concentration of MB was 160 mg/l (stock). The other parameters, such as the volume of the stirring tank, temperature, stirring speed, and adsorbate masse were V = 50ml, T = **25 ± 2°C**, stirring speed = 250 rpm, m_{PACK} = 25mg.

2.8.2. The effect of humic acid on the adsorption

Textile wastewater, as it is known contains variable concentrations of organic and inorganic ions, mainly cations and anions such as nitrates, chlorides, sulfates, carbonates, and hydrogeno-carbonates.In this part, the effect of humic acid on adsorption was examined to better understand the effect of his ions on the adsorption of the MB on the adsorbent. Indeed, humic acids are found in nature in significant quantities. Therefore, different humic acid quantities (5, 20, 30, and 50 mg) were added to 50 ml of a solution of MB at 800 mg/L in the presence of 25 mg of adsorbent. After stirring until the equilibrium time the results obtained were compared to the result of adsorption without humic acid.

2.8.3. Effect of the biosorbent dose on biosorption

The ratio of biosorbent-solution is an important factor in assessing the biosorption capacity of the material biosorbent. To discover the impact of the initial dose of PACK biosorbent on the MB dye, a range of doses between 10, 20, 30, 50, and 100 mg of adsorbent was examined in the 400 mg / L initial solution of the MB dye.

3. Result and discussions

3.1. Characterization of adsorbents

3.1.1. Infrared spectroscopy (FT-IR) interpretation of PACK material

The FT-IR spectrum of the PACK material before adsorption (Fig. 2) gives certain absorption bands that can be defined by the following functional groups. a broad absorption band of about 3600–3000 cm^{-1} which signifies the vibration of elongation of hydrogen from hydroxyl groups -OH (phenol alcohols, or carbonyls) It can also correspond to the vibration of elongation of the –OH groups of cellulose (lignin and pectin). Another band at 2360 cm^{-1} may correspond to the presence of a = N-H bond. The characteristic bands betwin1640 cm^{-1} and 1530 cm^{-1} can be identified as the carboxylic group bonding ionic (COO-) elongation vibrations and can be assigned to the C=C aromatic stretching. The characteristic band at 1380 cm^{-1} can be related to the C-H and O-H deformation vibration in hydroxyls, phenols, methyl, and olefins. In the comparison between the two FT-IR spectra before and after adsorption, similar peaks of different intensities were observed with the appearance of new peaks such as:

At 1321 cm^{-1}, a characteristic band attributed to the valence vibrations of the aliphatic C-H groups existing in the structure of the MB. The peek at 1120 cm^{-1} corresponds to the mode of vibration and elongation of the aromatic groups C-H existing in the structure of the MB, another band at 665 cm^{-1} may correspond to the presence of a C-S bond existing in the structure of the MB. These peaks confirmed the adsorption of MB onto the PACK material.

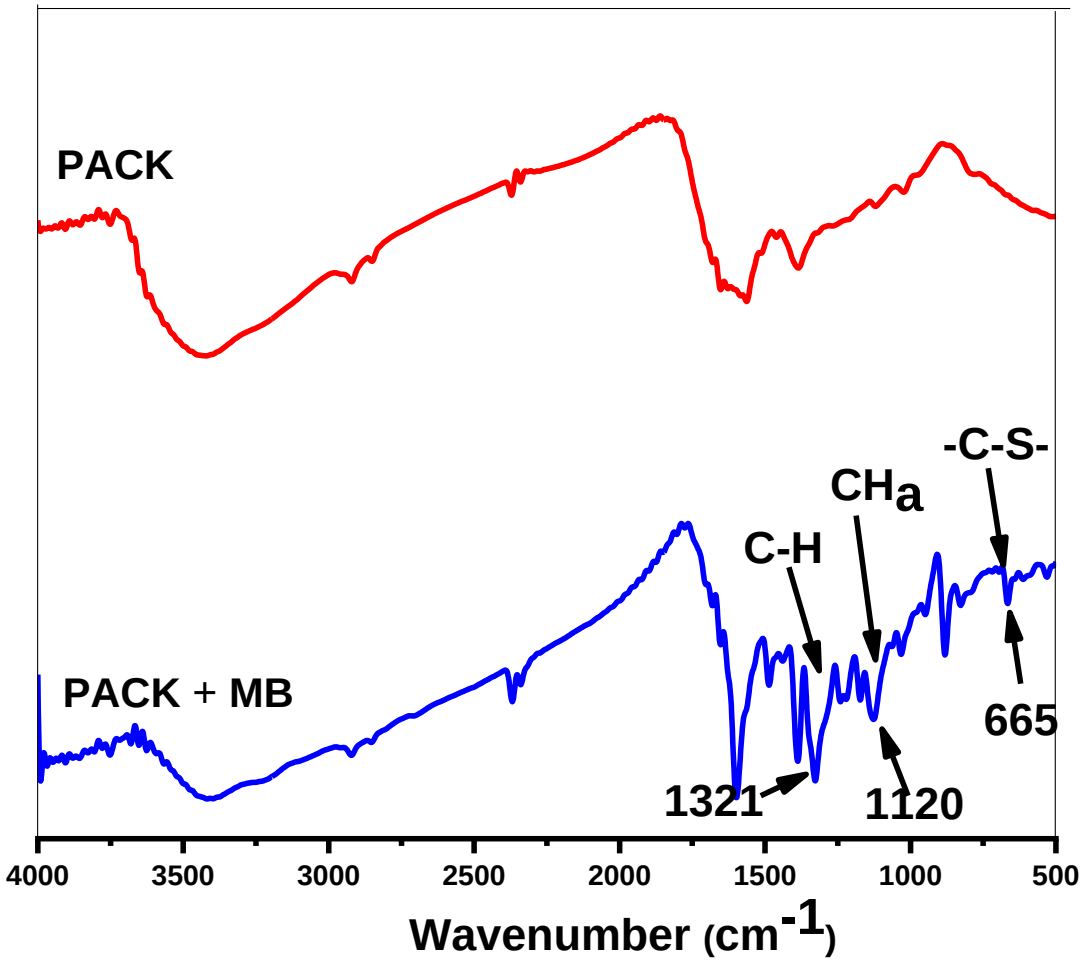

Figure 2. FT-IR spectrum of the PACK before and after adsorption of BM.

3.1.2. The Point of Zero Charge

From the graph presented in Fig. 3, the pH_{pzc} of adsorbate was equal to 8.3, which means that the surface of PACK was positively charged when the pH of the solution was lower than 8.3 and negatively charged when the pH of the solution was higher than 8.3.

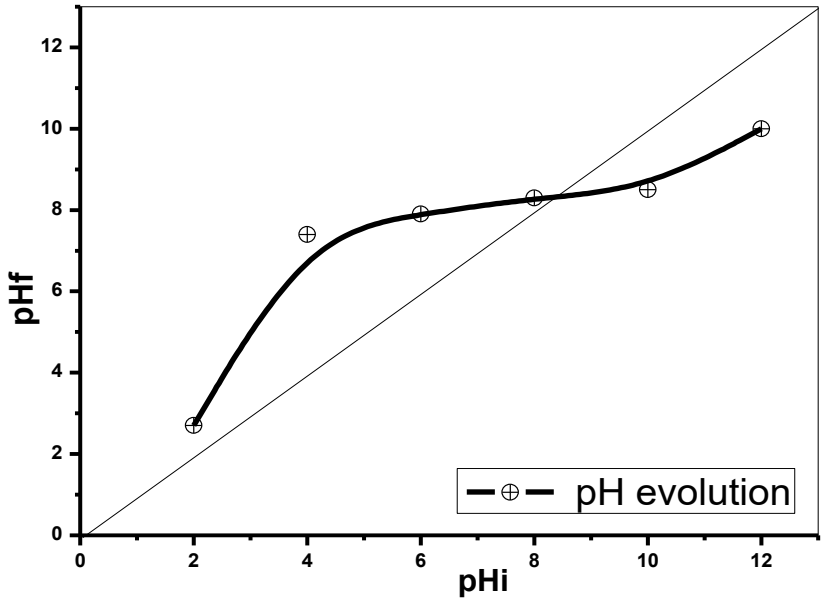

Figure 3. Isoelectric points of PACK (V = 50 ml, T = 25 ± 2 °C, stirring speed = 250 rpm, m_{PACK} = 25 mg).

3.1.3 Scanning electron microscopy (SEM)

It can be seen in the SEM surface images of PACK in Fig. 4. Images extracts obtained at a one and ten-micron-meter scale showed a heterogeneous surface morphology composed of many cavities (micro-pores) of different sizes. This irregular morphology of the material can facilitate the sorption of MB, and for this, we can assume that the PACK material represented an appropriate morphological profile for the adsorption of the dyes[52].

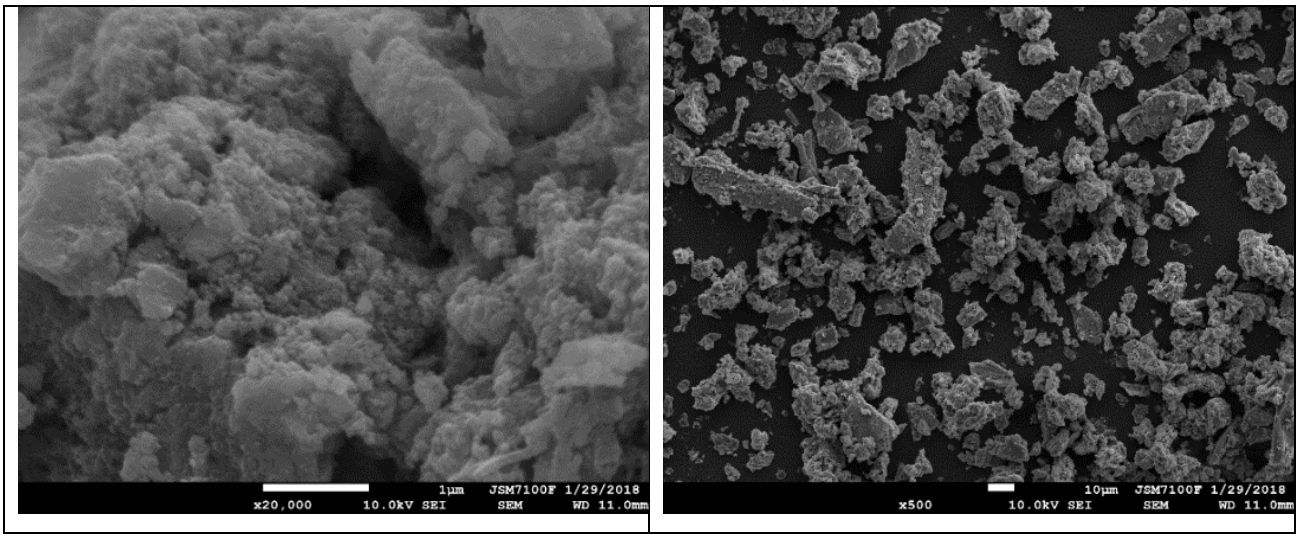

Figure 4. SEM captures of PACK

3.2. Kinetics analysis

Two initial concentrations 100 and 150 mg/L were considered. As expected, the adsorption capacity of PACK increased with the increase of the initial dye concentrations. As shown in Figure 5, the biosorption increases rapidly during the first 90 minutes, before reaching equilibrium, for both concentrations cited below. According to adsorption kinetics, more information on the adsorption mechanism (adsorbent/adsorbate) or in another way the transfer of a solute from the liquid phase to the solid phase can be provided. For this purpose, several kinetic models, namely the pseudo-first kinetic model (PFO), pseudo-second-order model (PSO), and pseudo-n^{th} order model (PNO)were applied to explain the adsorption mechanism. Fig.5 and Table 5 show the parameters obtained with the different kinetic models for the adsorption of MB onto the PACK material. It can be seen from this table, that all models accurately fitted the experimental data, leading to coefficients of correlation between 0.95 and 0.997; however, the values of the coefficients of correlation given by the PSO model were slightly lower than those given by PFO and PNO (Table 5).

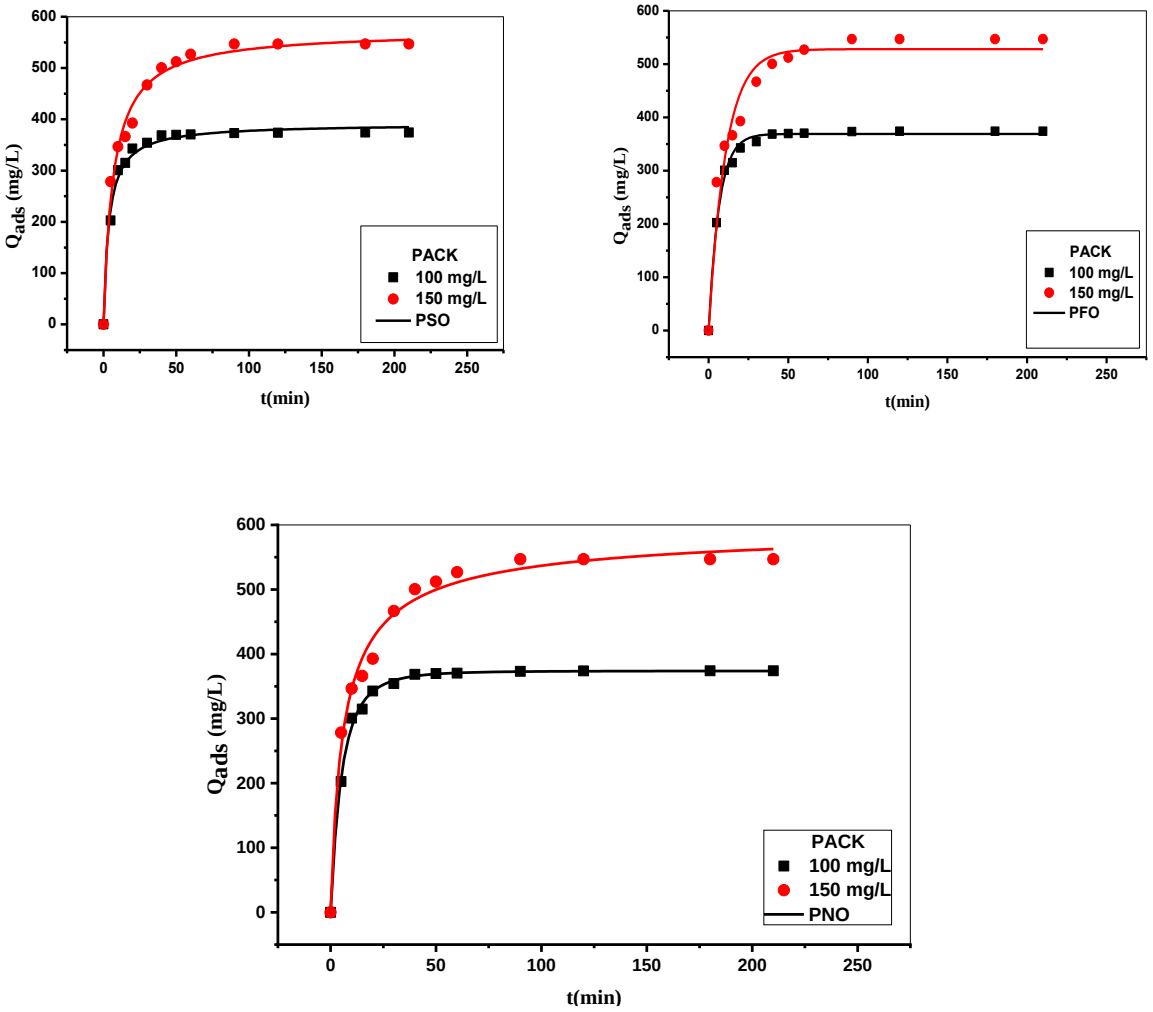

Figure 5. Kinetics data (symbol) of MB adsorption onto PACK and modeling data (lines) by PFO, PSO, and P^{nth}O with different initial concentrations. (V = 200 ml, T = 25 ± 2 °C, stirring speed = 250 rpm, m_{PACK} = 50 mg).

In addition, theoretically calculated Qt (373.87mg/g and 604.37mg/g) values from the PNO model agree very well with the experimental Qt (374mg/g and 547 mg/g)values, for both 100 and 150 mg/L, respectively, if compared to those obtained by both PFO and PSO models. Moreover, the rate constants (K1, K2, and Kn) for all models, declined in a significant way with an increased initial MB concentration from 100 to 150 mg/L. Furthermore, the coefficient n of the PNO goes from 1.31 to 2.5 for both concentrations 100 and 150 mg/L respectively. This result let's say that the order of the reaction is greater than 2 when the concentration is equal to 150 mg/L. In summary, according to the modeling results, it can be considered that experimental data were most accurately fitted in this order PNO-PFO-PSO models.

Table 5: Kinetic parameters and correlation coefficients for nonlinear regression of PFO PSO and PNO models for the adsorption of MB onto PACK at room temperature.

Material	Model	Parameters	100	150
PACK	PFO	Qexp	**374**	**547**
		Qe	368.88	528.05
		K_1	0.153	0.093
		R^2	**0.994**	**0.9494**
	PSO	Qe	391.46	572.70
		K_2*10^{+4}	6.94	2.60
		R^2	**0.989**	**0.986**
	PNO	Qe	373.87	604.37
		k_n	0.029	1.16E-05
		n	1.31	2.50
		R^2	**0.997**	**0.986**

3.3. Isotherm analysis

Adsorption isotherm is very important both theoretically and practically to optimize the adsorption system design for the elimination of MB by the material used; the corresponding results are shown in Fig.6. The two isotherms showed an L-type appearance (Langmuir type). The L shape of the adsorption isotherms means that there is no strong competition between the solvent and the adsorbent to occupy the adsorption sites; consequently, the affinity between the adsorbate and the adsorbent is relatively high. This was confirmed by the modeling of the adsorption isotherms (the affinity between the adsorbent and the adsorbate increases when the value of the K_L constant decreases). The maximum values of the adsorption capacity at equilibrium were1285.34 mg/g and 1528.02 mg/g for the two temperatures 20 and 30 °C, respectively. According to the results obtained, there was a positive temperature effect on the adsorption of MB-PACK. To properly define the sorption process for the elimination of dyes from the effluent, the most appropriate correlation for the equilibrium data should be determined.

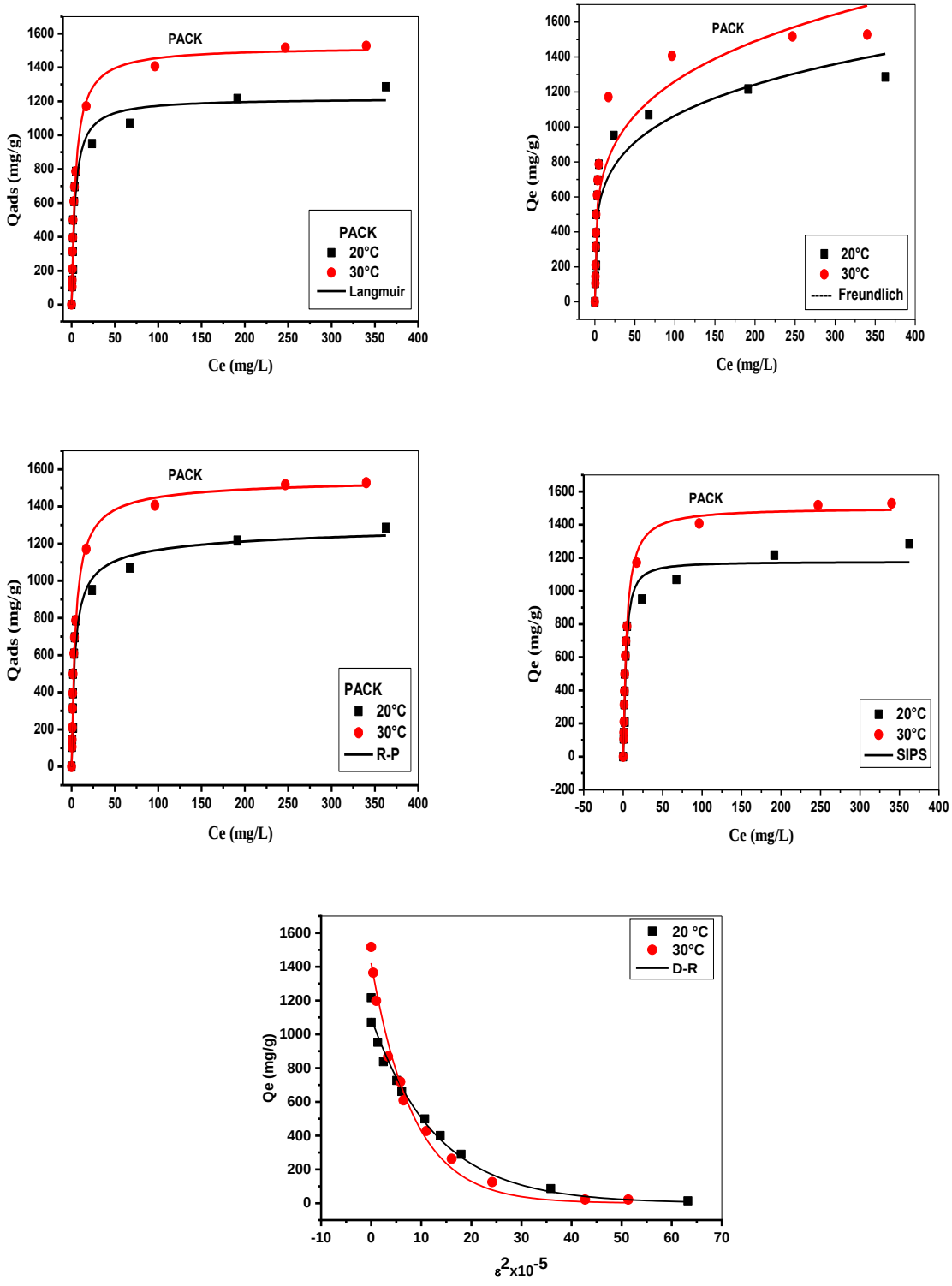

Figure 6. Experimental data (points) of MB adsorption onto PACK. Modeling Data (lines) by Langmuir, Freundlich, Sips, Redlich-Peterson, and D-R models models at different temperatures. (Stirring speed= 250 rpm, pH=6.5)

Isotherm models cited in Table 3 were used and the fitting was carried out using the Marquard-Levenberg program. It is clear that the adsorption capacity increased with increasing equilibrium concentration of MB and reached saturation progressively for all tested models. In the case of the two-parameter models, both Langmuir and Dubinin-Radushkevich isotherm models are the most appropriate to describe experimental data. The calculated parameters are provided in Table 6 and their graph is shown in Fig.6. It can be seen from Table 6, that the values of the coefficient of determination, R^2, obtained for Langmuir and Dubinin-Radushkevich(D-R) were closer to 1.00 than the Freundlich model. This indicates that there is strong positive evidence that the biosorption of methylene blue molecules onto PACK follows the adsorption of methylene blue molecules localized without adsorbate-adsorbent interaction[53]. The adsorption capacity for Langmuir and Dubinin-Radushkevich (D-R) (Table 6) using nonlinear regression was found to increase from 1219.83 mg/g to 1522.34 mg/g and from 1096.76 mg/g to 1419.95 mg/g for Langmuir and Dubinin-Radushkevich (D-R) respectively, namely close to those found experimentally for an increase in temperatures from 20to 30 °C. The biosorption constant, K_L; increases and decreases respectively from 256 L/mg to 219 L/mg, respectively using the Langmuir model as temperatures varied from 20 to 30 °C. Besides, from Table 6, it can be evaluated that the adsorption behavior of MB on PACK fitted very well with the Langmuir isotherm model, better than the Freundlich model as reflected by the correlation coefficients and the $\mathbf{F_{error}}$ of the experimental data. On the other hand, the three-parameter models, R-P, and Sips Eqs. were also applied to examine the adsorption of MB. The calculated isotherm parameters and their corresponding coefficient of determination R^2 values are also shown in Table 6. The high values of R^2 and the low values of F_{error} for the the R-P model suggest the applicability of this model to represent the equilibrium sorption of MB on PACK in comparison with the sips model. Several studies showed that the R-P isotherm was more accurate than the Langmuir and Freundlich isotherms as it contains three unknown parameters. Indeed, the Langmuir and Freundlich isotherms can result from the R-P isotherm, since forβ_R = 1, the R-P Eq. becomes the Langmuir isotherm and for β_R =0, it is closer to the FreundlichEq.Otherwise, the Sips model is a combination of Langmuir and Freundlich models. From this and Table 6, it is very understood that the adsorption capacity obtained from the Langmuir, Sips, and R-P Eqs could be more realistic than that from the Freundlich Eq. Moreover, the Redlich–Peterson (R–P) model was close to the Sips and Langmuir isotherm in the range of studied temperatures (when m and β value approach 1).

The isotherm constant α_R decreased with temperature; while inversely, the β_R exponent increased with temperature. From Table 6, we can note that β_R values were close to unity (i.e., the data could preferably be fitted with the Langmuir model). Finally Regarding the statistic parameters given by F_{error} and R^2, it can be noted that the R-P model was the most suitable to describe experimental data owing to its low F_{error} and the high R^2, compared to the other models in the range of temperatures considered. Also, The Dubinin-Radushkevich (D-R) isotherm model, provides us with more information about whether the adsorption process is physical or chemical depending on its measured E_{DR} parameter (if the E_{DR} value is between 8-16 $KJmol^{-1}$ the adsorption process is a chemisorption process and is a physisorption process if E_{DR}< 8 KJ mol^{-1})[54]. As mentioned, E_{DR} is independent of temperature, it depends on the nature of the adsorbate-adsorbent couple[55]. From the D-R model, the sorption energy E_{DR} is 0.65 KJ mol^{-1}. It is within the range of values for physical adsorption reactions. This result suggests that the biosorption process of the MB dye onto PACK biosorbent is physical in nature because the biosorption energy is less than 8 KJ mol^{-1}.

Table 6. Langmuir. Freundlich. Sips, Redlich-Peterson (R-P), and Dubinin-Radushkevich (D-R) constants for the adsorption of MB onto PACK

product	Models	parameters	20°C	30°C
PACK		**Q_{exp}(mg/g)**	**1285.34**	**1528.02**
	Langmuir	Q_m(mg/g)	1219.23	1522.34
		K_L (L/mg)x 10^3	0.256	0.219
		F_{error}	**0.365**	**0.926**
		R^2	**0.949**	**0.992**
	Freundlich	1/n	0.22	0.24
		K_F (mg/g)(L/mg)$^{1/n}$	381.59	414.21
		F_{error}	**0.857**	**0.950**
		R^2	**0.843**	**0.877**
	Sips	Q_m(mg/g)	1176.18	1502.57
		K_S (L/mg)	0.299	0.235
		m	1.26	1.08
		F_{error}	**0.471**	**0.329**
		R^2	**0.948**	**0.992**
	Redlich-Peterson	k_R(L/g)	341.261	343.545
		α_R (L/ mg)	0.325	0.238
		β_R	0.969	0.989
		F_{error}	**0.386**	**0.322**
		R^2	**0.9477**	**0.991**
	Dubinin-Radushkevich	Q_{DR}(mg/g)	1096.76	1419.95
		K_{DR}*10^6	**0.77**	1.20
		R^2	**0.983**	**0.988**

3.4. Statistical physics

According to the results obtained by the three statistical models used in this study (Fig.7**),** it seems that the two-energy monolayer model has the best modeling results according to the R^2 values obtained

(Table 7) for the two temperatures tested (20 and 30 °C). The two other models were therefore not further considered in the interpretations of the different parameters since they gave lower R^2 values.

Table 7: Results of calculations of the various anchoring parameters

	Model 1			**Model 2**			**Model 3**	
	20°C	**30°C**		**20°C**	**30°C**		**20°C**	**30°C**
n	1.262	1.079	**n_1**	1.775	3.553	**n**	1.26	1.078
Nm	931.99	1392.80	**Nm1**	548.26	101.82	**Nm**	932.48	1392.73
$C_{1/2}$	3.3464	4.259	**C_1**	2.433	1.289	**C_1**	3.347	4.259
R^2	0.9778	0.9966	**n_2**	1.957	1.025	**C_2**	732.22	753.18
			Nm_2	173.94	1146.87	**R^2**	0.9778	0.9966
			C_2	113.86	8.326			
			R^2	0.9873	0.9996			

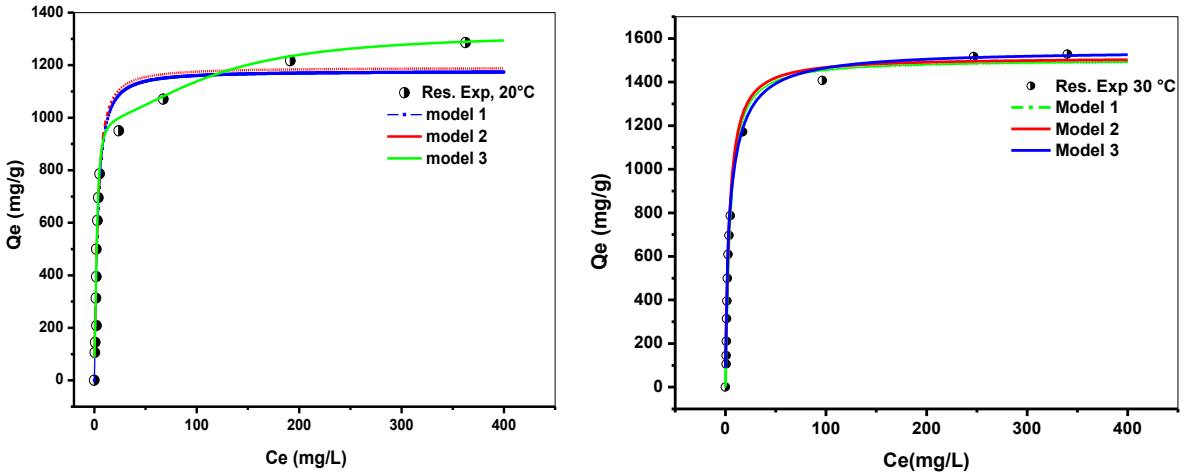

Figure 7. Simulation of statistical physics models, monolayer single-energy (Model 1), monolayer two-energy (Model 2), and Double-layer two-energy (Model 3).

3.4.1 Steric parameters ni and Nmi

The steric parameters n_1 and n_2 of the two-energy monolayer model are very useful in proposing an adsorption mechanism for the MB dye on the adsorbent. Three cases are possible concerning the value of n. The value n can be less than 0.5, 0.5<n <1, and in the last case n> 1. In the case where 0.5 <n <1, the molecules of the solute can orient themselves on the surface of the adsorbate in two different ways, parallel and non-parallel with a certain centering for each type of orientation. The case where n < 0.5 corresponds to adsorption where the molecules of the solute are oriented in a parallel way on the surface of the adsorbent. n> 1 shows that the molecules are anchored vertically on a site, leading to an aggregation. It is noted that the anchoring of the molecule on the adsorbent depends on its size, its structure, and also on its charge. The results of calculations of the various anchoring parameters are summarized in Table 7. It should be observed from Table 7 that at a temperature equal to 20 °C the value of n was= 1.775, namely between n = 1 (only one molecule is anchored at one site) and n=2 (two molecules are anchored at one site). The following Eq. (6) was considered to measure the percentage of MB molecules with a mono anchorage, (noted with X), and with two anchorage (noted with (1-X)).

$$n = X \times 1 + (1 - X) \times 2 \quad (8)$$

for the first n (n_1=1.775) It was found that 22.5% of the sites (type one) were occupied by one molecule, and the rest of the sites were occupied by two molecules (77.5%)[56]. Regarding the second n (n_2=1.957) at 293 K, it was found that 4.3% of the sites (type two) were occupied by one molecule, while the majority of the sites were occupied by two molecules (95.7%).

The values of n_1 increased from 1.775 for 20 °C to n1 = 3.553 °C for 30 °C, showing that the arrangement of the MB molecules on the surface of the adsorbent was affected by the temperature. It can easily be concluded that when the temperature increases, the number of molecules adsorbed per site decreases. On the contrary, the n_2 values decreased from 1.956 for 20 °C to n_2 = 1.025 for 30 °C. This shows that the percentage of sites (type two) that anchor two molecules decreased from 95.7% to 2.5%. This can be due to an increase in temperature that eliminates the bindings between MB dey molecules. It should be noted that this observation deserves further study concerning the different functions existing on the surface of the adsorbent material capable of creating an interaction or anchoring, since the sites n_1 and n_2 are not physically defined, which complicates the conclusion. It can be noticed that n_1 increases and n_2 decreases when the temperature increases; showing, an exchange or a compromise between the sites n_1 and n_2 concerning the adsorbed molecules when the

temperature varies. Concerning the Nmi parameters, is defined as the number of receptor sites occupied at saturation throughout adsorption, Nm1 is the number of receptors of the type one sites occupied and Nm2 is the number of receptors of the type two sites occupied. From Table 7. It can be noted that the increase in temperature caused a decrease in the first type of density Nm1 and an increase in the second type Nm2. Note that each density for each different site varied with an inverse trend compared to the number of MB products captured the reduction in the number of MB molecules captured per site created free space for the PACK biosorbent that contributed to the adsorption producing an increase in the number of anchorages ($n' = 1 / n$), followed by an increase in density Nmi.

3.5. Study of the effect of the parameters governing adsorption

3.5.1. The effect of pH

In Fig.8, the influence of the initial pH is shown. We have observed a very low adsorbed quantity for a very low pH range compared to pH_{pzc} and this may be due to the repulsion force between the positively charged material and the MB cationic dye. The adsorbed quantity is increased as the pH is increased towards pH_{pzc} until the maximum adsorbed quantity is obtained in a natural solution ph (ph = 6.5). This increase can be explained by the increase in the negative charges on the PACK surface by the increase in pH. The availability of negative charges on the PACK biosorbent surface makes the cationic dye MB adsorption better and more suitable [38]. Above the natural pH, there is a color change of the solution from blue to green color, associated with a maximum wavelength change from 664 nm to 570 nm with the emergence of the wavelength of the MB color. This color alteration can be attributed to secondary chemical reactions in the pH range above the natural pH between the MB dye and the PACK modifying material, and that caused the changes in the MB dye's ionic character.

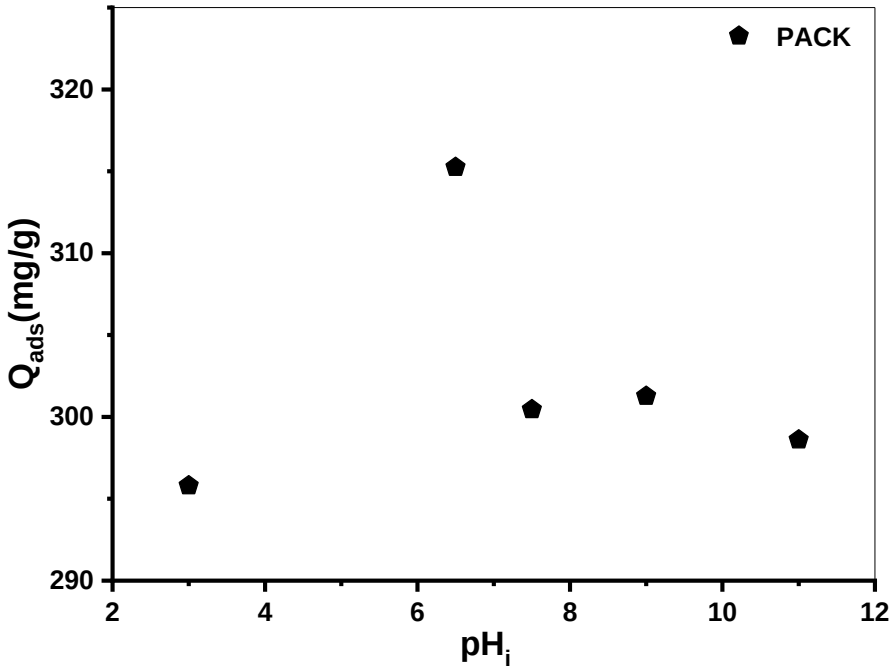

Figure 8. pH effect of MB adsorption onto PACK (V = 50 ml, T = 25 ± 2 °C, stirring speed = 250 rpm, m_{PACK} = 25 mg).

3.5.2. The effect of the temperature

25 mg of PACK adsorbent was added to 50 ml of an MB solution at a concentration of 800 mg/Lat the natural pH. The suspension was stirred for the equilibrium time. The protocol was repeated at 20, 30 and 40 ° C. To determine whether the adsorption process of the dye is endothermic or exothermic, the effect of temperature (20, 30, and 40 ° C) on the adsorption of MB on PACK has been examined. Figure 9 shows that the adsorption capacity increased with increasing temperature.

As the temperature increases, it is usual for the viscosity of the solution to decrease, thus increasing mobility for the dye as well, and thus an increase in penetration MB molécules through the pores of the PACK. At the same time, there could be more chemical interaction between the adsorbate and the surface of the bisorbent[57, 58]. Tan et al [59]reported a similar pattern in the adsorption of MB on activated oil palm fiber carbon.

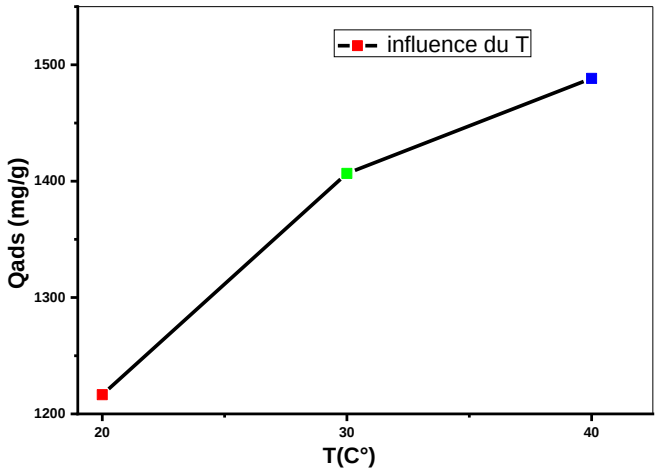

Figure 9. Temperature effect of MB adsorption onto PACK (V = 50 ml, stirring speed = 250 rpm, m_{PACK} = 25 mg).

3.5.3. The humic acid effect

According to the results obtained and compared to the maximum quantity adsorbed for a concentration of 400 mg/L of MB in the absence of humic acid (total elimination), there was a stable negative effect for each addition of different amounts of humic acid. This result can be explained by the adsorption competition between the cations of the component humic acid in the solution and the MB dye on the PACK material. The adsorption competition between cations of the component humic acid in the solution and the MB dye on the PACK material may explain this result. However, Fig. 10 demonstrates the ability of the PACK to maintain high MB removal at high ionic strength. Therefore, Textile wastewater treatment, which may include this group of compounds, may be effective with this material.

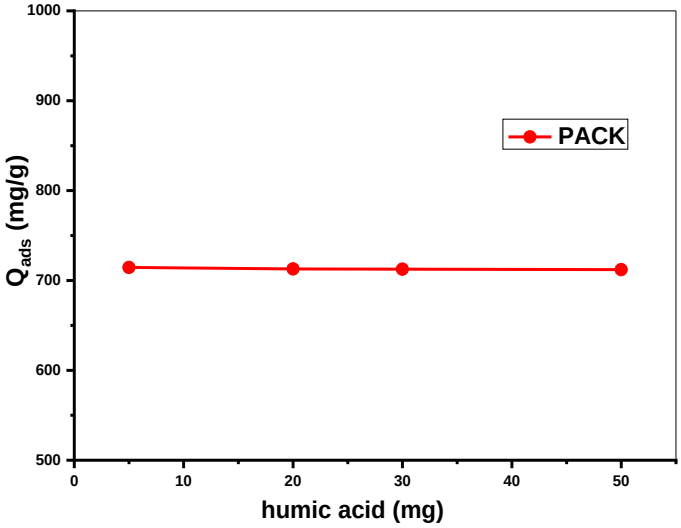

Figure 10. effect of humic acid on adsorption of MB on PACK material

3.5.4. The Effect of the biosorbent dose on biosorption

Figure 11 demonstrates the effect of the adsorbent Dosage on the adsorption capacity of BM dye. This figure indicates that the rise in the mass of the adsorbent contributes to a reduction in the adsorption capacity per unit mass of the adsorbent, but at the same time to an increase in the rate of biosorption, so a greater removal of the pollutant. This can be due to an increase in the available surface area and an increase in the number of active sites on the surface of the PACK material[8].

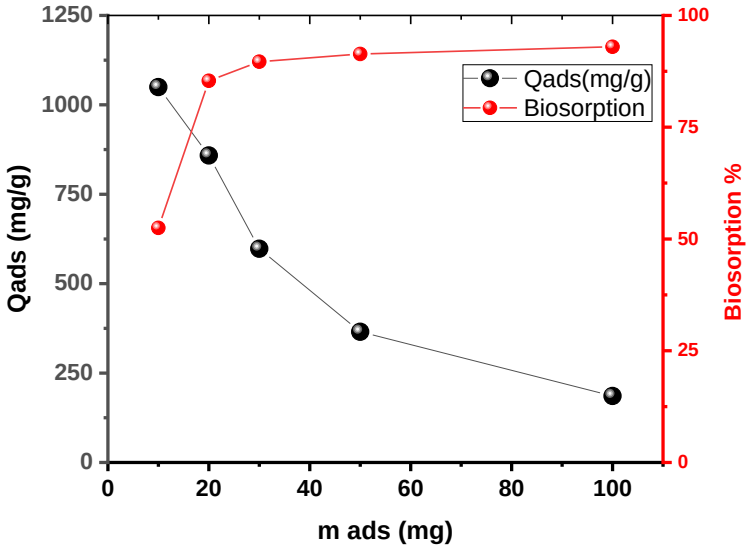

Figure 11. The effect of biosorbent dosage on the biosorption of MB onto PACK.

3.6. Desorption study

To determine the recovery rates of the PACK product, the desorption of the adsorbed MB dye after adsorption was carried out in three different solution media of 0.1 M HCl, 0.1 M NaOH, and 0.1 M ethanol, and the results are shown in **Figure 12**. After experiments of the adsorption of MB at an initial concentration of 400 mg/L, the solid phases (PACK) were separated from the solution and placed in the three solutions of HCl, NaOH, and ethanol and stirred until reached the equilibrium time for the desorption. At equilibrium, the quantities of MB desorbed in the three solutions were determined using spectrophotometry. Using an HCl acid solution the amount of desorption of the MB dye was recovered at the highest rate (52.88%) unlike the other two solutions. It is probably related to the breakage of the physical bonds (van der Waals) between the MB dye and the PACK product at low pH. However, nearly half of the adsorbed dye has not been retrieved. This may be due to the loss of the amount of absorbent material during the transition from the absorption process to the desorption process and also to the possibility that the dye that has been diffused into the particle or chemically bound has not been fully recovered[37].

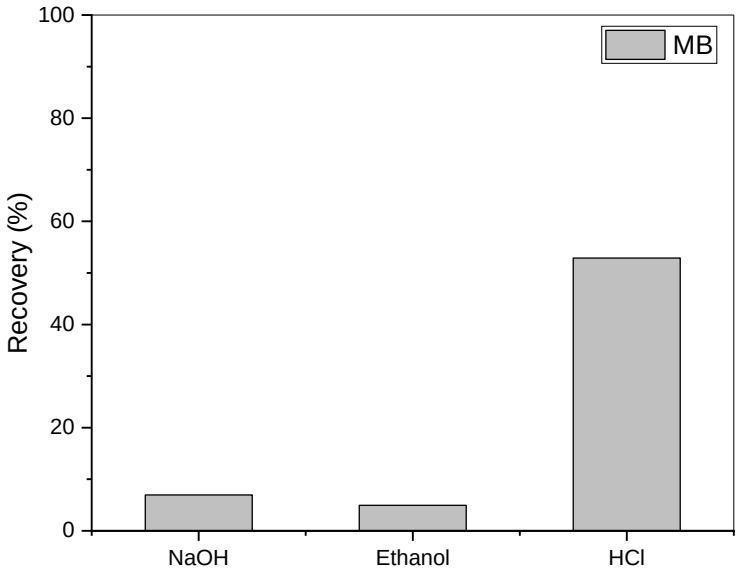

Figure 12: Recovery percent of various solvents for desorption of MB dye onto PACK. (C_0 =400 mg /L, m= 0.05 g, contact time: 24 h, temperature: 25 °C).

3.7. Proposed mechanism of adsorption of MB on PACK material

Based on the findings of the isoelectric point, the pH effect, the FT-IR analysis, and the results of the D.K isotherm model. The adsorption mechanism of MB on the PACK is supposed to be globally guided by electrostatic interactions (physical adsorption) Between the adsorbent which becomes negatively charged Each time we switch from the acid pH to its pHz and the positively charged dye, by weak hydrogen bonds between the nitrogen atoms present in the molecules of MB and the hydrogen atoms in the functional groups available on the surface of the adsorbent, and also with cation exchange. In addition and according to the analysis result of the FTIR, a π-π interaction can also occur in the process of biosorption MB_PACK, the MB dye is a polycyclic aromatic compound therefore contains several benzene rings, Benzene rings were also confirmed in the biosorbent with FT-IR analysis which revealed the presence of a C = C aromatic stretch. As these benzene rings are electron-rich areas, they can produce a donor-acceptor stacking interaction between MB and PACK. The description of the MB biosorption process is shown in Figure 13.

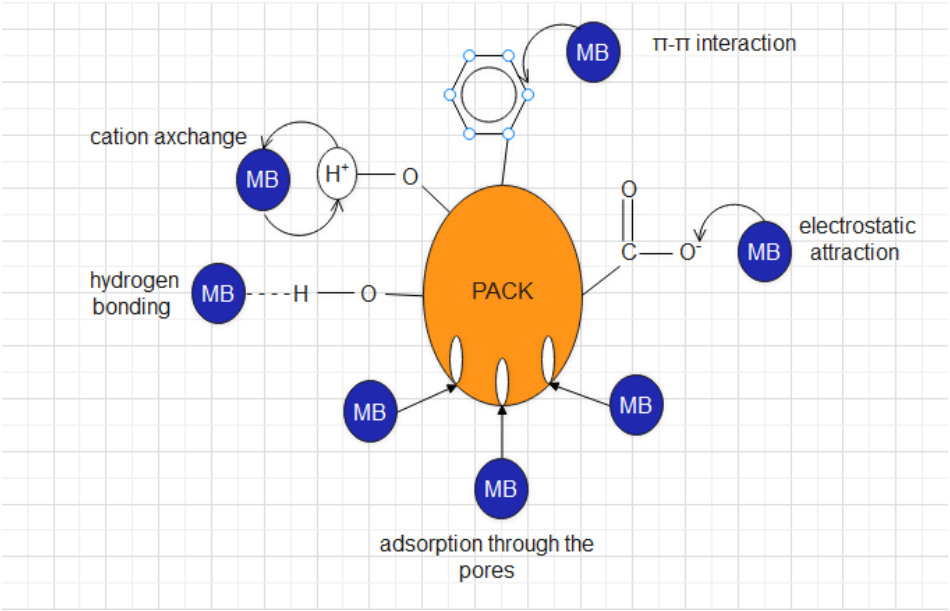

Figure 13: Mechanism of interaction MB dye with PACK in aqueous solution

3.8. Comparison of the maximum adsorption capacity of MB dye on certain adsorbents

The comparison of the maximum adsorption capacity of some adsorbents on methylene blue is displayed in **Table 8.** It should be noted that the adsorption capacity of the modified powder of Acorus calamus on MB appeared to be greater than that of other adsorbents, including activated carbon. The potential of PACK, an easily available and low-cost material, to be used as an alternative biosorbent material for the removal of a dye, MB, from aqueous solutions was therefore confirmed.

Table 8. Comparison of maximum monolayer adsorption of MB on some adsorbent in the literature

Adsorbent	Adsorption Capacity (mg/g)	References
Bentonite (alginate beads)	2024	[60]
PACK	1500	This study
Ziziphus jujuba stones (BZJS1) (alginate beads)	737.13	[39]
pectin from orange industry residues (alginate beads	398.40	[34]
graphene oxide	357.14	[61]
OP-H_3PO_4	307.63	[38]
Palm fiber-activated carbon	278	[59]
Activated carbon from Mangosteen fruit peel	230	[62]
Wild carob-activated carbon	218	[63]
Chitosan flakes-activated carbon	144	[64]
Fe_3O_4 particle	20.40	[65]

3.9. Thermodynamic analysis

Thermodynamic parameters reflect the possibility and the spontaneity of a biosorption process. Parameters such as the free energy change (ΔG), the enthalpy change (ΔH), and the entropy change (ΔS) can be estimated from the variations of the equilibrium constants with the temperature.

The free enthalpy change of the biosorption reaction is given using Eq. 9 as reported by Milonjic[30]:

$$\Delta G^{\circ} = -RT\ln(\rho Kc) \quad (9)$$

Where ΔG° is the free energy change ($kJ.mol^{-1}$), R the universal gas constant ($8.31J.mol^{-1}K^{-1}$), T is the absolute temperature (K), Kc the thermodynamic equilibrium constant ($L.g^{-1}$) and ρ the water density ($g.L^{-1}$).

ΔH° and ΔS° Values of the biosorption mechanism were calculated from Van't Hoff Eqs.10, and 11:

$$\ln(\rho K_C) = -\frac{\Delta H^o}{RT} + \frac{\Delta S^o}{R} \quad (10)$$

$$K_C = \frac{Q_e}{C_e} \quad (11)$$

ΔH and ΔS can be then deduced from the slope (ΔH/R) and the intercept (ΔS/R) of the plot of ln (ρK_C) versus 1/T.

In general, change in free energy values between −20 and 0 kJ mol^{-1} is reported for physisorption, while these values are in a range of −400 to −80 kJ mol^{-1} for chemisorption processes [63, 66].

Table 9 gives the calculation of the thermodynamic parameters. The value obtained for the free energy is about -20 KJ/mol for our material in the range of temperature from 20 to 40°C indicating that adsorption took place physically[63]. This result confirms the one found with the Dubinin-Radushkevich (D-R) model. Increased randomness at the interface of the solid solution during the biosorption MB on biosorbent was demonstrated by the positive value of entropy change.

Table 9: The calculation of the thermodynamic parameters

Température (K)	Kc (L/g)	ΔH^0(KJ/mol.)	ΔS^0(J/mol.K)	ΔG^0(KJ/mol.)
293	6.36	54.703	259.72	-21.32
303	14.60			-24.14
313	26.65			-26.65

4. Conclusion

New material was obtained by physical treatment from a low-cost and abundant biosorbent, powder of *Acoruscalamus*, with $H_2SO_4$and $KMnO_4$, denoted by PACK material, this material had a high maximum experimental capacity, 1285.34 and 1528.02 mg/g at 20 °C and 30 °C, respectively. Isotherm models with two and three parameters, namely Langmuir, Freundlich, Redlich-Peterson, and Sipswere applied to fit experimental data. Redlich-Peterson isotherms indicated a better fit compared to the Langmuir, Freundlich, and Sips isotherm models. According to the results of the kinetic modeling of adsorption of MB onto the PACK material, the pseudo-n^{th} order model has a better adjustment of the experimental results, if compared to both pseudo-first and pseudo-second-order kinetics models. As per the R^2 values obtained from the simulation of the results with the three advanced models, monolayer single-energy, monolayer two-energy, and double-layer two-energy models as statistical physics models, the two-energy monolayer model led to the best result of the processes of MB adsorption onto the PACK material. For this result, we can assume that the adsorption of MB on PACK exists on two different sites in energy (type one and two), each site can interact with a variable number of MB molecules (n), n1 interacts with type one and n2 with type two. According to this study, the promising potential of the PACK material, a very abundant material, easily obtainable, and renewable, for removing basic dyes from aqueous solution was demonstrated.

5. Reference

1. Novel activated carbon prepared from an agricultural waste, Stipa tenacissima, based on ZnCl2 activation—characterization and application to the removal of methylene blue: Desalination and Water Treatment: Vol 57, No 50. https://www.tandfonline.com/doi/abs/10.1080/19443994.2015.1137231. Accessed 9 Mar 2020
2. Robinson T, McMullan G, Marchant R, Nigam P (2001) Remediation of dyes in textile effluent: a critical review on current treatment technologies with a proposed alternative. Bioresource Technology 77:247–255. https://doi.org/10.1016/S0960-8524(00)00080-8
3. Soloman PA, Basha CA, Velan M, et al (2009) Electrochemical Degradation of Remazol Black B Dye Effluent. Clean Soil Air Water 37:889–900. https://doi.org/10.1002/clen.200900055
4. Miyah Y, Lahrichi A, Idrissi M, et al (2017) Assessment of adsorption kinetics for removal potential of Crystal Violet dye from aqueous solutions using Moroccan pyrophyllite. Journal of the Association of Arab Universities for Basic and Applied Sciences 23:20–28. https://doi.org/10.1016/j.jaubas.2016.06.001
5. Juang RS, Wu FC, Tseng RL (1997) The Ability of Activated Clay for the Adsorption of Dyes from Aqueous Solutions. Environmental Technology 18:525–531. https://doi.org/10.1080/09593331808616568
6. Rangabhashiyam S, Anu N, Selvaraju N (2013) Sequestration of dye from textile industry wastewater using agricultural waste products as adsorbents. Journal of Environmental Chemical Engineering 1:629–641. https://doi.org/10.1016/j.jece.2013.07.014
7. Ahmed MJ, Dhedan SK (2012) Equilibrium isotherms and kinetics modeling of methylene blue adsorption on agricultural wastes-based activated carbons. Fluid Phase Equilibria 317:9–14. https://doi.org/10.1016/j.fluid.2011.12.026
8. Şenol ZM (2020) Effective biosorption of Allura red dye from aqueous solutions by the dried-lichen (*Pseudoevernia furfuracea*) biomass. International Journal of Environmental Analytical Chemistry 1–15. https://doi.org/10.1080/03067319.2020.1785439
9. Badr S, Ashmawy AA, El Sherif I, Moghazy R (2016) Non-conventional low-cost biosorbents for adsorption and desorption of heavy metals. Research Journal of Pharmaceutical, Biological and Chemical Sciences 7:3110–3122

10. Berrios M, Martín MÁ, Martín A (2012) Treatment of pollutants in wastewater: Adsorption of methylene blue onto olive-based activated carbon. Journal of Industrial and Engineering Chemistry 18:780–784. https://doi.org/10.1016/j.jiec.2011.11.125
11. Suárez-García F, Martínez-Alonso A, Tascón JMD (2001) Porous texture of activated carbons prepared by phosphoric acid activation of apple pulp. Carbon 39:1111–1115. https://doi.org/10.1016/S0008-6223(01)00053-7
12. Ubago-Pérez R, Carrasco-Marín F, Fairén-Jiménez D, Moreno-Castilla C (2006) Granular and monolithic activated carbons from KOH-activation of olive stones. Microporous and Mesoporous Materials 92:64–70. https://doi.org/10.1016/j.micromeso.2006.01.002
13. Attia AA, Girgis BS, Fathy NA (2008) Removal of methylene blue by carbons derived from peach stones by H3PO4 activation: Batch and column studies. Dyes and Pigments 76:282–289. https://doi.org/10.1016/j.dyepig.2006.08.039
14. El-Hendawy A-NA, Samra SE, Girgis BS (2001) Adsorption characteristics of activated carbons obtained from corncobs. Colloids and Surfaces A: Physicochemical and Engineering Aspects 180:209–221. https://doi.org/10.1016/S0927-7757(00)00682-8
15. Baquero M (2003) Activated carbons by pyrolysis of coffee bean husks in presence of phosphoric acid. Journal of Analytical and Applied Pyrolysis 70:779–784. https://doi.org/10.1016/S0165-2370(02)00180-8
16. Kyzas GZ, Lazaridis NK, Mitropoulos ACh (2012) Removal of dyes from aqueous solutions with untreated coffee residues as potential low-cost adsorbents: Equilibrium, reuse and thermodynamic approach. Chemical Engineering Journal 189–190:148–159. https://doi.org/10.1016/j.cej.2012.02.045
17. Namane A, Mekarzia A, Benrachedi K, et al (2005) Determination of the adsorption capacity of activated carbon made from coffee grounds by chemical activation with ZnCl and HPO. Journal of Hazardous Materials 119:189–194. https://doi.org/10.1016/j.jhazmat.2004.12.006
18. Yagmur E, Ozmak M, Aktas Z (2008) A novel method for production of activated carbon from waste tea by chemical activation with microwave energy. Fuel 87:3278–3285. https://doi.org/10.1016/j.fuel.2008.05.005
19. Valix M, Cheung WH, McKay G (2004) Preparation of activated carbon using low temperature carbonisation and physical activation of high ash raw bagasse for acid dye adsorption. Chemosphere 56:493–501. https://doi.org/10.1016/j.chemosphere.2004.04.004

20. Laine J, Calafat A, labady M (1989) Preparation and characterization of activated carbons from coconut shell impregnated with phosphoric acid. Carbon 27:191–195. https://doi.org/10.1016/0008-6223(89)90123-1
21. Önal Y (2006) Kinetics of adsorption of dyes from aqueous solution using activated carbon prepared from waste apricot. Journal of Hazardous Materials 137:1719–1728. https://doi.org/10.1016/j.jhazmat.2006.05.036
22. Patel R, Suresh S (2008) Kinetic and equilibrium studies on the biosorption of reactive black 5 dye by Aspergillus foetidus. Bioresource Technology 99:51–58. https://doi.org/10.1016/j.biortech.2006.12.003
23. Aksu Z (2005) Application of biosorption for the removal of organic pollutants: a review. Process Biochemistry 40:997–1026. https://doi.org/10.1016/j.procbio.2004.04.008
24. Dotto GL, Pinto LAA (2011) Adsorption of food dyes onto chitosan: Optimization process and kinetic. Carbohydrate Polymers 84:231–238. https://doi.org/10.1016/j.carbpol.2010.11.028
25. Dotto GL, Vieira MLG, Esquerdo VM, Pinto LAA (2013) Equilibrium and thermodynamics of azo dyes biosorption onto Spirulina platensis. Braz J Chem Eng 30:13–21. https://doi.org/10.1590/S0104-66322013000100003
26. Kaur H, Thakur A (2014) Adsorption of Congo red dye from aqueous solution onto Ash of Cassia Fistula seeds: Kinetic and Thermodynamic Studies. chemical science review and letters 3:159–169
27. Low cost adsorbents from agricultural waste for removal of dyes - Ramaraju - 2014 - Environmental Progress & Sustainable Energy - Wiley Online Library. https://aiche.onlinelibrary.wiley.com/doi/full/10.1002/ep.11742. Accessed 6 Nov 2020
28. Ramakrishnaiah C (2014) Removal of Colour from Textile Effluent by Adsorption Using Low Cost Adsorbents. IRJPAC 4:568–577. https://doi.org/10.9734/IRJPAC/2014/5772
29. Chebli D, Bouguettoucha A, Mekhalef T, et al (2015) Valorization of an agricultural waste, *Stipa tenassicima* fibers, by biosorption of an anionic azo dye, Congo red. Desalination and Water Treatment 54:245–254. https://doi.org/10.1080/19443994.2014.880154
30. (PDF) The use of a forest waste biomass, cone ofPinus brutiafor the removal of an anionic azo dye Congo red from aqueous medium. https://www.researchgate.net/publication/264554082_The_use_of_a_forest_waste_biomass_co

ne_ofPinus_brutiafor_the_removal_of_an_anionic_azo_dye_Congo_red_from_aqueous_medium. Accessed 7 Nov 2020

31. Reffas A, Bouguettoucha A, Chebli D, Amrane A (2016) Adsorption of ethyl violet dye in aqueous solution by forest wastes, wild carob. Desalination and Water Treatment 57:9859–9870. https://doi.org/10.1080/19443994.2015.1031707
32. Chebli D, Bouguettoucha A, Reffas A, et al (2016) Removal of the anionic dye Biebrich scarlet from water by adsorption to calcined and non-calcined Mg–Al layered double hydroxides. Desalination and Water Treatment 57:22061–22073. https://doi.org/10.1080/19443994.2015.1128365
33. Gündüz F, Bayrak B (2017) Biosorption of malachite green from an aqueous solution using pomegranate peel: Equilibrium modelling, kinetic and thermodynamic studies. Journal of Molecular Liquids 243:790–798. https://doi.org/10.1016/j.molliq.2017.08.095
34. Kebaili M, Djellali S, Radjai M, et al (2018) Valorization of orange industry residues to form a natural coagulant and adsorbent. Journal of Industrial and Engineering Chemistry 64:292–299. https://doi.org/10.1016/j.jiec.2018.03.027
35. HASDEMİR ZM, ŞİMŞEK S (2018) Removal of cationic dye in aquatic medium by using a new composite material. Cumhuriyet Science Journal 39:181–191
36. Patel RK, Kumar S, Chawla AK, et al (2019) Elimination of Fluoride, Arsenic, and Nitrate from Water Through Adsorption onto Nano-adsorbent: A Review. CNANO 15:557–575. https://doi.org/10.2174/1573413715666190101113651
37. Şenol ZM, Gürsoy N, Şimşek S, et al (2020) Removal of food dyes from aqueous solution by chitosan-vermiculite beads. International Journal of Biological Macromolecules 148:635–646. https://doi.org/10.1016/j.ijbiomac.2020.01.166
38. Guediri A, Bouguettoucha A, Chebli D, et al (2020) Molecular dynamic simulation and DFT computational studies on the adsorption performances of methylene blue in aqueous solutions by orange peel-modified phosphoric acid. Journal of Molecular Structure 1202:127290. https://doi.org/10.1016/j.molstruc.2019.127290
39. Guediri A, Bouguettoucha A, Chebli D, Amrane A (2020) The use of encapsulation as a proposed solution to avoid problems encountered with conventional materials in powder form: Application in methylene blue removal from aqueous solutions. Journal of Molecular Liquids 316:113841. https://doi.org/10.1016/j.molliq.2020.113841

40. Lin J, Wang L (2009) Comparison between linear and non-linear forms of pseudo-first-order and pseudo-second-order adsorption kinetic models for the removal of methylene blue by activated carbon. Front Environ Sci Eng China 3:320–324. https://doi.org/10.1007/s11783-009-0030-7
41. Simonin J-P (2016) On the comparison of pseudo-first order and pseudo-second order rate laws in the modeling of adsorption kinetics. Chemical Engineering Journal 300:254–263. https://doi.org/10.1016/j.cej.2016.04.079
42. Oladipo AA, Gazi M (2014) Enhanced removal of crystal violet by low cost alginate/acid activated bentonite composite beads: Optimization and modelling using non-linear regression technique. Journal of Water Process Engineering 2:43–52. https://doi.org/10.1016/j.jwpe.2014.04.007
43. Tseng R-L, Wu P-H, Wu F-C, Juang R-S (2014) A convenient method to determine kinetic parameters of adsorption processes by nonlinear regression of pseudo-nth-order equation. Chemical Engineering Journal 237:153–161. https://doi.org/10.1016/j.cej.2013.10.013
44. Eastoe J, Dalton JS (2000) Dynamic surface tension and adsorption mechanisms of surfactants at the air–water interface. Advances in Colloid and Interface Science 85:103–144. https://doi.org/10.1016/S0001-8686(99)00017-2
45. Sellaoui L, Bouzid M, Duclaux L, et al (2016) Binary adsorption isotherms of two ionic liquids and ibuprofen on an activated carbon cloth: simulation and interpretations using statistical and COSMO-RS models. RSC Adv 6:67701–67714. https://doi.org/10.1039/C6RA03405E
46. Bouaziz N, Ben Manaa M, Aouaini F, Ben Lamine A (2019) Investigation of hydrogen adsorption on zeolites A, X and Y using statistical physics formalism. Materials Chemistry and Physics 225:111–121. https://doi.org/10.1016/j.matchemphys.2018.12.024
47. Sellaoui L, Dotto GL, Lamine AB, Erto A (2017) Interpretation of single and competitive adsorption of cadmium and zinc on activated carbon using monolayer and exclusive extended monolayer models. Environ Sci Pollut Res 24:19902–19908. https://doi.org/10.1007/s11356-017-9562-8
48. Sellaoui L, Edi Soetaredjo F, Ismadji S, et al (2017) New insights into single-compound and binary adsorption of copper and lead ions on a treated sea mango shell: experimental and theoretical studies. Phys Chem Chem Phys 19:25927–25937. https://doi.org/10.1039/C7CP03770H

49. Lawal IA, Lawal MM, Akpotu SO, et al (2018) Theoretical and experimental adsorption studies of sulfamethoxazole and ketoprofen on synthesized ionic liquids modified CNTs. Ecotoxicology and Environmental Safety 161:542–552. https://doi.org/10.1016/j.ecoenv.2018.06.019
50. Sellaoui L, Guedidi H, Knani S, et al (2015) Application of statistical physics formalism to the modeling of adsorption isotherms of ibuprofen on activated carbon. Fluid Phase Equilibria 387:103–110. https://doi.org/10.1016/j.fluid.2014.12.018
51. Silva LS, Lima LCB, Ferreira FJL, et al (2015) Sorption of the anionic reactive red RB dye in cellulose: Assessment of kinetic, thermodynamic, and equilibrium data. Open Chemistry 13:. https://doi.org/10.1515/chem-2015-0079
52. El-Sikaily A, El Nemr A, Khaled A (2011) Copper sorption onto dried red alga Pterocladia capillacea and its activated carbon. Chemical Engineering Journal 168:707–714. https://doi.org/10.1016/j.cej.2011.01.064
53. Khelifa A (2001) Adsorption de CO2 par des zeolithes X echangees par des cations bivalents. Annales de Chimie Science des Matériaux 26:55–66. https://doi.org/10.1016/S0151-9107(01)80046-5
54. Şenol ZM, Gül ÜD, Gürkan R (2020) Bio-sorption of bisphenol a by the dried- and inactivated-lichen (Pseudoevernia furfuracea) biomass from aqueous solutions. J Environ Health Sci Engineer. https://doi.org/10.1007/s40201-020-00508-6
55. Eren E (2008) Removal of copper ions by modified Unye clay, Turkey. Journal of Hazardous Materials 159:235–244. https://doi.org/10.1016/j.jhazmat.2008.02.035
56. Aouaini F, Souhail B, Khemiri N, et al (2019) Study of the CO_2 adsorption isotherms on El Hicha clay by statistical physics treatment: microscopic and macroscopic investigation. Separation Science and Technology 54:2577–2588. https://doi.org/10.1080/01496395.2018.1548487
57. Khattri SD, Singh MK (2009) Removal of malachite green from dye wastewater using neem sawdust by adsorption. Journal of Hazardous Materials 167:1089–1094. https://doi.org/10.1016/j.jhazmat.2009.01.101
58. Cherifi H, Fatiha B, Salah H (2013) Kinetic studies on the adsorption of methylene blue onto vegetal fiber activated carbons. Applied Surface Science 282:52–59. https://doi.org/10.1016/j.apsusc.2013.05.031

59. Tan IAW, Hameed BH, Ahmad AL (2007) Equilibrium and kinetic studies on basic dye adsorption by oil palm fibre activated carbon. Chemical Engineering Journal 127:111–119. https://doi.org/10.1016/j.cej.2006.09.010
60. Harrache Z, Abbas M, Aksil T, Trari M (2019) Thermodynamic and kinetics studies on adsorption of Indigo Carmine from aqueous solution by activated carbon. Microchemical Journal 144:180–189. https://doi.org/10.1016/j.microc.2018.09.004
61. Rahmi, Ishmaturrahmi, Mustafa I (2019) Methylene blue removal from water using H2SO4 crosslinked magnetic chitosan nanocomposite beads. Microchemical Journal 144:397–402. https://doi.org/10.1016/j.microc.2018.09.032
62. Liu X, Cui B, Liu S, Ma Q (2019) Methylene Blue Removal by Graphene Oxide/Alginate Gel Beads. Fibers Polym 20:1666–1672. https://doi.org/10.1007/s12221-019-9011-z
63. Bounaas M, Bouguettoucha A, Chebli D, et al (2020) Role of the Wild Carob as Biosorbent and as Precursor of a New High-Surface-Area Activated Carbon for the Adsorption of Methylene Blue. Arab J Sci Eng. https://doi.org/10.1007/s13369-020-04739-5
64. Marrakchi F, Ahmed MJ, Khanday WA, et al (2017) Mesoporous-activated carbon prepared from chitosan flakes via single-step sodium hydroxide activation for the adsorption of methylene blue. International Journal of Biological Macromolecules 98:233–239. https://doi.org/10.1016/j.ijbiomac.2017.01.119
65. Ravi, Pandey LM (2019) Enhanced adsorption capacity of designed bentonite and alginate beads for the effective removal of methylene blue. Applied Clay Science 169:102–111. https://doi.org/10.1016/j.clay.2018.12.019
66. Milonjic S (2007) A consideration of the correct calculation of thermodynamic parameters of adsorption. J Serb Chem Soc 72:1363–1367. https://doi.org/10.2298/JSC0712363M

Chapter III:

Experimental and Theoretical Study of Methylene Blue Adsorption on a New Raw Material, Cynara Scolymus—A Statistical Physics Assessment

1 Introduction

Throughout the world, many industries, such as the cosmetic, food, and paper industries, use dyes in large quantities. Most of these dyes are used in the textile industry [1] for their chemical stability and ease of synthesis. The global coloring production is more than 7×10^5 tons per year, with Azo coloration accounting for 60 to 70% of the total [2]. However, there are serious environmental problems with the use of these synthetic dyes. These industrial aqueous effluents may include tinctorial effluents, which may contain chemicals that are toxic to microbial populations as well as toxic or carcinogenic to humans or animals [3].

Methylene blue is not known to be very dangerous, but it can have a variety of side effects. It can cause short periods of fast or difficult breathing if inhaled. Swallowing by mouth causes a burning sensation and may cause gastritis, diarrhea, nausea, and vomiting [4].

Several physical, chemical, and biological methods have been introduced to remove this type of dye, such as flocculation, electro flocculation, membrane filtration, liquid–liquid extraction, irradiation, coagulation, ion exchange, advanced oxidation, ozonation, and electrochemical destruction [5]. However, due to the high cost of these processes and their limited capacity to adapt to a wide range of dye wastewater, their use is somewhat limited [6].

Consequently, due to its advantages and ease of use, adsorption remains the most used method in recent years [7]. Several materials, including activated carbon and synthetic clay, are used as adsorbents support in this method. The problem with these materials is the high cost of preparation. For this reason, several researchers are trying to find new materials to lower the preparation cost.

Because of their abundance in nature and the simplicity of their transformation into effective adsorbents, biosorbents attract a lot of attention [8]. For instance, lignocellulosic materials (biosorbents) have been proposed for the treatment of colored effluents, such as orange peel [7], cone of Pinusbrutia [1], Stipatenacissima [2] and its fibers [9], cupuassu shell [10], Saw dust and neem bark [11], raw pomegranate [12], Phragmitesaustralis [13], green macro alga [14], and Acorus calamus [15].

Artichoke, or *Cynara Scolymus*, is a vegetable of the Asteraceae family largely consumed in the Mediterranean regions. The edible section of the plant is the flower, known as the head, which is protected by leaf sheaths called bracts [16]. The *Cynara Scolymus* canning industry produces solid waste, primarily the stems and external bracts of the flowers, which make up 60–80% of the total *Cynara Scolymus* flowers and are unfit for human consumption, and it is generally disposed of as cattle feed or green manure [17]. Recently, this artichoke residue biomass has been investigated for potential use as a bioactive adsorbent precursor in a few research works [18,19].

The adsorption of methylene blue onto such adsorbents was estimated using classical models (i.e., Langmuir, Freundlich, Redlich–Peterson (RP), Sips, and Dubinin–Radushkevich isotherms) at equilibrium, and the parameters of these models can provide information on the classification of active sites and elimination capability without inspecting the absorption mechanism of methylene blue [20,21].

In this study, we employed novel physical models developed based on the grand canonical ensemble to relate the macroscopic features of molecules with the adsorption properties of materials [22,23]. These statistical thermodynamics-based models allow for the estimation of parameters such as the removed amount at saturation (Q_e), the number of adsorbed ions per active site (n), the density of receptor sites (N_m), and the uptake energy (E). All of the parameters were evaluated as a function of the temperature, resulting in a more detailed description of the adsorbate–adsorbent adsorption system [24].

The physical parameters collected from the simulation using these models allow us to describe the adsorption process at a molecular level if the adsorbate characteristics, adsorbent porosity, and surface charge are well characterized. Langmuir's model, for example, indicates that the adsorption site accepts one molecule of adsorbate, while physical models indicate that the acceptor site can accept n molecules of the adsorbate [25,26]. In recent years, numerous researchers have employed these physical models to describe the adsorption mechanism of their adsorbent materials, such as; porous heterostructured MXene/biomass activated carbon composites [27], lignin-based activated carbon [28], carbon foam hybrid aerogels [29], organo-sepiolite[30], Alginate/Carbon-based Films [31], cocoa shell [32], bone char [33], Acorus calamus [15], and Binary Mixture of Forest Waste Biopolymer [34].

To our current knowledge, the understanding of the interaction mechanism between *Cynara Scolymus* (Cs) direct powder and MB ions remains limited, particularly with regard to utilizing advanced physical models for studying this interaction. Hence, the primary objective of this study is to significantly enhance our understanding by achieving the following key objectives: (a) Assess the adsorption capacity of *Cynara Scolymus* direct powder (Cs) for the effective uptake of MB from aqueous solutions. This investigation will provide valuable insights into the potential of Cs powder as a viable adsorbent for removing MB contaminants. (b) Explore the adsorption properties of MB uptake at various temperatures (298 K, 303 K, and 313 K) using a range of equilibrium equations. By examining the temperature dependence of MB adsorption, we can gain a deeper understanding of the thermodynamics and kinetics of the adsorption process. (c) Analyze the adsorption process by considering classical models, such as Langmuir, Freundlich, Redlich–Peterson (RP), Sips, and Dubinin–Radushkevich isotherms. By applying these well-established models, we can evaluate the adsorption behavior of MB onto the Cs material and compare it with existing literature. (d) Obtain a comprehensive understanding of the underlying mechanism of MB adsorption onto the Cs material by employing statistical physics. This approach will allow us to delve into the microscopic details of the adsorption process and gain insights into the molecular interactions between Cs and MB ions. (e) Define the adsorption phenomena in macroscopic terms by utilizing thermodynamic functions. This analysis will enable us to characterize the energetics and spontaneity of the adsorption process and provide valuable information on the feasibility and stability of MB adsorption onto Cs. It is worth noting that the preparation of Cs direct powder will be a straightforward and cost-effective procedure, ensuring the practicality and applicability of this material for potential environmental remediation applications.

2 Materials and Methods

This research contributes to sustainability in several ways. Firstly, it aims to evaluate the adsorption capacity of Cs direct powder to effectively remove MB from aqueous solutions. By understanding the adsorption properties of Cs, this study can provide valuable insights into its potential as a viable adsorbent for removing contaminants like MB. Developing efficient adsorption materials can contribute to water decontamination and the preservation of water resource quality. Additionally, this research explores the adsorption properties of MB at different temperatures using a range of equilibrium equations.

This analysis will improve our understanding of the thermodynamics and kinetics of the MB adsorption process, enabling the optimization of operating conditions for more efficient and energy-saving adsorption processes, thus contributing to the sustainability of water decontamination processes. In this study, classical models such as Langmuir, Freundlich, Redlich–Peterson (RP), Sips, and Dubinin–Radushkevich have been employed to analyze the adsorption process of MB onto Cs. These established models allow for the evaluation of the adsorption behavior and its comparison with existing literature. This evaluation of adsorption models will provide a better understanding of the interactions between Cs and MB ions, facilitating the design of more efficient and sustainable adsorption materials. Furthermore, this research adopts a statistical physics approach to gain a comprehensive understanding of the underlying mechanism of MB adsorption onto Cs. By studying the microscopic details of the adsorption process, researchers can gather insights into the molecular interactions between Cs and MB ions. This in-depth knowledge can be utilized to improve the design of more selective and specific adsorption materials, promoting more efficient and sustainable resource utilization. Finally, this research utilizes thermodynamic functions to characterize the adsorption phenomena on a macroscopic scale. The analysis of thermodynamic properties allows for the determination of the energetics and spontaneity of the MB adsorption process, providing valuable information on the feasibility and stability of MB adsorption onto Cs. This information is crucial for evaluating the practical applicability of Cs as an adsorbent in environmental remediation applications, thereby contributing to the sustainable utilization of resources and environmental preservation.

This research provides in-depth knowledge of the adsorption mechanisms of MB onto Cs direct powder. By improving our understanding of adsorption processes and optimizing adsorption materials, this study contributes to sustainability by advancing water decontamination practices, promoting efficient resource utilization, and preserving the environment.

2.1 Materials

The *Cynara Scolymus* biomass (external bracts) waste used in this research was collected after consumption. Hydrochloric acid (HCl) with 35% (*w*/*w*), Sodium hydroxide (NaOH) with 98.8 % (*w*/*w*), sodium chloride (NaCl) with 95% (*w*/*w*), and humic acid (HA) with 99.9% (*w*/*w*) were obtained from Sigma–Aldrich.

2.2 Adsorbent Preparation

Cynara Scolymus residue wastes were passed through several stages of crushing, washing drying, grinding, and sieving to produce the final product powder (Cs) used in this work.

Large quantities of collected *Cynara Scolymus* were ground, washed multiple times with tap water and then distilled water to remove unwanted impurities, dried in an oven at around 333 K, and finally ground to a uniform powder. The particle sizes utilized in the adsorption tests were selectively separated with sieves with mesh widths ranging from 0.3 to 0.5 mm. The finished powder was kept in a desiccator until needed.

2.3 Effluent Preparation (MB)

Bis-(dimethylamino)–3.7 phenazathionium chloride, or methylene blue as it is commonly named, and containing an ammonium base, was in the form of a dark green powder. Its crude chemical formula is $C_{16}H_{18}ClN_3S$ with a molar mass of 319.85 g•mol^{-1} and solubility of 4 g•L^{-1} at 293 K. All the MB solutions used in this work were prepared from the stock solution at a concentration of 1 g•L^{-1}. All the glassware was washed with distilled water and dried in an oven at 323 K before being used. HCl and NaOH were used to adjust the pH to the desired value. The absorbance of each residual concentration was determined using a UV-vis spectrophotometer SP-8001 from Axiom (Frankfurt, Germany, Shimadzu).

2.4 Characterization of the Adsorbent

Various characterization techniques were used in this study and are detailed below.

FTIR analysis allows the determination of functional material surface groups. Infra-red spectroscopy was performed on natural and loaded Cs with MB dye (Cs-MB) using the Fourier Transform Infrared spectrometer (FTIR) model IRAffinity-1S from Shimadzu (Nakagyo-Ku, Japan), employing a high-pressure KBr disc technique in the band of 4000 to 400 cm^{-1}.

Additionally, the Cs material fine powder was analyzed using a PW3071/xx diffractometer operating at 45 KV and 35 mA with a copper anticathode emitting Ka radiation (λ = 1.5405 A). The XRD graphs were made with a step of 0.02° and a time step of 6.985 s/step throughout a 2θ angle range of 4 to 90°.

Scanning electron microscopy (SEM) of the Cs product before biosorption was visualized using the JCM-5000 NeoScope TM from Jeol (Tokyo, Japan) to examine the morphological features of the Cs biosorbent.

To evaluate the thermal characteristics of the Cs material, a thermogravimetric examination was performed in the temperature range of 303 to 1053 K using an SDT Q600 V20.9 Build 20 thermal gravimetric from TA Instruments (New Castle, Delaware, USA).

Finally, electrostatic interactions with a material surface are among the most important factors in deciding on the functionality and compatibility between the adsorbent and the adsorbate to give an idea of the adsorption mechanism. To determine the pH_{pzc} of our materials, a very simple protocol was considered. A series of suspensions: biosorbent (10 mg)/distilled water (10 mL) stirred for 24 h, each with a different initial pH (range 2 to 12), and the final pH was measured. The results are graphically represented (when $\Delta pH = 0$, the pH_{pzc} point equals the pHi).

2.5 Effect of the Initial pH

A factor that plays a very important role in the adsorption phenomenon is pH, which can alter the surface function and the distribution of anions and cations of any material.

To test the effect of this parameter, in each 25 mL Erlenmeyer flask, 10 mL of a methylene blue solution at 250 mg•L^{-1} was mixed with 10 mg of Cs. Every suspension was adjusted to a given initial pH (range of 2.4 to 12).

At room temperature, the mixture was stirred for 24 h at a speed of 250 ppm. The suspension was centrifuged, and the final concentration of the filter was measured by UV.

2.6 Effect of Humic Acid and NaCl

Textile wastewater is known to contain inorganic and organic ions in varying concentrations, mainly cations and anions such as chlorides, nitrates, hydrogen, sulfates, and carbonates. Consequently, and to get information on the effect of these ions on the retention process of MB dye by the Cs material, NaCl and humic acid (HA) have been considered as test ions.

A small amount of NaCl (0.1 M) was added to 10 mL of MB and 10 mg of biosorbent for different concentrations of MB dye (from 50 to 800 mg•L^{-1}). The mixture was stirred until the equilibrium time, and then the suspension was separated and analyzed. The same protocol was repeated with the second HA ion (0.1 M).

2.7 Study of Adsorption

2.7.1 Adsorption Kinetics

The following experiment was performed on three different MB concentrations (50. 100, and 200 mg•L^{-1}). In a 50 mL Erlenemayer series, at optimal pH (pH chosen in the section: pH Influence) and ambient temperature, 20 mg of adsorbent was introduced into 20 mL of MB dye solution. The mixture was stirred for a given time at a speed of 250 rpm on stir plates. Then, the centrifugation of each suspension was centrifuged, and the absorbance was measured to determine the residual MB. The adsorbed quantity was calculated using the following Equation:

$$Q_t = \frac{(C_0 - C_t)V}{m} \quad (1)$$

where Q_t is the quantity adsorbed, C_0 is the initial concentration of MB, C_t is the final concentration of MB, V is the volume of the mixture, and m is the mass of the mixture.

2.7.2 Kinetic Modeling

Some kinetic models such as pseudo-first-order, pseudo-second-order [35], and Pseudo-n^{th}-order [36] were used. Their Equation and parameter are listed in Table 1.

Table 1. Equations of PFO, PSO, and PNO models for nonlinear regression of Kinetic adsorption data.

Kinetics Model	Number	Equation
Pseudo-first order	(2)	$Q_t = Q_e(1 - e^{-kt})$
Pseudo-second order	(3)	$Q_t = \frac{k_2 {Q_e}^2 t}{1 + k_2 Q_e t}$
Pseudo-nthorder	(4)	$Q_t = Q_e - [(no-1)k_{no}t + {Q_e}^{(no-1)}]^{\frac{1}{1-no}}$
Intraparticle diffusion	(5)	$Q_t = k_{id}.t^{1/2} + C$
Boyd	(6)	$F_t = \frac{Q_t}{Q_e} = 1 - \frac{6}{\pi^2} e^{-\beta_t}$
	(7)	$\beta_t = -0.4977 - \ln(1 - F)$

The intraparticle diffusion model and the Boyd model were considered to evaluate the diffusion mechanism and the rate control step.

2.7.3 Isotherm Adsorption

The capacity of adsorbents to adsorb the different components of a mixture is the most critical factor in the efficiency of most adsorption processes. Therefore, it is important to have a clear understanding of the properties of the adsorbent-adsorbate equilibrium. For planning and scaling precisely the adsorption process, three isotherms were performed at the three temperatures (T = 298, 303.313 K) by the protocol outlined below.

For each Erlenemayer (25 mL), 10 g of adsorbent was added to 10 mL of MB of variable concentration solution at the optimal pH. The mixture was stirred at 250 ppm up to equilibrium. A wide range of MB concentrations was used (from 50 to 800 mg•L^{-1}).

The adsorbed quantity was determined using Equation (8).

$$Q_e = \frac{(C_0 - C_e)V}{m} \quad (8)$$

where Q_e is the quantity adsorbed, C_0 is the initial concentration of MB, C_e is the final concentration of MB in the solution, V is the volume of the mixture, and m is the mass of the mixture.

2.7.4 Isotherm modeling

Mathematical simulations were carried out to evaluate accurately the interaction between the Cs and the MB dye.

2.7.4.1 Classical Models

Three models, each with a two-parameter equation, Langmuir, Freundlich, and Dubinin–Radushkevich [37], and two models, each with a three-parameter equation, Redlich–Peterson [38] and Sips [39], are the most widely used models in the literature to describe the nonlinear equilibrium at a constant temperature between the adsorbed pollutant (Q_e) and the rest of the pollutant in solution (C_e). Table 2 shows the equations and parameters of such models.

Table 2. Langmuir, Freundlich, Dubinin–Radushkevich, Redlich–Peterson (R–P), and Sips equations and Equation.

Isotherme Model	Number	Equation
Langmuir	(9)	$\frac{Q_e}{Q_m} = \frac{K_L C_e}{1 + K_L C_e}$
Freundlich	(10)	$Q_e = K_F C_e^{1/nf}$
Sips	(11)	$\frac{Q_e}{Q_m} = \frac{(K_S C_e)^{ms}}{1 + (K_S C_e)^{ms}}$
Redlich–Peterson	(12)	$Q_e = \frac{k_R C_e}{1 + \alpha_R {C_e}^{\beta_R}}$
Dubinin–Radushkevich	(13)	$Q_e = Q_m e^{(-k_{DR}\varepsilon^2)}$ with: $\varepsilon = RT\ln\left(1 + \left(\frac{1}{C_e}\right)\right)$

2.7.4.2 Advanced Statistical Physics Models for Analyzing the Experimental Results of Adsorption Isotherm of MB on Cs

To better understand the mechanism of MB adsorption on Cs, advanced adsorption models were considered to confirm the results obtained using classical models, as well as to provide more information on the behavior of the adsorbent-adsorbate system [40].

Five advanced models were selected for this analysis. These models are briefly represented in Table 3.

Table 3. The Advanced statistical physics models AM1, AM2, AM3, AM4, and AM5.

Model	Num	Equation	Ref
Single-energy single-layer model (AM1)	(14)	$Q_e = \frac{Q_0}{1+\left(\frac{C_{1/2}}{C_e}\right)^n} = \frac{n.N_m}{1+\left(\frac{C_{1/2}}{C_e}\right)^n}$	[38]
Double-energy single-layer model (AM 2)	(15)	$Q_e = \frac{n_1.N_{m1}.}{1+\left(\frac{C_1}{C_e}\right)^{n_1}} + \frac{n_2.N_{m2}}{1+\left(\frac{C_2}{C_e}\right)^{n_2}}$	[39]
Single-energy double-layer model (AM 3)	(16)	$Q_e = n.N_m.\frac{\left(\frac{C_e}{C_{1/2}}\right)^n + 2.\left(\frac{C_e}{C_{1/2}}\right)^{2n}}{1+\left(\frac{C_e}{C_{1/2}1}\right)^n + \left(\frac{C_e}{C_{1/2}}\right)^{2n}}$	[20]
Double-energy double-layer model (AM 4)	(17)	$Q_e = n.N_m.\frac{\left(\frac{C_e}{C_1}\right)^n + 2.\left(\frac{C_e}{C_2}\right)^{2n}}{1+\left(\frac{C_e}{C_1}\right)^n + \left(\frac{C_e}{C_2}\right)^{2n}}$	[21]
Finitemultilayer (AM 5)	(18)	$Q_e = n.N_m.\frac{F_1(C_e)+F_2(C_e)+F_3(C_e)+F_4(C_e)}{G(C_e)}$ With: $F_1(C_e) = \frac{\left(-2.\left(\frac{C_e}{C_1}\right)^{2n}\right)}{\left(1-\left(\frac{C_e}{C_1}\right)^n\right)} + \frac{\left(\frac{C_e}{C_1}\right)^n\left(1-\left(\frac{C_e}{C_1}\right)^{2n}\right)}{\left(1-\left(\frac{C_e}{C_1}\right)^n\right)^2}$ $F_2(C_e) = \frac{2.\left(\frac{C_e}{C_1}\right)^n\left(\frac{C_e}{C_2}\right)^n\left(1-\left(\frac{C_e}{C_2}\right)^{(nN_2)}\right)}{\left(1-\left(\frac{C_e}{C_2}\right)^n\right)}$ $F_3(C_e) = \frac{-\left(\frac{C_e}{C_1}\right)^n\left(\frac{C_e}{C_2}\right)^n\left(\frac{C_e}{C_2}\right)^{(nN_2)}N_2}{\left(1-\left(\frac{C_e}{C_2}\right)^n\right)}$ $F_3(C_e) = \frac{\left(\frac{C_e}{C_1}\right)^n\left(\frac{C_e}{C_2}\right)^{(2n)}\left(1-\left(\frac{C_e}{C_2}\right)^{(nN_2)}\right)}{\left(1-\left(\frac{C_e}{C_2}\right)^n\right)^2}$ $G(C_e) = \frac{\left(1-\left(\frac{C_e}{C_1}\right)^{(2n)}\right)}{\left(1-\left(\frac{C_e}{C_1}\right)^n\right)} + \frac{\left(\frac{C_e}{C_1}\right)^n\left(\frac{C_e}{C_2}\right)^n\left(1-\left(\frac{C_e}{C_2}\right)^{(nN_2)}\right)}{\left(1-\left(\frac{C_e}{C_2}\right)^n\right)}$	[39]

2.7.5 Statistical Assessment of Equilibrium Parameters

The average percentage errors APE (%) function, represented by Equation (19), was used to evaluate nonlinear adsorption curves of kinetics and isotherms. This function allows comparing experimental data to the adjusted model's results point by point. The models with the lowest APE (%) values are the best for describing the experimental behavior.

$$\mathrm{APE}(\%) = \frac{\sum_{i=1}^{N} \frac{|Qi.mod - Qi.exp|}{Qi.exp}}{N} \times 100 \quad (19)$$

where Qi.mod is the model's adsorption capacity, Qi.exp is the experimental adsorption capacity, and N is the number of experimental points performed [40].

3 Results and Discussion

3.1 Adsorbent Characterization

The FTIR analysis was utilized to determine the functional groups existing on the *Cynara Scolymus* surface (Cs) material before and after the adsorption of MB color (Cs-MB). The acquired results are depicted in Figure 1a.

Broadband between 3700 and 3000 cm^{-1} demonstrated that the surface of Cs contains a greater amount of alcoholic and phenolic –OH functional groups than cellulose, Pectin, and lignin in powder of leaf structure [41]. The peak at 2939 cm^{-1} correlated to the methyl group's C–H stretching bond [42]. The peak at 1745 cm^{-1} corresponded to the bending of the C=O functional group found in quinones and lactones. The sharp peak at 1648 cm^{-1} was associated with the bending vibrations of C=O derived from a carboxylic acid [43]. The peak at 1429 cm^{-1} was assigned to the carboxylate functional group (COO^{-}). The peak at 1256 cm^{-1} was associated with the bending modes of the ligands O–C–H, C–C–H, and C–O–H. A prominent band of about 1036 cm^{-1} verified the presence of the functional group C–O–C in the cellulose and lignin molecules of Cs [44]. These functional groups on the Cs surface could serve as active sites for cationic dye adsorption. Figure 1a illustrates the changes in FTIR spectra caused by dye adsorption. There was a considerable drop in the strength of the C–H and C–O–C peaks at 2939 cm^{-1} and 1036 cm^{-1}, respectively, which could be due to MB adsorption onto Cs adsorbent [7].

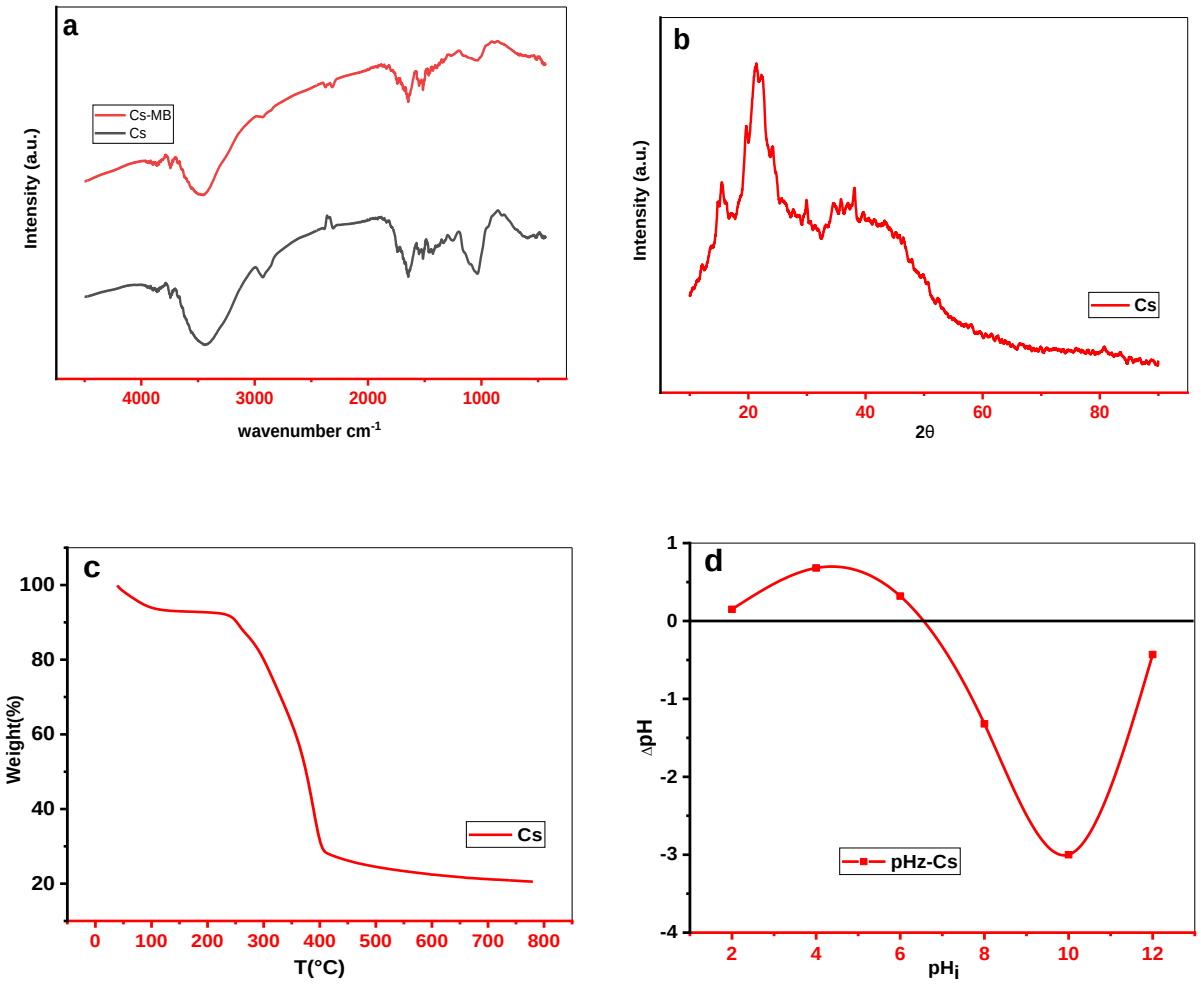

Figure 1. *Cynara Scolymus* (Cs) Characterization (**a**) FTIR spectrum, (**b**) XRD shape, (**c**) Thermogravimetric analysis, (**d**) isoelectric point.

Figure 1b depicts the XRD pattern for Cs. As can be seen, the sample diffraction pattern had two planes at approximately 15° and 21°2θ. The plane (0 0 2) of cellulose I was responsible for a high-intensity peak near 21.5° at 2θ. The plane (1 0 1) of cellulose I, which was near 15.5°, exhibited significantly less diffraction and overlap. This could be due to the comparatively large concentrations of lignin and hemicellulose in natural lignocellulose Cs. which contribute to its amorphous nature [44,45].

The thermogravimetric analysis (TGA) results are displayed in Figure 1c. Thermal analysis revealed two regions; the first suggested that the Cs biomass lost weight between 35 and 230 °C as a result of moisture evaporation. The second zone was 230–400 °C and demonstrated the greatest weight loss due to hemicellulose and cellulose degradation. The final weight reduction was at 450 °C, which was entirely due to lignin degradation [46].

From Figure 1d, the pH_{pzc} of the Cs substance was 6.55. Therefore, above this value, the surface of this material was negatively charged by the excess of OH^- anions, and the surface was positively charged below this value by the excess of H^+cations[47].

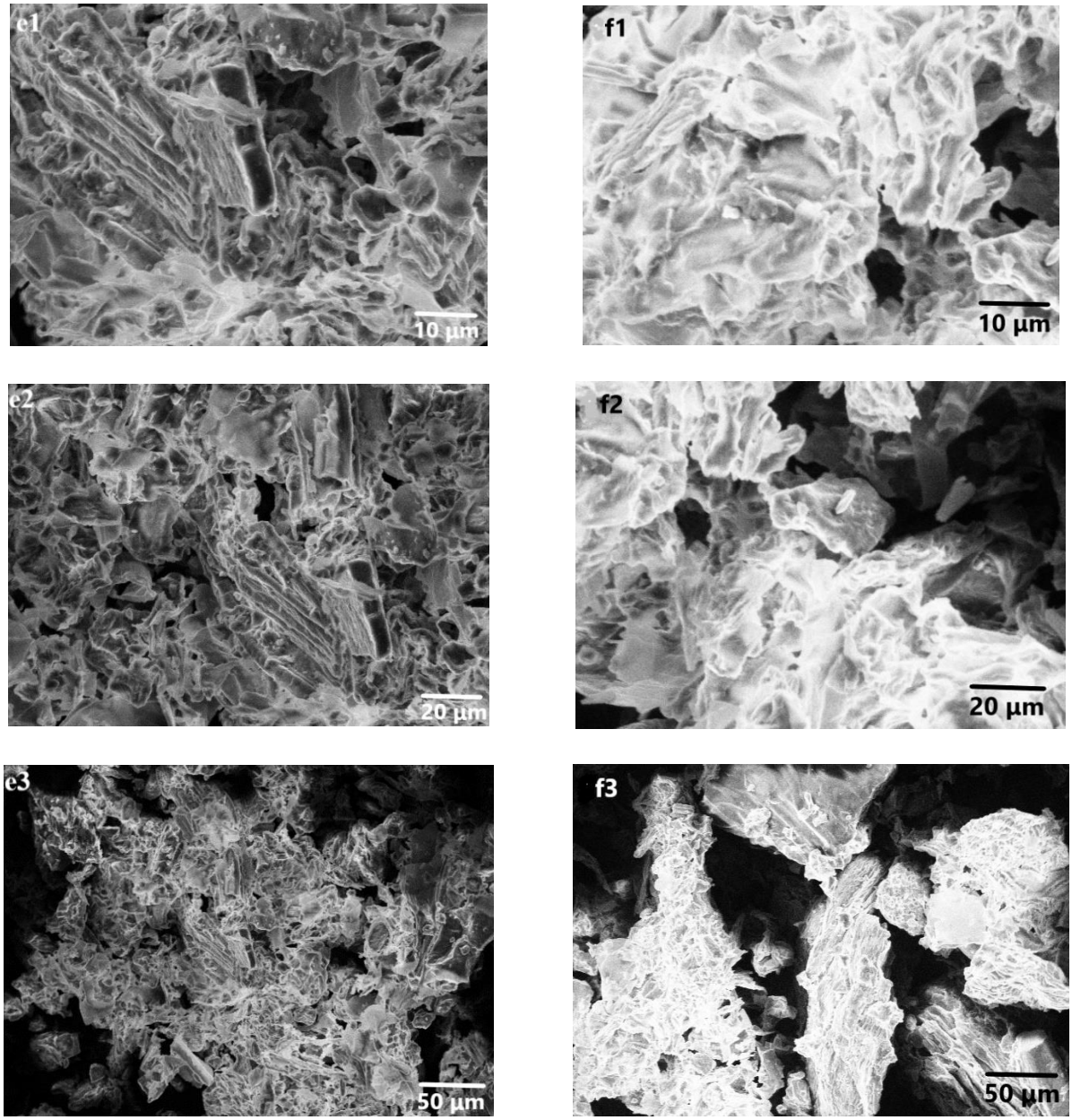

Figure 2. SEM images (**e**) before and (**f**) after adsorption.

Figure 2e1–e3 show SEM surface images of the Cs product before adsorption on a scale of 10, 20, and 50 μm, respectively, and Figure 2f1–f3 after adsorption. Figure 2e1–e3 revealed a heterogeneous surface structure with many cavities of varying sizes. As a result of the irregular morphology of the material, we can deduce that the Cs material represented a suitable morphological profile for dye adsorption. After adsorption and from Figure 2f1–f3, the coverage of the adsorbent surface (Cs) due to the adsorption of adsorbate molecules (MB), presumably leading to the formation of a monolayer of adsorbate molecules on the adsorbent surface, is visible from the formation of a white spreading layer (molecular cloud) of uniform thickness and coverage [48].

3.2 Effect of the Initial pH on Adsorption of MB with Cs

The pH impact of the aqueous solution on MB adsorption on Cs material is shown in Figure 3, which shows a very weak adsorbed quantity for a very low pH range (pH < pHpzc). This may be due to the repulsion force between the positively charged Cs product and the MB cationic dye. The adsorption capacity increased significantly as the pH of the solution increased as a result of an increase in negative charges (OH^- ions) [49] on the Cs surface as the pH increased. At pH 10, the maximum capacity was reached. This confirms that electrostatic interaction plays a significant role in MB adsorption on Cs. We observed a decrease in the adsorbed amount of MB between 10 and 12 pH as a result of the modification of the MB structure in this interval, where the maximum wavelength decreases from 654 to about 550 nm. By these findings, a pH of 10 was considered thereafter.

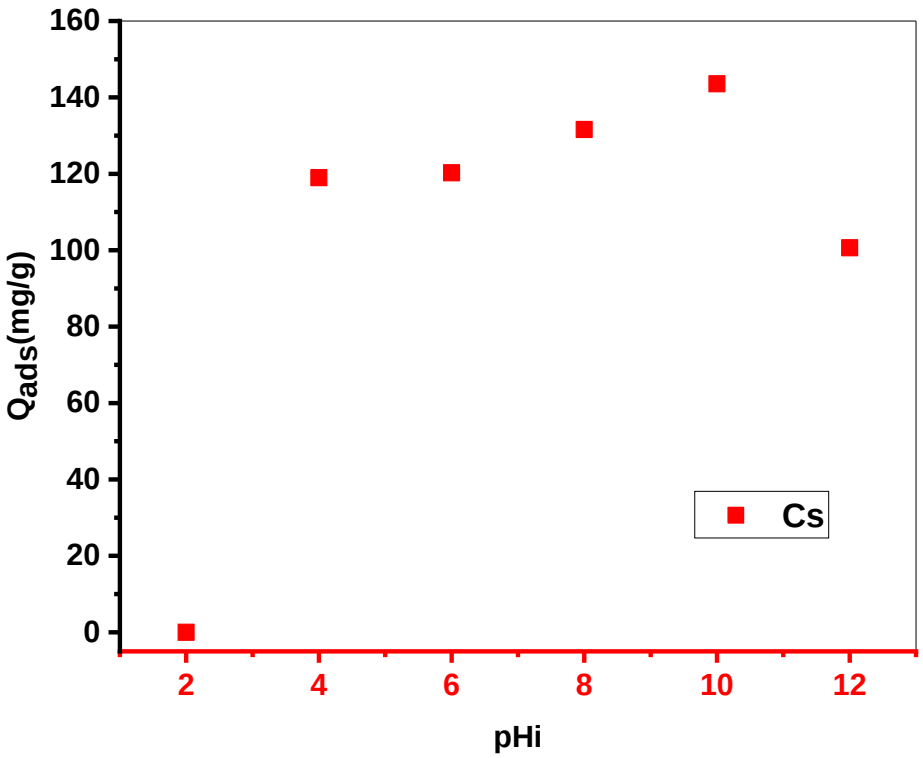

Figure 3. The effect of initial pH on adsorption of MB with Cs (m = 10 mg, V = 10 mL, pH = 10, stirring = 250 ppm, Tambient).

3.3 Influence of Humic Acid (HA) and NaCl on Adsorption of MB on Cs

In the presence of NaCl, the quantity adsorbed (Q_e) decreased from a maximum value of 203 mg•g^{-1} to 180 mg•g^{-1}. As shown in Figure 4, the competitiveness of adhesion onto adsorbent between MB cationic molecules and the Na^+ cations of the inorganic salt was most likely the reason for this decrease.

In the presence of HA, there was a slight rise in the amount of adsorbed MB (Figure 4), and the amount adsorbed (Qe) increased from 203 mg•g^{-1} to 210 mg•g^{-1}. It can be said that there is no effect of HA in the MB adsorption process. There are two possible explanations for this result: the first is that HA interacts directly with the MB [50], and the second is that HA can create other active sites on the adsorbent Cs where the MB molecules can be captured.

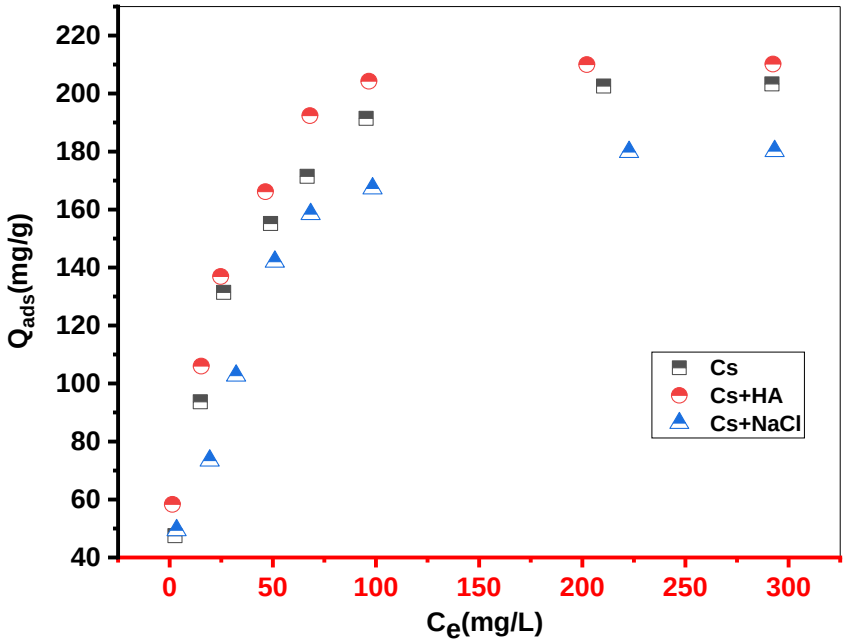

Figure 4. Influence of NaCl and humic acid (HA) on the discoloration of MB solutions by Cs (m = 10 mg, V = 10 mL, stirring = 250 ppm, pH = 10, Tambient).

3.4 Kinetics Analysis

From the graph presented in Figure 5, the studied material showed three phases of adsorption kinetics:

The first phase displays a higher removal rate of MB due to vacant adsorbent sites and the large concentration gradient at the beginning of the process. A slower adsorption rate when the solute is adsorbed owing to decreased adsorption sites and gradient concentration in the second phase. The third phase is the saturation or equilibrium step, where there are no more accessible adsorption sites; the beginning of this step is indicated by the equilibrium time, and it was equal to 120 min in our case.

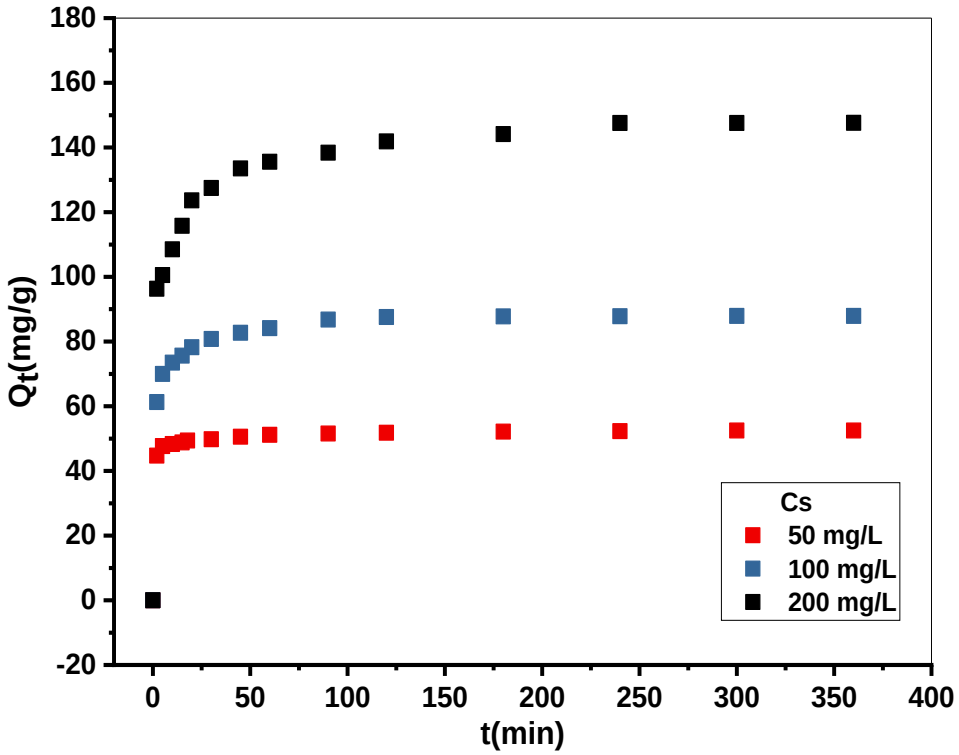

Figure 5. Representative curve of experimental adsorption kinetics of MB on Cs material (m = 10 mg, V = 10 mL, stirring = 250 ppm, pH = 10, Tambient).

There was also an increase in the quantity adsorbed when the initial concentration of MB increased due to the driving forces, which increased with the initial concentration [51,52].

The Boyds equation was applied to determine the actual control phase. If the plots describe linear simulation for the Boyd model line crossing the origin, then the control phase is the intra-particle diffusion step. If not, the adsorption process is controlled by the film diffusion step [49]. From Figure 6, the $B_t$vs t curves were not linear and did not cross the origin, suggesting that the film diffusion step controlled the adsorption process [53,54].

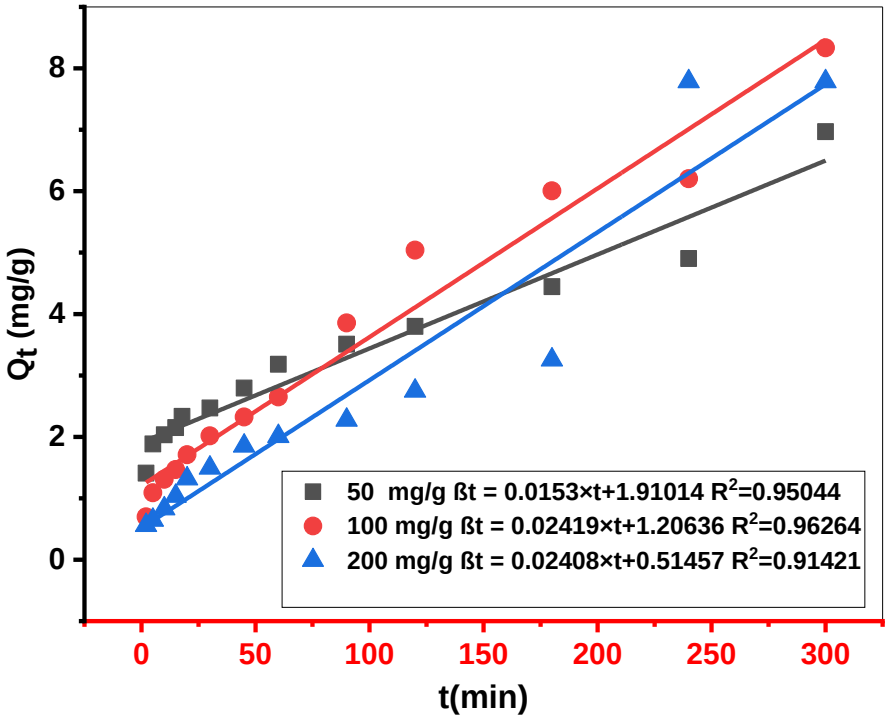

Figure 6. The curves representative of linear simulation of MB adsorption on Cs using the Boyd model.

Figure 7 illustrates the results of the nonlinear regression of the PFO, PSO, and PNO equations, and the corresponding parameters are collected in Table 4. At the initial stages and for the three concentrations (50, 100, and 150 mg•L^{-1}), the PFO-derived curves are above the experimental adsorption data (less than 60 min). On the contrary, they are lower than the experimental data for the final stage of adsorption. The same observation holds for the PSO-derived curves with a slight difference in the initial stage time (less than 100 min). As a result, there exists an order n other than 1 and 2 that provides the lowest deviation throughout the adsorption process [32], as shown by the PNO-derived curves that have the least deviation from the experimental data and confirmed through the values of the correlation coefficients R^2 and the average percentage errors APE (%) given in Table 4. The pseudo-nth-order kinetic model accurately fitted the experimental data and outperformed the pseudo-first and pseudo-second-order equations. The order of adsorption reaction n was found to be between 4.97, 4.365, and 8.04 for 50, 100, and 150 mg•L^{-1} concentrations, respectively. All these results are clearly proved with the two Figures 8 and 9, digital photographic images of a series of adsorption of MB with Cs material and UV-Visible spectrophotometer adsorption of MB for each time interval.

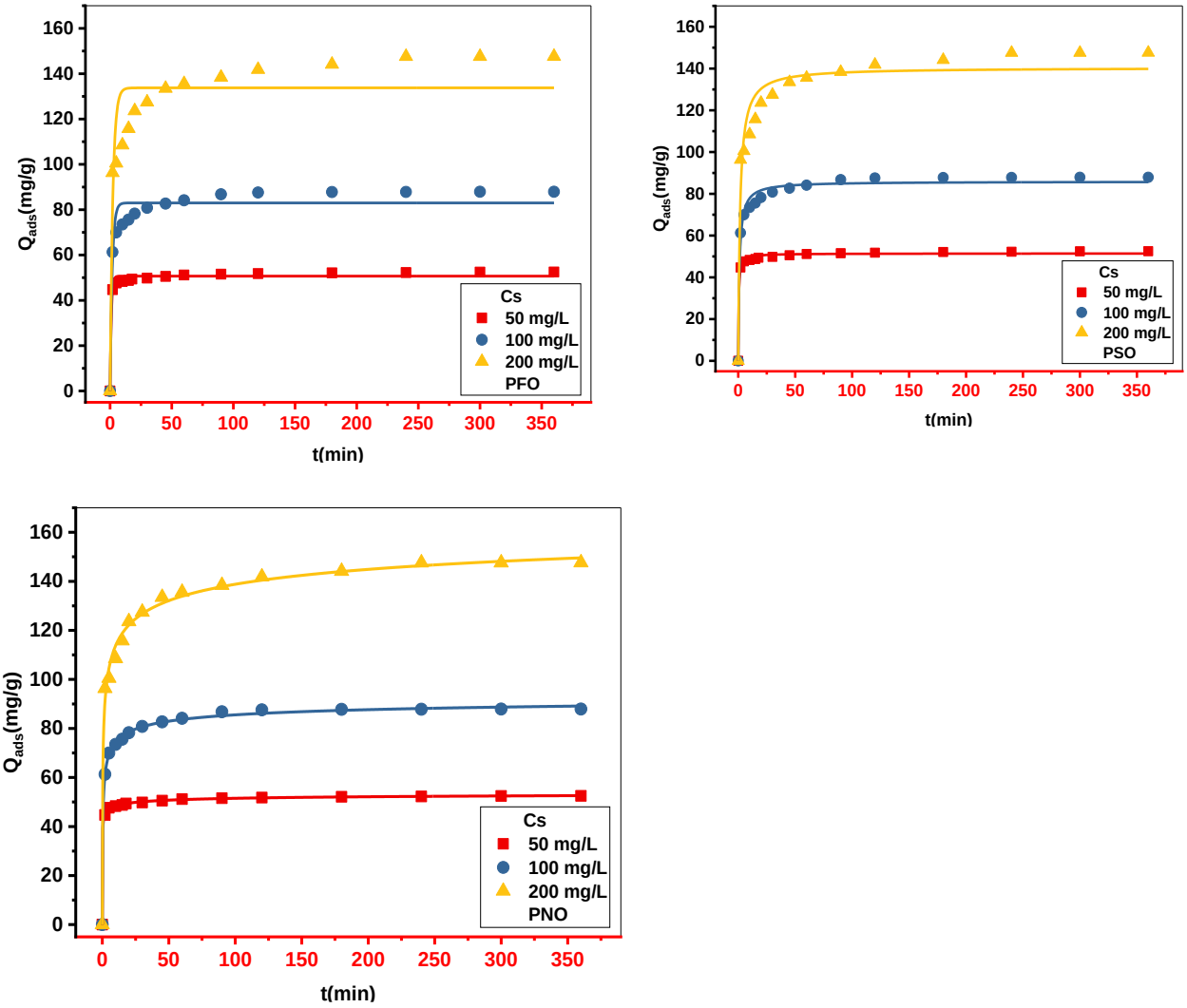

Figure 7. The curves representative of nonlinear simulation of the pseudo-first-order (PFO), pseudo-second-order (PSO), and pseudo-nth-order kinetic models (PNO).

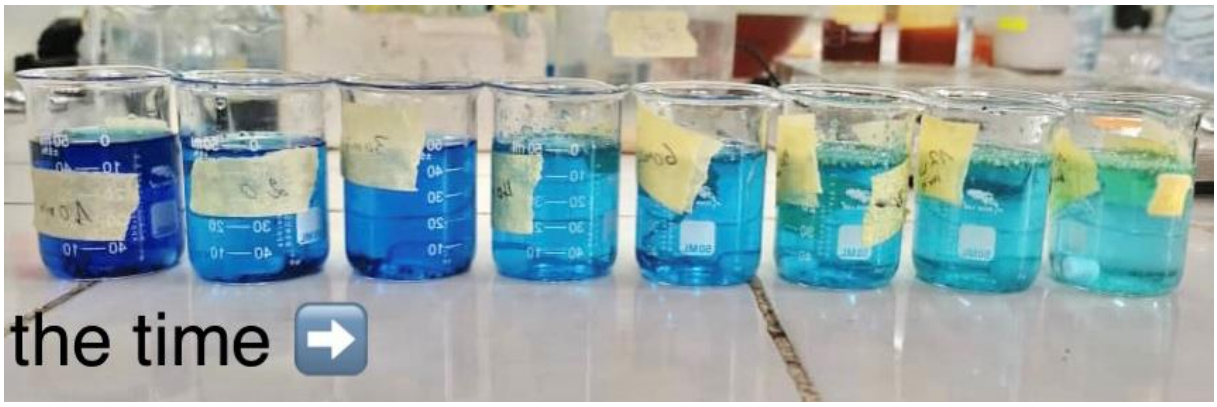

Figure 8. Sequence of digital photographs proving MB adsorption with Cs material.

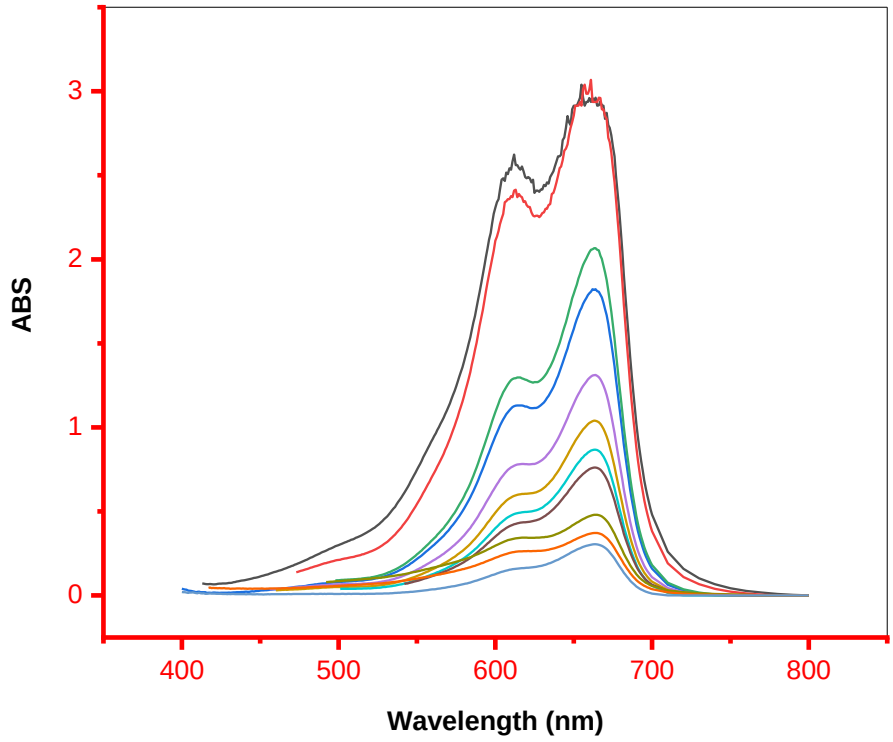

Figure 9. UV-Visible spectrophotometer sorption of MB for each time interval.

Table 4. Parameters of Kinetic for nonlinear regression of PFO, PSO, and PNO models for the adsorption of MB on Cs.

Models	Parameters	50 mg•L^{-1}	100 mg•L^{-1}	150 mg•L^{-1}
PFO	Qexp	52.5	87.92	147.61
	Qe	50.68	82.98	133.75
	K_1	1.044	0.58	0.461
	R^2	0.985	0.939	0.865
	APE (%)	2.664	5.973	9.474
PSO	Qe	51.43	85.88	140.42
	$K_2 \times 10^{+4}$	0.055	0.011	0.0046
	R^2	0.994	0.982	0.947
	APE (%)	1.657	5.714	5.795
PNO	Qe	55.46	96.89	203.56
	k_n	1.073×10^{-5}	8.38×10^{-7}	2.49×10^{-16}
	no	4.97	4.365	8.04
	R^2	0.999	0.998	0.994
	APE (%)	0.328	0.889	1.851

3.5 Isotherms Analysis

Figure 10 illustrates the MB dye adsorption isotherm on Cs. The adsorption capacity increased with the initial dye concentration until equilibrium was reached. The adsorption ability of MB on Cs decreased as the temperature increased (the adsorption amounts at temperatures of 298, 303, and 313 K were 203.33, 192.188, and 179.38 mg•g^{-1}, respectively). These results suggest an exothermic MB-Cs adsorption mechanism [51,55,56].

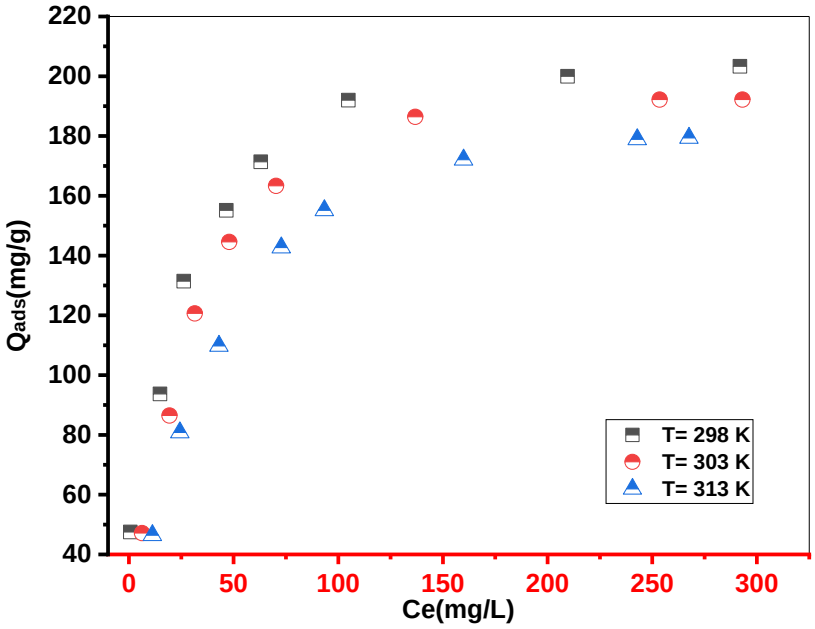

Figure 10. Experimental isotherms of MB adsorption onto Cs. (m = 10 mg, V = 10 mL, stirring = 250 ppm, pH=10, $T_{ambient}$).

3.5.1 Classical Models

Figure 11 depicts the nonlinear regression findings of the five models Langmuir, Freundlich, Dubinin–Radushkevich (D–R), Redlich–Peterson (R–P), and Sips, and Table 5 provides the fitting parameters as well as the average percentage of errors APE (%) for each. By comparing the R^2 and APE% values, the Redlich–Peterson isotherm model gave the best result of adjusting the MB adsorption on the Cs adsorbent. Because of the three parameters involved in the R–P model, Several studies [51,55] have shown its relevance in describing the adsorption process. It can be noted that the Freundlich and Langmuir isotherms can be derived from the R–P isotherm based on the b_R value. It becomes the Langmuir isotherm when $b_R = 1$ and the Freundlich isotherm for $b_R = 0$. The b_R values were very close to unity for the three temperatures tested, indicating that the R–P model was close to the Langmuir model in our adsorption case.

The E values obtained from the Dubinin–Radushkevich (D–R) model were <8.0 $kJ \cdot mol^{-1}$, confirming the physical nature of the MB adsorption onto the Cs material at all examined temperatures.

The five traditional models considered are insufficient to construct the MB uptake dynamic, and so theoretical treatment via advanced models appears to be a required tool to support the setup/management of the MB–Cs interaction.

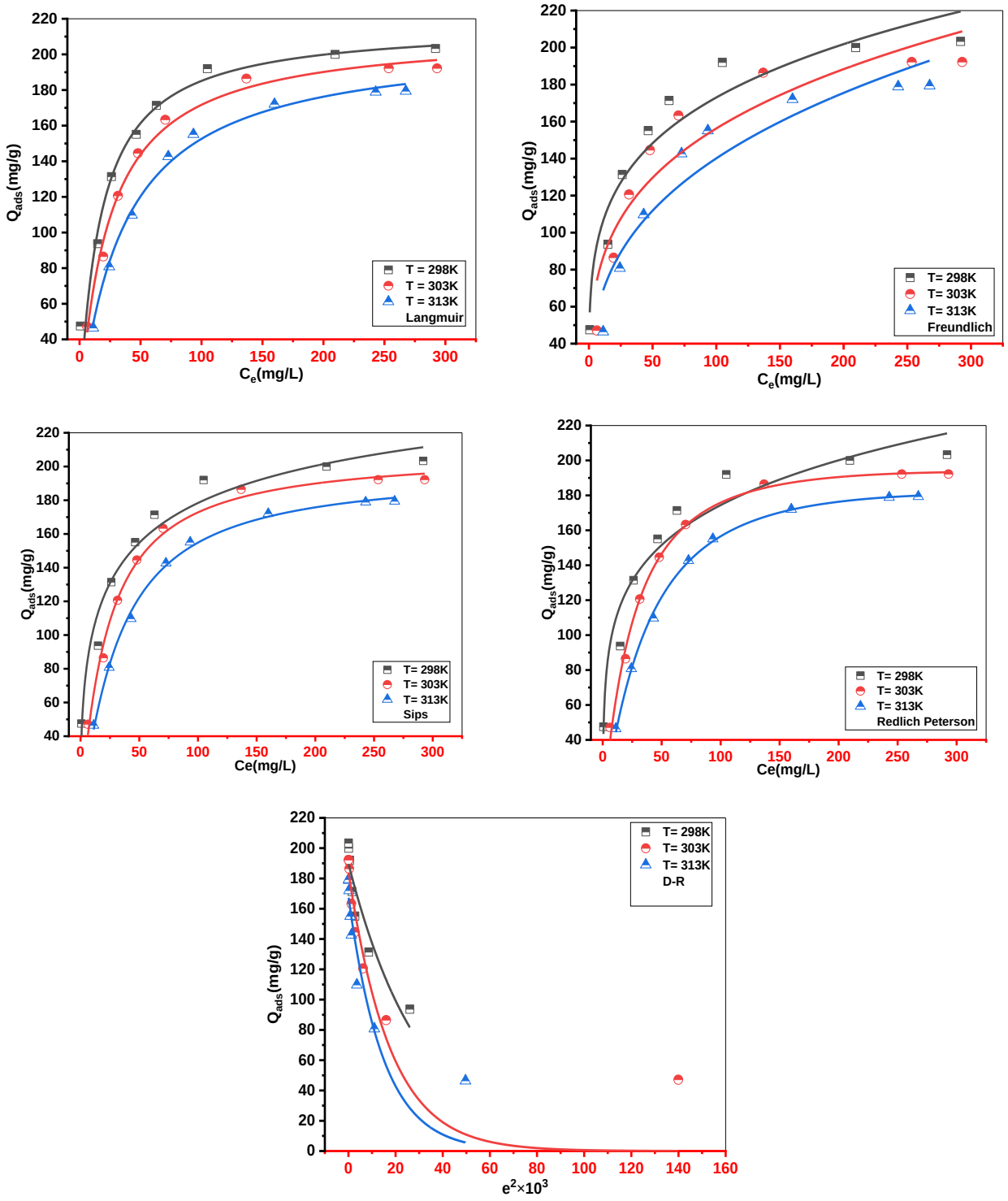

Figure 11. Result of fitting isotherms data of MB adsorption onto Cs with Langmuir, Freundlich, D− –R, Redlich–Peterson (R–P), and Sips.

Table 5. Langmuir, Freundlich, D–R, Redlich-Peterson (R–P), and Sips parameters for the adsorption of MB onto Cs.

Models	Parameters	298 K	303 K	313 K
Langmuir	Q_e (mg•g^{-1})	203.333	192.187	179.380
	Q_m (mg•g^{-1})	217.075	213.012	208.577
	K_L (L•mg^{-1})	0.0579	0.04155	0.0272
	R^2	0.911	0.990	0.994
	APE (%)	12.143	3.506	2.707
Freundlich	nf	4.499	3.7136	3.078
	K_F (mg•g^{-1}) (L/mg)$^{1/n}$	62.16	45.219	31.38
	R^2	0.926	0.866	0.899
	APE (%)	9.569	15.586	12.618
Sips	Q_m (mg•g^{-1})	294.691	208.441	197.356
	K_S (L•mg^{-1})	0.0248	0.04314	0.031
	ms	0.4714	1.0793	1.1606
	R^2	0.949	0.989	0.996
	APE (%)	7.645	3.908	1.994
Redlish–Peterson	k_R(L•g^{-1})	181.46	7.294	4.637
	β_R	2.496	0.022	0.011
	R^2	0.926	0.993	0.999
	APE (%)	7.544	3.187	1.224
D–R	Q_m (mg•g^{-1})	189.969	184.75	168.348
	E (kJ•mol^{-1})	3.927	2.967	2.7048
	R^2	0.869	0.832	0.819
	APE (%)	10.614	18.477	17.246

3.5.2 Advanced Statistical Physics Models

The simulation of the experimental isotherm data was performed using the software ORIGIN (version 2018) (Figure 12). The choice of the most relevant model(s) for understanding the MB adsorption process onto the Cs material depended on the APE (%) values and correlation coefficient R^2 given in Table 6.

The best advanced statistical physics model for fitting the MB adsorption onto the Cs adsorbent was found to be the AM2 (double-energy single-layer model), which was therefore considered thereafter.

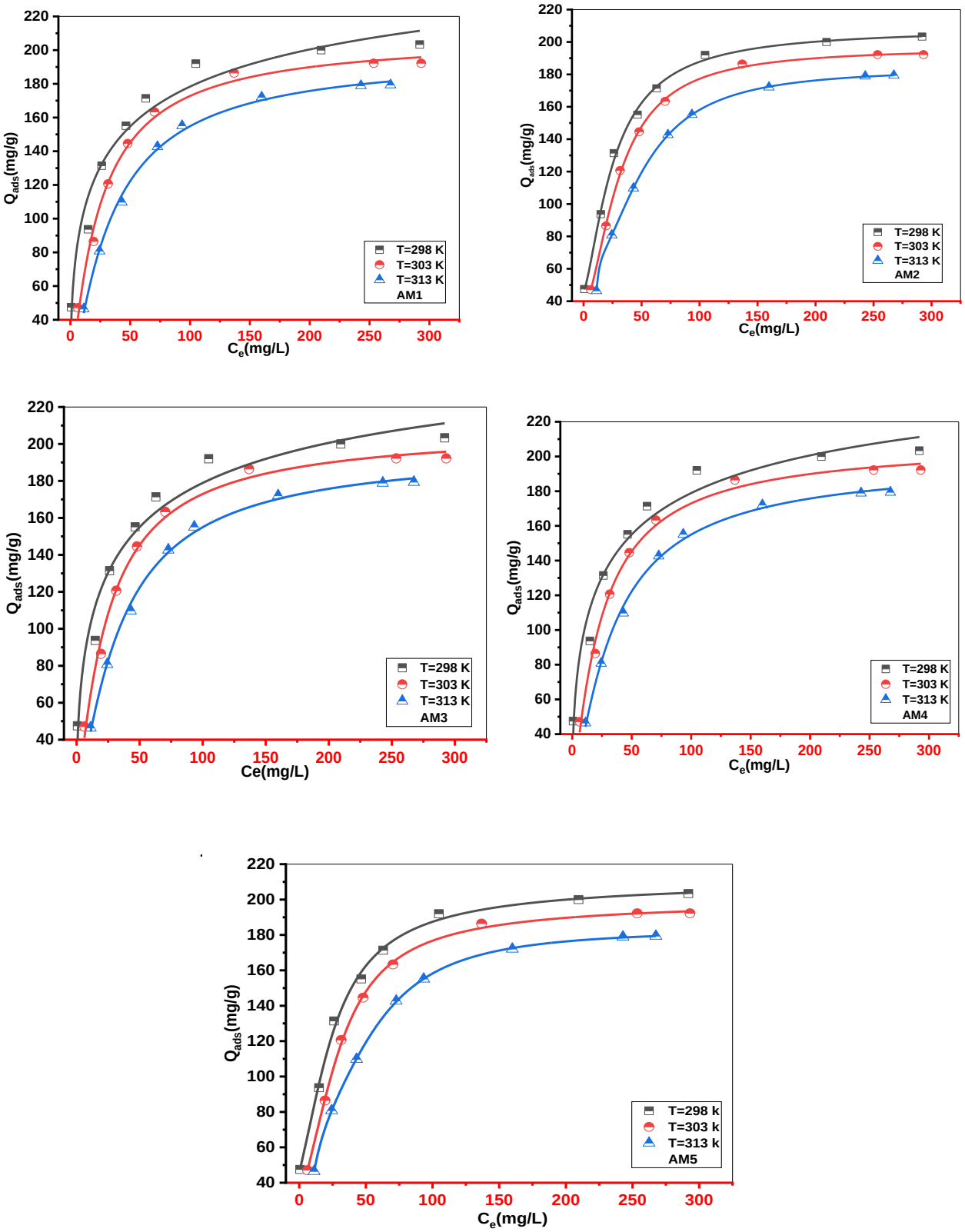

Figure 12. Result of fitting isotherms data of MB adsorption onto Cs with AM1, AM2, AM3, AM4, and AM5 models.

Table 6. Values of the estimated parameters of models AM1, AM2, AM3, AM4, and AM5 of the MB-Cs adsorption process.

Models	Parameters	T = 298 K	T = 303 K	T = 313 K
AM1	n	0.471	1.079	1.161
	N_m	624.728	193.109	170.044
	$C_{1/2}$	40.359	23.182	32.839
	R^2	0.949	0.989	0.996
	APE (%)	7.646	3.908	1.995
AM2	n_1	0.129	0.610	6.833
	n_2	1.444	1.676	2.036
	N_{m1}	360.902	59.874	8.5241
	N_{m2}	112.073	95.507	61.579
	C_1	2.419×10^{-35}	9.807×10^{-13}	9.851
	C_2	26.414	30.566	51.191
	R^2	0.99218	0.99781	0.99994
	APE (%)	1.354960	0.766527	0.096792
AM3	n	0.374	0.811	0.867
	N_m	382.960	130.008	115.298
	$C_{1/2}$	35.781	23.896	33.782
	R^2	0.95233	0.99038	0.99675
	APE (%)	7.527145	3.706916	1.792957
AM4	n	0.363	0.76608	0.81213
	N_m	394.458	137.7444	123.15063
	C_1	45.7492	30.3144	43.7831
	C_2	35.848	23.911	33.791
	R^2	0.94044	0.98802	0.99596
	APE (%)	7.519079	3.701431	1.805403
AM5	n	0.717	0.779	1.986
	N_2	3.842	4.176	1.334
	C_1	1.229×10^{-11}	0.835	9.879
	C_2	27.059	31.696	58.628
	Nm	61,556	49,993	39,537
	R^2	0.99421	0.99812	0.9999
	APE (%)	1.405965	0.8529428	0.17386

3.5.3 Steric and Energetic Parameters

The physicochemical parameters governing the interaction between MB ions and the Cs material were calculated and intensively interpreted according to the AM2 model in the following sections.

3.5.3.1. n. N_m. and Q_{ads} Steric Parameter Interpretation

The n value can be used to determine the geometric position (vertical or horizontal) and mechanism (multi–ionic or multimolecular) of the trapped MB ions on the Cs adsorbent surface. When n is less than 1, the adsorbed molecule adopts a parallel (horizontal) orientation with a multi–docking mode. When n is more than 1, the adsorbed molecules are anchored in a non-parallel (vertical) orientation with a multimolecular mode [21,23,39]. Figure 13a depicts n_1 and n_2 as the temperature goes up from 298 to 313 K, and the obtained values of these parameters are shown in Table 6. The n_1 was found to be 0.129, 0.610, and 6.833, while the n_2 values were 1.444, 1.675, and 2.036 at 298, 303, and 313 K, respectively.

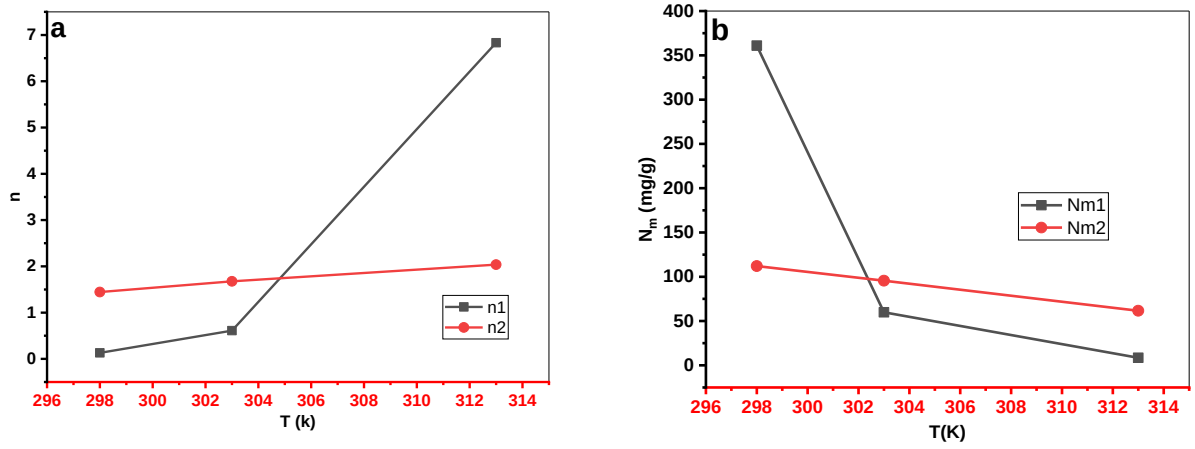

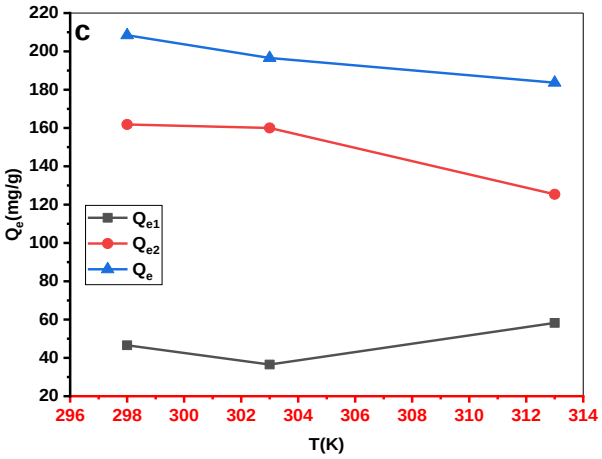

Figure 13. The evolution of (**a**) n, (**b**) Nm, and (**c**) Qe as a function of temperature for MB-Cs adsorption.

At 298 and 303 K, the MB–Cs interaction revealed a horizontal orientation and multi–docking mechanism for the n_1. The adsorbed MB behavior was changed to vertical positioning and multimolecular mode by increasing the solution temperature to 313 K. The second parameter, n_2, displayed a vertical setting and multimolecular mode for the three temperatures. When the temperature increases, the two parameters n_1 and n_2 increase [54,57], as illustrated in Figure 13a. This result demonstrated that the chemical behavior of the MB molecules in solution was the same and that the two parameters, n_1 and n_2, were aggregated but to different degrees (lower degree for the second parameter, n_2). This behavior could be related to the enhanced thermal agitation, which may have resulted in thermal collisions between the MB molecules, increasing the number of captured MB molecules per site.

Figure 13b shows the density (N_m) of the receptor site as a function of temperature. The density of the Cs receptor sites N_{m1} and N_{m2} was reduced as the temperature increased. This evolution is connected to an increase in the number of trapped molecules n_1 and n_2 per site as the temperature increases (the tendency to aggregation) [38,58].

The total saturation adsorption amount (Q_e) is affected by the number of captured molecules per site and the density of receptor sites ($Q_{ei} = N_{mi} \times n_i$), and the total Q_e is the sum of Q_{ei}, this value measures the ability of the Cs surface ability to retain the MB molecules.

The total amount of saturation adsorption (Qe) was plotted as a function of temperature in Figure 13c, showing that this parameter was significantly affected by the temperature alteration.

Indeed, when the temperature rose, the amount adsorbed decreased due to exothermic adsorption, as is usual in classical adsorption phenomena.

3.5.3.2. Energetic (E) Parameter Interpretation

The energetic interaction (E) between the MB ions and the Cs surface was calculated using the following equations [59]:

$$C_1 = C_{SM} e^{\frac{-E_1}{RT}} \quad (20)$$

$$C_2 = C_{SM} e^{\frac{-E_2}{RT}} \quad (21)$$

where C_1 and C_2 are the half-saturation concentrations, and C_{SM} is the adsorbate (MB) solubility.

This solubility was considered to remain constant at all adsorption temperatures for simplicity [52]. The solubility was assumed to be constant at all adsorption temperatures.

According to Table 6, the C_1 concentrations at the two temperatures, 298 and 303 K, were found to be relatively low, resulting in inconsistent E_1 values. In this instance, we chose to interpret the energy according to the last temperature (313 K) [52].

For 313 K, the calculated energies were −2.345 kJ•mol^{-1} for the first type of energy (E_1) and −6.633 kJ•mol^{-1}for the second type of energy (E_2). It was discovered that the first energy was lower than the second, demonstrating that the free active sites of the first type were the most prevalent. Moreover, the calculated energy values were low and <40 kJ/mol [47]. As a result, MB adsorption on the Cs adsorbent corresponds to a physical process with the expected existence of a van der Waals interaction or hydrogen bonding.

3.5.4 Thermodynamicynamic Function Study

To conduct a thermodynamic investigation of the MB adsorption mechanism on the Cs materials, the advanced double-energy single-layer model (AM2) could be used to calculate thermodynamic parameters, including entropy, Gibbs free enthalpy, and internal energy [20,21,60].

3.5.4.1 Entropy

The adsorption process can provide useful information on the order and/or disorder of the adsorbed ions (MB) on the Cs-material through the examination of configurational entropy (i.e., the degree of regularity of the adsorption system). The entropy variation of the second, advanced model as a function of the adsorbate equilibrium concentration is given in Table 7 by Equation (22) [61,62].

The theoretical entropy calculation is displayed in Figure 14a as a function of the MB concentration at various temperatures. As can be shown, entropy behaves very differently according to the MB concentration. Before reaching half-saturation ($C_{1/2} > C$), the entropy increased, indicating a disordered state until it reached a maximum value (Figure 14a). At low MB concentrations, this random state was indicated by the existence of more active sites on the Cs composite that are suited for MB ion adsorption. On the other hand, the entropy increased with increasing MB concentration ($C_{1/2} < C$), indicating an ordered state [63]. The rise in this order state was associated with a decrease in the number of accessible active sites on the Cs material adsorbent [38,64].

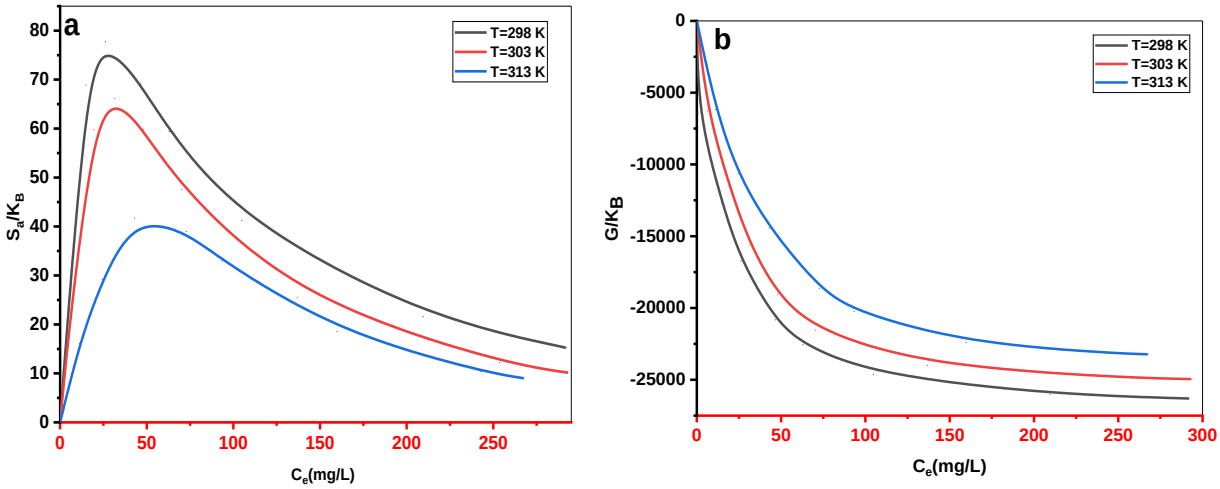

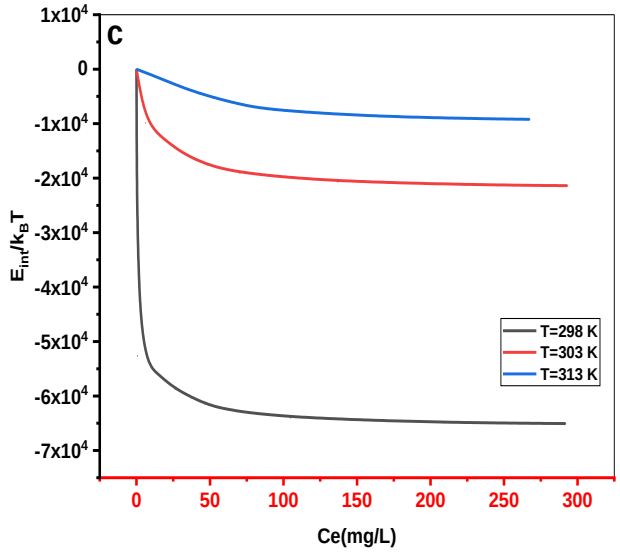

Figure 14. (**a**) Entropy, (**b**) free enthalpy, and (**c**) internal energy evolution as a function of concentration for MB absorption by Cs adsorbent at various temperatures.

3.5.4.2 Free Gibbs Enthalpy

The free Gibbs enthalpy was determined using Equation (23), stated in Table 7, based on the AM2.

The Gibbs free enthalpy was plotted as a function of the adsorbate concentration at various temperatures for the Cs adsorbent (Figure 14b). As shown in Figure 14b, the Gibbs free energy was negative, showing the spontaneous nature of the adsorption process. Additionally, the feasibility of the adsorption process was reduced as the temperature increased due to the decrease in the free enthalpy [64,65].

Table 7. Entropy, free enthalpy, and internal energy function according to the AM2 model.

Function	Num	Equation
Entropy	(22)	$\frac{S_a}{K_B} = N_1\left[\ln\left(1+\left(\frac{C_e}{C_1}\right)^{n_{1m}}\right)+\frac{n_1\ln\left(\frac{C_1}{C_e}\right)}{1+\left(\frac{C_1}{C_e}\right)^{n_{1m}}}\right]+N_2\left[\ln\left(1+\left(\frac{C_e}{C_2}\right)^{n_2}\right)+\frac{n_2\ln\left(\frac{C_2}{C_e}\right)}{1+\left(\frac{C_2}{C_e}\right)^{n_2}}\right]$
Gibbs free enthalpy	(23)	$G = K_B T\ln\left(\frac{C_e}{Z_v}\right)\left[\frac{Q_{sat1}}{1+(\frac{C_1}{C_e})^{n_{1m}}}+\frac{Q_{sat2}}{1+(\frac{C_2}{C_e})^{n_{2m}}}\right]$ With: $Z_v = \frac{Z_{gtr}}{V} = \left(\frac{2\pi m K_B T}{h^2}\right)^{3/2}$
Internal energy	(24)	$E_{int} = K_B T\left[N_{1s}\frac{\ln(\frac{C_e}{Z_v})+n_{1m}\ln(\frac{C_1}{C_e})}{1+(\frac{C_1}{C_e})^{n_{1m}}}+N_{2s}\frac{\ln(\frac{C_e}{Z_v})+n_{2m}\ln(\frac{C_2}{C_e})}{1+(\frac{C_2}{C_e})^{n_{2m}}}\right]$

3.5.4.3 Internal Energy

Internal energy can be considered to evaluate all forms of energy provided to the MB adsorption system. Equation (24) in Table 7 gives the general form of the internal energy [66]. The estimates for this thermodynamic parameter are shown in Figure 14c. The internal energy values were all negative, showing that the MB adsorption systems happened spontaneously [37].

3.6 Comparison of Adsorption Capacity with Literature

To prove the effectiveness of *Cynara Scolymus* powder as a low-cost biosorbent for MB removal, it is essential to compare its adsorption capacity with that of other low-cost adsorbents. In this study, we compared the adsorption capacity of Cs with other adsorbents reported by various researchers. Numerous studies have been conducted to investigate MB removal from water using different types of adsorbents modified with various chemical agents. The Qmax of these adsorbents is listed in Table 8. The data presented in Table 8 demonstrate that certain materials, such as Acorus calamus (PACK) and Ziziphus jujuba (BZJS), exhibit higher adsorption capacities than *Cynara Scolymus* (Cs) powder. It is important to note that PACK is a modified material treated with H2SO4 and subsequently with KMnO4, while BZJS is a material modified with H3PO4 and encapsulated with alginate. These results highlight the relatively low production cost of Cs compared to the aforementioned materials. Furthermore, it is worth noting that the direct powder form of Cs has a significantly higher maximum adsorption capacity compared to *Cynara*

Scolymus activated carbon (ACE@CSNB), as indicated in the table. This finding emphasizes the effectiveness and cost-efficiency of Cs as a support material for methylene blue disposal.

Overall, the comparison of Cs with other low-cost adsorbents demonstrates its potential as a promising biosorbent for efficient MB removal.

Table 8. Comparison of maximum methylene blue adsorption on some literature adsorbents.

Adsorbent Material	Qmax (mg/g)	Reference
PACK	1500	[15]
BZJS1	737.13	[67]
Pectin from orange industry residues in alginate beads form	398.40	[68]
Cynara Scolymus Powder (Cs)	203.333	This work
Carboxymethyl cellulose/carboxylated graphene oxide composite microbeads	183.23	[69]
Ziziphus jujuba (PZJS)	160.85	[67]
ACE@CSNB	15	[70]

4 Conclusions

The natural powder of *Cynara Scolymus* (Cs) was used as an adsorbent in this investigation to remove methylene blue ions (MB). The ideal pH for removing MB color was determined to be 10, which resulted in the greatest amount of adsorption.

The Cs material had a maximum experimental adsorption capacity of 203.333, 192.187, and 179.380 mg•g^{-1} at 298, 303, and 313 K, respectively. Langmuir, Freundlich, Redlich-Peterson (R–P), Sips, and Dubinin–Radushkevich (D–R) were used as classical models to describe experimental results. The Redlich–Peterson (R–P) equation provided the best fit for the adsorption data without elucidating the process of MB absorption. Five statistical physics models (AM1, AM2, AM3, AM4, and AM5) were considered to better explain the interaction between the MB ions and the Cs active sites. The steric, energetic, and thermodynamic parameters resulting from the double-energy single-layer model that gave the appropriate fit of the MB–Cs interaction were thoroughly interpreted. The MB adsorption on the Cs composite was mediated by multi–docking

and multimolecular modes. The receptor's site density (N_m) decreased with increasing solution temperature for both N_{m1} and N_{m2}. Adsorption energies were estimated to be negative and <40 kJ•mol^{-1}, indicating exothermic and physical processes. As the temperature dropped, Q_e increased, confirming the exothermic nature of the uptake processes. Entropy, Gibbs free enthalpy, and internal energy indicated that MB adsorption onto the novel Cs adsorbent was possible and spontaneous.

5 References

1. Bouguettoucha, A.; Chebli, D.; Mekhalef, T.; Noui, A.; Amrane, A. The use of a forest waste biomass, cone of *Pinus brutia* for the removal of an anionic azo dye Congo red from aqueous medium. *Desalin. Water Treat.* **2015**, *55*, 1956–1965.
2. Bouguettoucha, A.; Reffas, A.; Chebli, D.; Mekhalif, T.; Amrane, A. Novel activated carbon prepared from an agricultural waste, *Stipa tenacissima*, based on ZnCl2 activation—Characterization and application to the removal of methylene blue. *Desalin. Water Treat.* **2016**, *57*, 24056–24069.
3. Tsai, W.T.; Chang, Y.M.; Lai, C.W.; Lo, C.C. Adsorption of ethyl violet dye in aqueous solution by regenerated spent bleaching earth. *J. Colloid Interface Sci.* **2005**, *289*, 333–338.
4. Bhattacharyya, K.G.; Sharma, A. Kinetics and thermodynamics of methylene blue adsorption on neem (*Azadirachta indica*) leaf powder. *Dye Pigment.* **2005**, *65*, 51–59.
5. Srinivasan, A.; Viraraghavan, T. Decolorization of dye wastewaters by biosorbents: A review. *J. Environ. Manage.* **2010**, *91*, 1915–1929.
6. Yao, Z.; Wang, L.; Qi, J. Biosorption of methylene blue from aqueous solution using a bioenergy forest waste: *Xanthoceras sorbifolia* seed coat. *CLEAN Soil Air Water* **2009**, *37*, 642–648.
7. Guediri, A.; Bouguettoucha, A.; Chebli, D.; Chafai, N.; Amrane, A. Molecular dynamic simulation and DFT computational studies on the adsorption performances of methylene blue in aqueous solutions by orange peel-modified phosphoric acid. *J. Mol. Struct.* **2020**, *1202*, 127290.
8. Crini, G. Non-conventional low-cost adsorbents for dye removal: A review. *Bioresour. Technol.* **2006**, *97*, 1061–1085.

9. Chebli, D.; Bouguettoucha, A.; Mekhalef, T.; Nacef, S.; Amrane, A. Valorization of an agricultural waste, *Stipa tenassicima* fibers, by biosorption of an anionic azo dye, Congo red. *Desalin. Water Treat.* **2015**, *54*, 245–254.

10. Cardoso, N.F.; Lima, E.C.; Pinto, I.S.; Amavisca, C.V.; Royer, B.; Pinto, R.B.; Alencar, W.S.; Pereira, S.F.P. Application of cupuassu shell as biosorbent for the removal of textile dyes from aqueous solution. *J. Environ. Manage.* **2011**, *92*, 1237–1247.

11. Naiya, T.K.; Chowdhury, P.; Bhattacharya, A.K.; Das, S.K. Saw dust and neem bark as low-cost natural biosorbent for adsorptive removal of Zn (II) and Cd (II) ions from aqueous solutions. *Chem. Eng. J.* **2009**, *148*, 68–79.

12. Ben-Ali, S.; Jaouali, I.; Souissi-Najar, S.; Ouederni, A. Characterization and adsorption capacity of raw pomegranate peel biosorbent for copper removal. *J. Clean. Prod.* **2017**, *142*, 3809–3821.

13. Southichak, B.; Nakano, K.; Nomura, M.; Chiba, N.; Nishimura, O. Phragmites australis: A novel biosorbent for the removal of heavy metals from aqueous solution. *Water Res.* **2006**, *40*, 2295–2302.

14. Aravindhan, R.; Rao, J.R.; Nair, B.U. Application of a chemically modified green macro alga as a biosorbent for phenol removal. *J. Environ. Manage.* **2009**, *90*, 1877–1883.

15. Djama, C.; Chebli, D.; Bouguettoucha, A.; Doudou, I.; Amrane, A. Statistical physics modelling of azo dyes biosorption onto modified powder of *Acorus calamus* in batch reactor. *Biomass Convers. Biorefinery*. **2021**, *13*, 1–16.

16. Pandino, G.; Lombardo, S.; Monaco, A.L.; Mauromicale, G. Choice of time of harvest influences the polyphenol profile of globe artichoke. *J. Funct. Foods* **2013**, *5*, 1822–1828.

17. Salem, M.B.; Affes, H.; Ksouda, K.; Dhouibi, R.; Sahnoun, Z.; Hammami, S.; Zeghal, K.M. Pharmacological studies of artichoke leaf extract and their health benefits. *Plant Foods Hum. Nutr*. **2015**, *70*, 441–453.

18. Saavedra, M.I.; Miñarro, M.D.; Angosto, J.M.; Fernandez-Lopez, J.A. Reuse potential of residues of artichoke (*Cynara scolymus* L.) from industrial canning processing as sorbent of heavy metals in multimetallic effluents. *Ind. Crops Prod.* **2019**, *141*, 111751.

19. Mahmoud, M.E.; Abou-Ali, S.A.A.; Elweshahy, S.M.T. Efficient and ultrafast removal of Cd (II) and Sm (III) from water by leaves of *Cynara scolymus* derived biochar. *Mater. Res. Bull.* **2021**, *141*, 111334.

20. Mobarak, M.; Mohamed, E.; Selim, A.; Sellaoui, L.; Lamine, A.B.; Erto, A.; Seliem, M.K. Surfactant–modified serpentine for fluoride and Cr (VI) adsorption in single and binary systems: Experimental studies and theoretical modeling. *Chem. Eng. J.* **2019**, *369*, 333–343.

21. Mobarak, M.; Mohamed, E.A.; Selim, A.Q.; Mohamed, F.M.; Sellaoui, L.; Bonilla-Petriciolet, A.; Seliem, M.K. Statistical physics modeling and interpretation of methyl orange adsorption on high–order mesoporous composite of MCM–48 silica with treated rice husk. *J. Mol. Liq.* **2019**, *285*, 678–687.

22. Sellaoui, L.; Bouzid, M.; Duclaux, L.; Reinert, L.; Knani, S.; Lamine, A.B. Binary adsorption isotherms of two ionic liquids and ibuprofen on an activated carbon cloth: Simulation and interpretations using statistical and COSMO-RS models. *RSC Adv.* **2016**, *6*, 67701–67714.

23. Li, Z.; Sellaoui, L.; Dotto, G.L.; Lamine, A.B.; Bonilla-Petriciolet, A.; Hanafy, H.; Belmabrouk, H.; Netto, M.S.; Erto, A. Interpretation of the adsorption mechanism of Reactive Black 5 and Ponceau 4R dyes on chitosan/polyamide nanofibers via advanced statistical physics model. *J. Mol. Liq.* **2019**, *285*, 165–170.

24. Sellaoui, L.; Soetaredjo, F.E.; Ismadji, S.; Lima, É.C.; Dotto, G.L.; Lamine, A.B.; Erto, A. New insights into single-compound and binary adsorption of copper and lead ions on a treated sea mango shell: Experimental and theoretical studies. *Phys. Chem. Chem. Phys.* **2017**, *19*, 25927–25937.

25. Lamine, A.B.; Bouazra, Y. Application of statistical thermodynamics to the olfaction mechanism. *Chem. Senses.* **1997**, *22*, 67–75.

26. Yahia, M.B.; Tounsi, M.; Aouaini, F.; Knani, S.; Yahia, M.B.; Lamine, A.B. A statistical physics study of the interaction of [7]-helicene with alkali cations (K+ and Cs+): New insights on microscopic adsorption behavior. *RSC Adv.* **2017**, *7*, 44712–44723.

27. Xue, H.; Gao, X.; Seliem, M.K.; Mobarak, M.; Dong, R.; Wang, X.; Fu, K.; Li, Q.; Li, Z. Efficient adsorption of anionic azo dyes on porous heterostructured MXene/biomass activated carbon composites: Experiments, characterization, and theoretical analysis via advanced statistical physics models. *Chem. Eng. J.* **2023**, *451*, 138735.

28. Sellaoui, L.; Gomez-Aviles, A.; Dhaouadi, F.; Bedia, J.; Bonilla-Petriciolet, A.; Rtimi, S.; Belver, C. Adsorption of emerging pollutants on lignin-based activated carbon: Analysis of adsorption mechanism via characterization, kinetics and equilibrium studies. *Chem. Eng. J.* **2023**, *452*, 139399.

29. Wang, X.; Xu, Q.; Zhang, L.; Pei, L.; Xue, H.; Li, Z. Adsorption of methylene blue and Congo red from aqueous solution on 3D MXene/carbon foam hybrid aerogels: A study by experimental and statistical physics modeling. *J. Environ. Chem. Eng.* **2023**, *11*, 109206.

30. Gómez-Avilés, A.; Sellaoui, L.; Badawi, M.; Bonilla-Petriciolet, A.; Bedia, J.; Belver, C. Simultaneous adsorption of acetaminophen, diclofenac and tetracycline by organo-sepiolite: Experiments and statistical physics modelling. *Chem. Eng. J.* **2021**, *404*, 126601.

31. Shamsudin, M.S.; Azha, S.F.; Sellaoui, L.; Badawi, M.; Bonilla-Petriciolet, A.; Ismail, S. Performance and interactions of diclofenac adsorption using Alginate/Carbon-based Films: Experimental investigation and statistical physics modelling. *Chem. Eng. J.* **2022**, *428*, 131929.

32. Al-Yousef, H.A.; Alotaibi, B.M.; Aouaini, F.; Sellaoui, L.; Bonilla-Petriciolet, A. Adsorption of ibuprofen on cocoa shell biomass-based adsorbents: Interpretation of the adsorption equilibrium via statistical physics theory. *J. Mol. Liq.* **2021**, *331*, 115697.

33. Sellaoui, L.; Dhaouadi, F.; Reynel-Avila, H.E.; Mendoza-Castillo, D.I.; Bonilla-Petriciolet, A.; Trejo-Valencia, R.; Taamalli, S.; Louis, F.; El Bakali, A.; Chen, Z. Physicochemical assessment of anionic dye adsorption on bone char using a multilayer statistical physics model. *Environ. Sci. Pollut. Res.* **2021**, *28*, 67248–67255.

34. Sarra, A.; Chaker, D.; Abdallah, B.; Derradji, C.; Abdeltif, A. Adsorption of a Cationic Dye Crystal Violet onto a Binary Mixture of Forest Waste Biopolymer: Advanced Statistical Physics Studies. *Adv. Mater. Res.* **2022**, *1168*, 93–113.

35. Tseng, R.-L.; Wu, P.-H.; Wu, F.-C.; Juang, R.-S. A convenient method to determine kinetic parameters of adsorption processes by nonlinear regression of pseudo-nth-order equation. *Chem. Eng. J.* **2014**, *237*, 153–161.

36. Oladipo, A.A.; Gazi, M. Enhanced removal of crystal violet by low cost alginate/acid activated bentonite composite beads: Optimization and modelling using non-linear regression technique. *J. Water Process Eng.* **2014**, *2*, 43–52. https://doi.org/10.1016/j.jwpe.2014.04.007.

37. Sadeghi, G.M.M.; Shamsi, R.; Sayaf, M. From Aminolysis Product of PET Waste to Novel Biodegradable Polyurethanes. *J. Polym. Environ.* **2011**, *19*, 522–534. https://doi.org/10.1007/s10924-011-0283-7.

38. Feng, J.; Liu, R.; Chen, P.; Yuan, S.; Zhao, D.; Zhang, J.; Zheng, Z. Degradation of aqueous 3,4-dichloroaniline by a novel dielectric barrier discharge plasma reactor. *Environ. Sci. Pollut. Res.* **2015**, *22*, 4447–4459. https://doi.org/10.1007/s11356-014-3690-1.

39. Ahmadpoor, F.; Shojaosadati, S.A.; Mousavi, S.Z. Magnetic silica coated iron carbide/alginate beads: Synthesis and application for adsorption of Cu (II) from aqueous solutions. *Int. J. Biol. Macromol.* **2019**, *128*, 941–947.

40. Yazidi, A.; Sellaoui, L.; Dotto, G.L.; Bonilla-Petriciolet, A.; Fröhlich, A.C.; Lamine, A.B. Monolayer and multilayer adsorption of pharmaceuticals on activated carbon: Application of advanced statistical physics models. *J. Mol. Liq.* **2019**, *283*, 276–286.

41. Guechi, E.-K.; Hamdaoui, O. Sorption of malachite green from aqueous solution by potato peel: Kinetics and equilibrium modeling using non-linear analysis method. *Arab. J. Chem.* **2016**, *9*, S416–S424.

42. Rangabhashiyam, S.; Selvaraju, N. Adsorptive remediation of hexavalent chromium from synthetic wastewater by a natural and ZnCl2 activated *Sterculia guttata* shell. *J. Mol. Liq.* **2015**, *207*, 39–49.

43. Khodabandehloo, A.; Rahbar-Kelishami, A.; Shayesteh, H. Methylene blue removal using *Salix babylonica* (Weeping willow) leaves powder as a low-cost biosorbent in batch mode: Kinetic, equilibrium, and thermodynamic studies. *J. Mol. Liq.* **2017**, *244*, 540–548.

44. Akar, T.; Anilan, B.; Gorgulu, A.; Akar, S.T. Assessment of cationic dye biosorption characteristics of untreated and non-conventional biomass: *Pyracantha coccinea* berries. *J. Hazard. Mater.* **2009**, *168*, 1302–1309.

45. Rangabhashiyam, S.; Lata, S.; Balasubramanian, P. Biosorption characteristics of methylene blue and malachite green from simulated wastewater onto *Carica papaya* wood biosorbent. *Surf. Interfaces* **2018**, *10*, 197–215.

46. Lopičić, Z.R.; Stojanović, M.D.; Marković, S.B.; Milojković, J.V.; Mihajlović, M.L.; Radoičić, T.S.K.; Kijevčanin, M.L. Effects of different mechanical treatments on structural changes of

lignocellulosic waste biomass and subsequent Cu (II) removal kinetics. *Arab. J. Chem.* **2019**, *12*, 4091–4103.

47. El Amri, A.; Bensalah, J.; Idrissi, A.; Lamya, K.; Ouass, A.; Bouzakraoui, S.; Zarrouk, A.; Lebkiri, A. Adsorption of a cationic dye (Methylene bleu) by *Typha Latifolia*: Equilibrium, kinetic, thermodynamic and DFT calculations. *Chem. Data Collect.* **2022**, *38*, 100834.
48. Postai, D.L.; Rodrigues, C.A. Adsorption of cationic dyes using waste from fruits of *Eugenia umbelliflora Berg* (*Myrtaceae*). *Arab. J. Sci. Eng.* **2018**, *43*, 2425–2440.
49. Namasivayam, C.; Kavitha, D. XRD and SEM studies on the mechanism of adsorption of dyes and phenols by coir pith carbon from aqueous phase. *Microchem. J.* **2006**, *82*, 43–48.
50. Luo, W.-J.; Gao, Q.; Wu, X.-L.; Zhou, C.-G. Removal of cationic dye (methylene blue) from aqueous solution by humic acid-modified expanded perlite: Experiment and theory. *Sep. Sci. Technol.* **2014**, *49*, 2400–2411.
51. Amri, A.E.L.; Bensalah, J.; Essaadaoui, Y.; Lebkiri, I.; Abbou, B.; Zarrouk, A.; Lebkiri, A. Elaboration, characterization and performance evaluation of a new environmentally friendly adsorbent material based on the reed filter (*Typha Latifolia*): Kinetic and thermodynamic studies and application in the adsorption of Cd (II) ion. *Chem. Data Collect.* **2022**, *39*, 100849.
52. Bensalah, J.; Berradi, M.; Habsaoui, A.; Allaoui, M.; Essebaai, H.; El Khattabi, O.; Lebkiri, A.; Rifi, E.-H. Kinetic and thermodynamic study of the adsorption of cationic dyes by the cationic artificial resin Amberlite® IRC50. *Mater. Today Proc.* **2021**, *45*, 7468–7472.
53. Bensalah, J.; Benhiba, F.; Habsaoui, A.; Ouass, A.; Zarrouk, A.; Lebkiri, A.; El Khattabi, O. The adsorption mechanism of the anionic and cationic dyes of the cationic resin A® IRC-50, kinetic study and theoretical investigation using DFT. *J. Indian Chem. Soc.* **2022**, *99*, 100512.
54. Bensalah, J.; Idrissi, A.; El Faydy, M.; Doumane, G.; Staoui, A.; Hsissou, R.; Lebkiri, A.; Habsaoui, A.; Abdelkader, Z. Investigation of the cationic resin as a potential adsorbent to remove MR and CV dyes: Kinetic, equilibrium isotherms studies and DFT calculations. *J. Mol. Struct.* **2023**, 134849. https://doi.org/10.1016/j.molstruc.2022.134849
55. Li, S.; Zeng, Z.; Xue, W. Adsorption of lead ion from aqueous solution by modified walnut shell: Kinetics and thermodynamics. *Environ. Technol.* **2019**, *40*, 1810–1820.

56. Kumar, A.S.K.; Warchol, J.; Matusik, J.; Tseng, W.-L.; Rajesh, N.; Bajda, T. Heavy metal and organic dye removal via a hybrid porous hexagonal boron nitride-based magnetic aerogel. *NPJ Clean Water* **2022**, *5*, 24.

57. Elabboudi, M.; Bensalah, J.; El Amri, A.; Azzouzi, N.E.L.; Srhir, B.; Zarrouk, A. Adsorption performance and mechanism of anionic MO dye by the adsorbent polymeric Amberlite® IRA-410 resin from environment wastewater: Equilibrium kinetic and thermodynamic studies. *J. Mol. Struct.* **2023**, *1277*, 134789.

58. Silva, L.S.; Lima, L.C.B.; Ferreira, F.J.L.; Silva, M.S.; Osajima, J.A.; Bezerra, R.D.S.; Filho, E.C.S. Sorption of the anionic reactive red RB dye in cellulose: Assessment of kinetic, thermodynamic, and equilibrium data. *Open Chem.* **2015**, *13*: 801–812.

59. Kumar, K.V.; Sivanesan, S. Equilibrium data, isotherm parameters and process design for partial and complete isotherm of methylene blue onto activated carbon. *J. Hazard. Mater.* **2006**, *134*, 237–244.

60. Selim, A.Q.; Sellaoui, L.; Mobarak, M. Statistical physics modeling of phosphate adsorption onto chemically modified carbonaceous clay. *J. Mol. Liq.* **2019**, *279*, 94–107.

61. Sellaoui, L.; Dotto, G.L.; Peres, E.C.; Benguerba, Y.; Lima, É.C.; Lamine, A.B.; Erto, A. New insights into the adsorption of crystal violet dye on functionalized multi-walled carbon nanotubes: Experiments, statistical physics and COSMO–RS models application. *J. Mol. Liq.* **2017**, *248*, 890–897.

62. Stovall, M.; Smith, S.A.; Langholz, B.M.; Boice, J.D., Jr.; Shore, R.E.; Andersson, M.; Buchholz, T.A.; Capanu, M.; Bernstein, L.; Lynch, C.F. Dose to the contralateral breast from radiotherapy and risk of second primary breast cancer in the WECARE study. *Int. J. Radiat. Oncol. Biol. Phys.* **2008**, *72*, 1021–1030.

63. Sellaoui, L.; Guedidi, H.; Knani, S.; Reinert, L.; Duclaux, L.; Lamine, A.B. Application of statistical physics formalism to the modeling of adsorption isotherms of ibuprofen on activated carbon. *Fluid Phase Equilib.* **2015**, *387*, 103–110.

64. Khalfaoui, M.; Knani, S.; Hachicha, M.A.; Lamine, A.B. New theoretical expressions for the five adsorption type isotherms classified by BET based on statistical physics treatment. *J. Colloid Interface Sci.* **2003**, *263*, 350–356.

65. Mobarak, M.; Mohamed, E.A.; Selim, A.Q.; Eissa, M.F.; Seliem, M.K. Experimental results and theoretical statistical modeling of malachite green adsorption onto MCM–41 silica/rice husk composite modified by beta radiation. *J. Mol. Liq.* **2019**, *273*, 68–82.

66. Sellaoui, L.; Li, Z.; Badawi, M.; Dotto, G.L.; Bonilla-Petriciolet, A.; Chen, Z. Origin of the outstanding performance of ZnAl and MgFe layered double hydroxides in the adsorption of 2-nitrophenol: A statistical physics assessment. *J. Mol. Liq.* **2020**, *314*, 113572.

67. Guediri, A.; Bouguettoucha, A.; Chebli, D.; Amrane, A. The use of encapsulation as a proposed solution to avoid problems encountered with conventional materials in powder form: Application in methylene blue removal from aqueous solutions. *J. Mol. Liq.* **2020**, *316*, 113841.

68. Kebaili, M.; Djellali, S.; Radjai, M.; Drouiche, N.; Lounici, H. Valorization of orange industry residues to form a natural coagulant and adsorbent. *J. Ind. Eng. Chem.* **2018**, *64*, 292–299.

69. Eltaweil, A.S.; Elgarhy, G.S.; El-Subruiti, G.M.; Omer, A.M. Carboxymethyl cellulose/carboxylated graphene oxide composite microbeads for efficient adsorption of cationic methylene blue dye. *Int. J. Biol. Macromol.* **2020**, *154*, 307–318.

70. Mahmoud, S.E.M.E.; Ursueguia, D.; Mahmoud, M.E.; Abel-Fattah, T.M.; Díaz, E. Functional surface homogenization of nanobiochar with cation exchanger for improved removal performance of methylene blue and lead pollutants. *Biomass Convers. Biorefinery* **2023**, 1–21. https://doi.org/10.1007/s13399-023-04098-9

Chapter IV: enhancement of H_2O_2 decomposition through the combined action of CuO-$NiFe_2O_4$ nanoparticles for methylene blue degradation

1 Introduction

Water pollution is a major global issue due to dangerous pollutants in our water sources. To address this problem, various conventional methods, including adsorption, coagulation [1], membrane treatments [2], and biological, physical, and chemical processes [3], have been employed to mitigate the impact of these harmful compounds in wastewater [4]. Nevertheless, all the previously suggested treatments suffer from the significant drawback of transferring pollutants from one phase to another instead of eliminating them [5].

Advanced oxidative processes (AOPs) based on highly reactive oxygen species (ROS) have been presented as an innovative and efficient strategy for the breakdown of antibiotics in wastewater. In 1894, H. J. [6] Fenton first reported the Fenton reaction. Under severe acid conditions, he observed the partial oxidation of tartaric acid into dihydroxymaleic acid in the presence of Fe^{2+} and H_2O_2. Since then, the Fenton reaction has been applied to process wastewater, including organic and biological contaminants [7]. However, the problems of the Fenton reaction mainly include the following aspects: incomplete pollutant mineralization; narrow pH range for obtaining the highest rate; waste of H_2O_2 for molecular oxygen production; low degradation rate for some chemicals; instability of the dissolved iron catalyst, which prevents their widespread application for wastewater treatment [8]. To alleviate the deficiency in homogeneous Fenton reactions, ultraviolet (UV) and ultrasonic (US) have been employed to increase the activation of H_2O_2. Although UV and US have substantially increased the beneficial effect, energy consumption is an inherent obstacle [9]. The heterogeneous Fenton reaction aims to broaden the practical operating pH range and limit the formation of the by-product iron mud. Considering its vast and practical use, the heterogenous Fenton reaction offers a viable alternative to H_2O_2 activation [10].

Spinel ferrites with narrow bandgaps have attracted considerable attention among various photocatalysts and Fenton catalysts due to their stability and outstanding magnetic characteristics. $NiFe_2O_4$, an inexpensive material with good magnetic properties and a narrow bandgap (2 eV), has received much attention in the photocatalytic treatment of pollutants [11]. $NiFe_2O_4$ has been shown to react with H_2O_2 to create •OH, which can show better performance under the Fenton process. Improving its catalytic performance remains a challenge. It is suggested that the combination of $NiFe_2O_4$ with metal oxides could be an effective strategy [12].

Due to its favorable physical and chemical properties, cupric oxide (CuO) is an important p-type metal oxide semiconductor with a narrow bandgap in the region of 1.2 to 2.2 eV that has been widely used in solar cells, catalysis [13], magnetic storage, and other applications. Cu+ and Cu^{2+}

in copper oxides can also react with H_2O_2 as a Fenton reaction, producing •OH and $•O^{2-}$, respectively. However, the CuO catalyst has some drawbacks such as its low stability as well as the high capacity of its charge carriers to recombine.

Whether $NiFe_2O_4$ could be mixed with CuO indicated above, a novel multicomponent nanocomposite material ($NiFe_2O_4$-CuO) will be constructed to catalyze H_2O_2, targeted to improve the decomposition efficiency of H_2O_2 under variable conditions [14].

In this chapter, a new catalyst based on $NiFe_2O_4$-CuO nanoparticles has been produced and initially employed for the H_2O_2 activation. The usual dye methylene blue was selected as the target pollutant.

2 Experimental

2.1.1 Chemicals and reagents

Metal nitrates, iron (III) nitrate nonahydrate (Fe $(NO_3)_3.9H_2O$) (99.99%), nickel (II) nitrate hexahydrate (Ni $(NO_3)_2$.6H2O) (99.9%), nitrate copper (II) trihydrate (Cu $(NO_3)_2.3H_2O$) (99.99%), hydrogen peroxide (H_2O_2), and polyethylene glycol (PEG). It was bought from Sigma-Aldrich.

2.2 Synthesis of catalysts

2.2.1 Synthesis of CuO

150 ml of 0.1 M Cu $(NO_3)_2.3H_2O$ solution will be sonicated for 2 h. Then, sodium hydroxide solution (2.2 M) will be added until the pH of the solution reaches 10, followed by stirring for 1 h. The residue will be washed with water after filtration in the next step. Finally, the dried product (80 ◦C, 3 h) will be calcined at 450 ◦C for 2 h.

2.2.2 Synthesis of $NiFe_2O_4$

2 mmol of Ni $(NO_3)_2.6H_2O$, 4 mmol of Fe $(NO_3)_3.9H_2O$ (the Ni^{2}+/Fe^{3}+ molar ratio was 1/2), and 5 g of PEG (Poly Ethylene Glycol) in 20 ml of aqueous alcohol 50% will be added to 100 ml of water. PEG will be added to obtain a small homogeneous particle size; after 10 min of stirring, the aqueous NaOH solution will be successively added drop by drop with continuous stirring until the pH reaches 11. Then the precursor solution will be treated by sonication for 30 min and transferred to a stainless-steel hydrothermal reactor for 12 hours of hydrothermal treatment at 190 ◦C. It will then be cooled to room temperature. The resulting product will be collected by centrifugation, washed several times with deionized water and ethanol, and then dried under a vacuum. The last step will be calcination at 300 ◦C for 2 hours.

2.2.3 Synthesis of $NiFe_2O_4$-CuO

A specific quantity of CuO (synthesized) was added with a CuO/$Nife_2O_4$ molar ratio of 1 to the previous mixture before the reaction in the autoclave and stirred for 30 min. The rest of the procedure will be the same as in Section (1.2.2). The last step will be calcination at 300 ◦C for 2 hours.

2.3 Analysis

Catalytic degradation studies were conducted in 200-mL conical flasks. The conical flasks containing the aqueous solution were agitated on a reciprocating shaker at 250 rpm and 303 K at pH 3 in the dark. The MB solution at a defined concentration was added to deionized water to reach the necessary initial concentration, and then the specific dose of sonicated nanoparticles was put into the solution. The resultant mixture was agitated for a certain interval to preserve the adsorption/desorption balance between the catalyst and the contaminant before adding the oxidizing solution. Samples taken at different time intervals were combined with 20 µL of methanol to deactivate the H_2O_2 solution, then immediately filtered through centrifuges before being evaluated using a visible UV spectrophotometer type Shimadzu Spectrophotometer UV Vis 1700.

2.4 Characterization of catalysts

The crystal phase of the produced materials was determined using an X-ray diffractometer (Smartlab9, Rigaku, Japan).

3 Results and discussion

3.1 Characterization of CuO-Nife$_2$O$_4$ nanoparticles

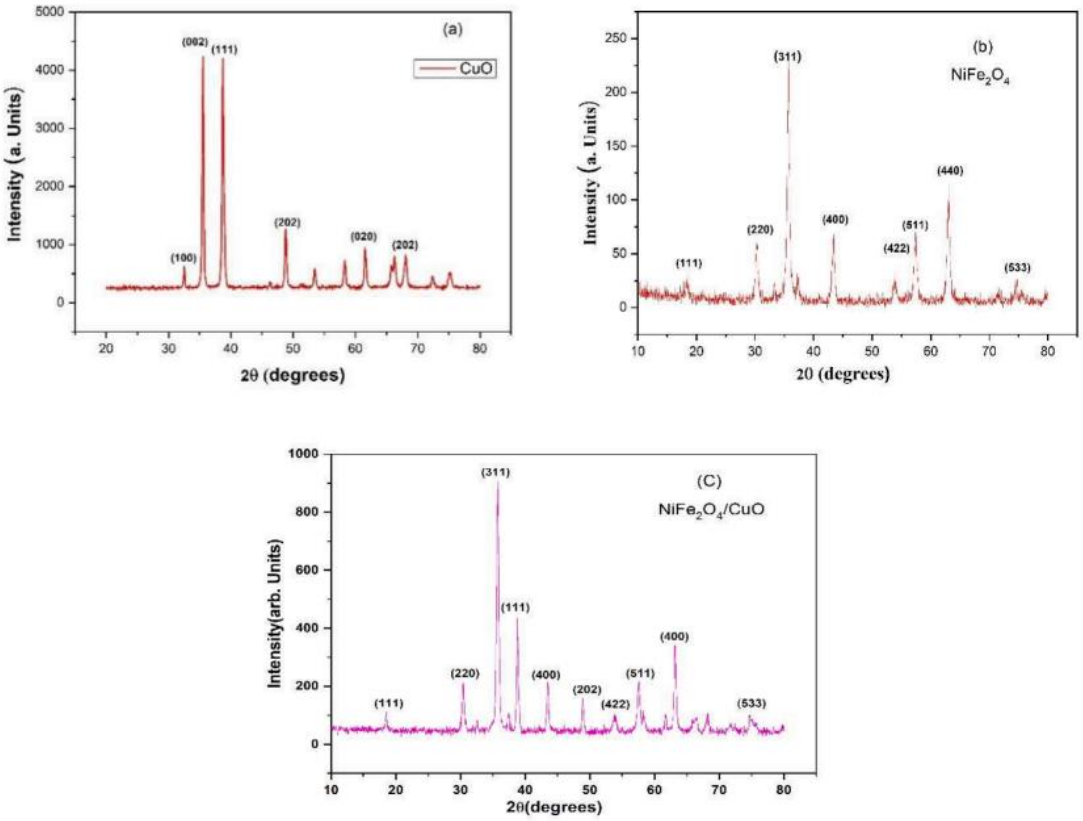

Figure1. X-ray diffraction pattern of (a) CuO, (b) $NiFe_2O_4$, (c) $NiFe_2O_4$-CuO nanocomposites.

X-ray diffraction (XRD) was utilized to examine the characteristics and compositions of peaks and phases. Various techniques, including the analysis of XRD patterns, have been employed to comprehensively examine metal oxides, ferrites, and nanocomposite materials. Figure 1 (a, b, c) illustrates the configurations of CuO, NiFe2O4, ferrite nanoparticles, and NiFe2O4-CuO composite materials.

Figure 1(a) illustrates the presence of peaks corresponding to the CuO crystallographic planes (100), (111), and (002), indicating the successful formation of a monoclinic structure. XRD data and peaks closely correspond with the details from the JCPDS card (961011195), which specifies the lattice parameters as a = 4.6700 Å, b = 3.4300 Å, and c = 5.1200 Å. No additional phases are observed in Fig. 1(a), indicating high purity and exceptional crystal growth, as evidenced by sharp and well-defined peaks. Figure 1(b) depicts the XRD pattern of synthesized NiFe2O4 nanoparticles. The X-ray analysis verifies the existence of diffraction peaks associated with the (220), (311), (400), (511), (400), and (533) crystallographic planes, signifying a cubic structure.

In Figure. 1(c), the XRD pattern of $NiFe_2O_4$-CuO nanocomposite reveals distinct peaks corresponding to the (220), (311), (400), (511), (422), (533), and (400) crystallographic planes, all indicative of a cubic system. The observed data aligns with the information provided by ICDS 01–070–6496 files. Additionally, the formation of new phases, notably the (111) and (202) peaks associated with CuO, is attributable to the ceramic technique adopted, the sintering temperature, and the reaction between the components. By utilizing established formulae, various structural characteristics were determined by the examination of the X-ray diffraction pattern. For CuO, NiFe2O4, and the $NiFe_2O_4$-CuO nanocomposite, the calculations involved the use of interplanar distance (d), lattice constant, and Bragg's angle [15].

$$a = d\sqrt{h^2 + k^2 + l^2} \quad (1)$$

In the X-ray patterns, the major peaks were attributed to the (311) plane of $N_iFe_2O_4$ nanoparticles and the (110) plane of CuO. The particle size (D) was estimated using Scherrer's equation, represented by Eq. (2):

$$D = \frac{0{,}9\lambda}{\beta\cos\theta} \quad (2)$$

Table 1 contains the values for the crystallite size (D) and lattice value.

Table 1 Lattice parameters and Values of crystallite size (D)

Composition	T Temp. ◦C	2 2Theta°	F WHM°	D nm	Lattice Constant Å
CuO	450	38.729	0.291	29.44	a = 4.670 b = 3.430 c = 5.120
$NiFe_2O_4$	300	35.662	1.25	6.9	a= 8.341
$NiFe_2O_4$/CuO	600	35.747	0.414	20.18	a= 8.321

3.2 Catalytic oxidation of MB by CuO, $NiFe_2O_4$, and, $NiFe_2O_4$-CuO

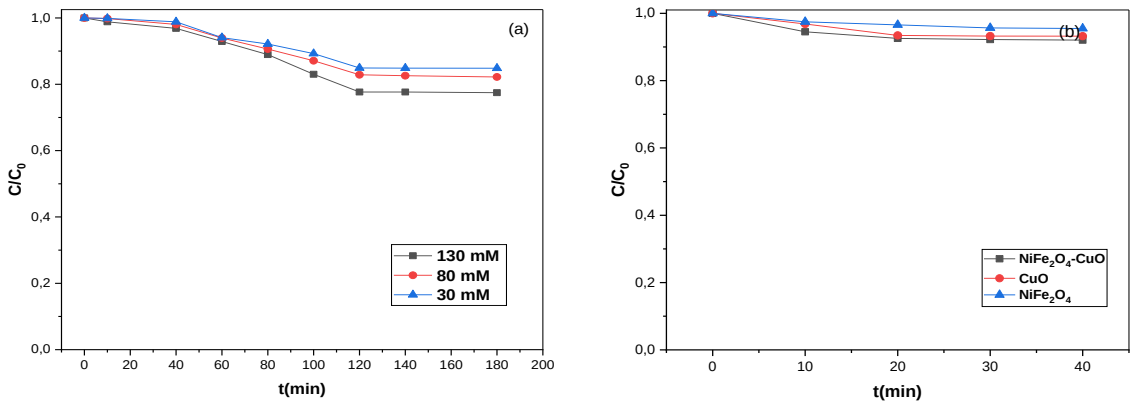

Figure 2. (a) only $NiFe_2O_4$, CuO, $NiFe_2O_4$-CuO; (b) only H_2O_2(30, 80, 130 mM).

Several systems, H_2O_2 alone, $NiFe_2O_4$, alone, CuO alone, $NiFe_2O_4$-CuO alone, $NiFe_2O_4$/ H_2O_2, CuO/ H_2O_2, and $NiFe_2O_4$-CuO/ H_2O_2 were tested for the removal of MB.

In the absence of H_2O_2, about 4.5%, 6.0%, and 8.0% reduction of MB were determined after 30 minutes due to the adsorption effect of $NiFe_2O_4$, CuO, and CuO- $NiFe_2O_4$ nanoparticles fig1. (a). For this, the catalyst/pollutant mixture will remain agitated for 40 minutes to ensure the removal of the adsorbed quantity before adding H_2O_2.

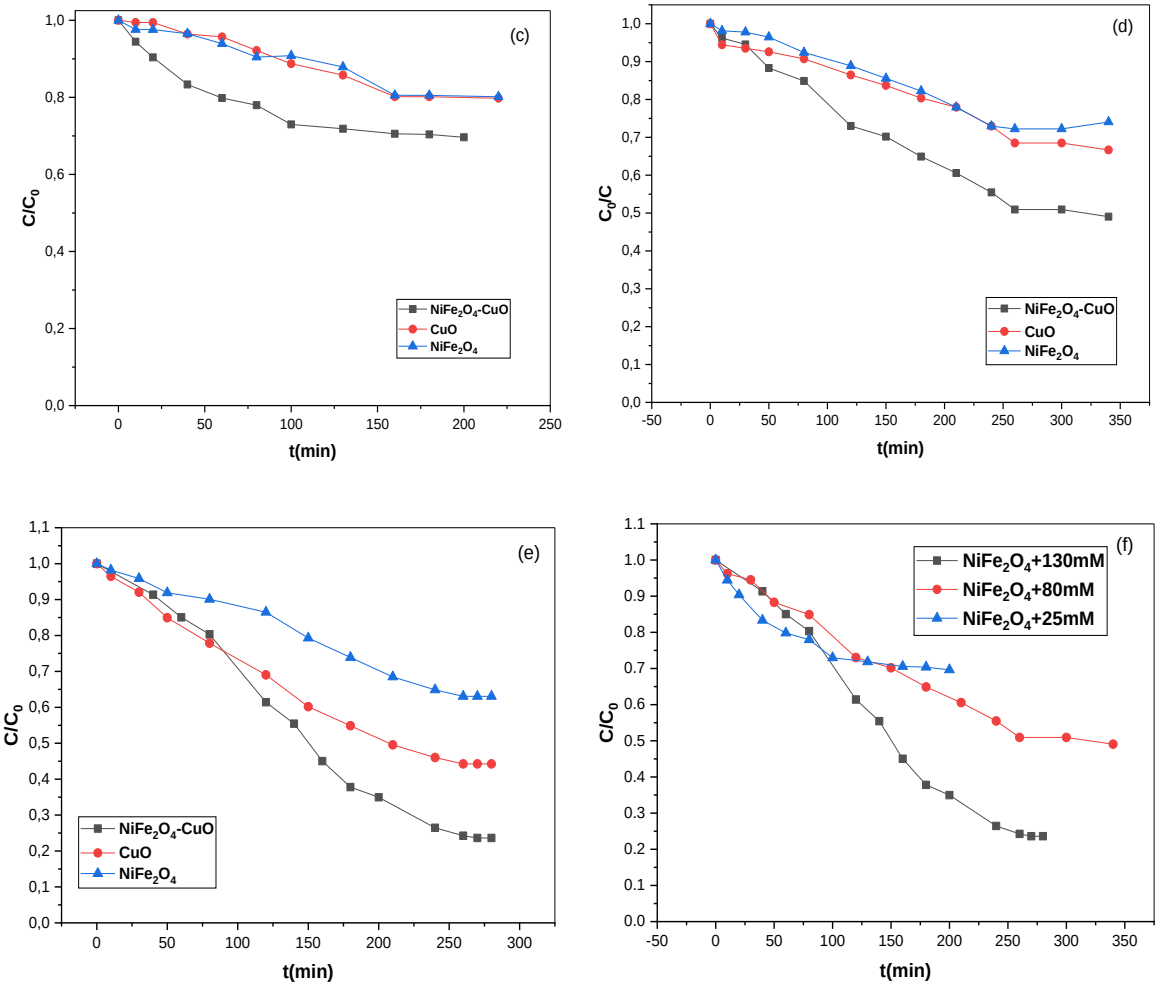

Figure 3. (c) $NiFe_2O_4$, CuO, $NiFe_2O_4$-CuO+H_2O_2(30mM) ; (d) $NiFe_2O_4$, CuO, $NiFe_2O_4$-CuO+H_2O_2(80mM) ; (e) $NiFe_2O_4$, CuO, $NiFe_2O_4$-CuO+H_2O_2(130mM) ; (f)CuO, $NiFe_2O_4$-CuO+H_2O_2(30, 80, 130mM).

Figure 3. (c) demonstrates MB deterioration of 20%, 20%, and 30%; Figure 3. (d) 25%, 35%, 50%; and Figure 3. (e) 40%, 55%, and 80%, respectively, $NiFe_2O_4$/H_2O_2, CuO/H_2O_2, $NiFe_2O_4$-CuO /H_2O_2, in approximately 300 min for all mixes. From these offers, the $NiFe_2O_4$-CuO complex gives a better degradation for the MB pollutant compared to the $NiFe_2O_4$ or CuO alone.

The effect of the H_2O_2 dose is remarkable in Figure 3. (f), the concentration of H_2O_2 increases the degradation of MB; this result shows the good performance of the complex for the decomposition of H_2O_2.

3.3 Identification of the reaction mechanism

According to the aforementioned experimental data, the probable mechanism for the activation of H_2O_2 on the $NiFe_2O_4$-CuO catalyst was hypothesized as summarized by Eqs. (1)– (14).

Firstly, H_2O_2 was initially associated with CuO-NiFe2O4 catalyst, then Fe (III) and Cu (II) were reduced to Fe (II) and Cu(I), while Ni (II) was oxidized to Ni (III), then some ROS like •OOH, •OH and $•O^{2-}$ were produced. Then, the generated Fe (II), Cu(I), and Ni (III) would continue to react with H_2O_2, while •OOH and •OH were released into the solution (Eqs. (4, 6, 8)). Furthermore, $•O^{2-}$ could react with H_2O and •OOH to produce •OOH and O_2 (Eqs. (9–10)).

The results suggested that there existed a synergistic interaction between CuO and $NiFe_2O_4$. Finally, the produced $•O^{2-}$/•OH/O_2 would attack the MB molecule, which was responsible for the MB breakdown.

$$\mathrm{Fe(III)} + H_2O_2 \rightarrow \mathrm{Fe\ (II)} + \bullet\,\mathrm{OOH} + \mathrm{H^+} \quad (3)$$

$$\mathrm{Fe(II)} + H_2O_2 \rightarrow \mathrm{Fe\ (II)} + \bullet\,\mathrm{OH} + \mathrm{OH^-} \quad (4)$$

$$\mathrm{Ni(II)} + H_2O_2 \rightarrow \mathrm{Ni\ (III)} + \bullet\,\mathrm{OH} + \mathrm{OH^-} \quad (5)$$

$$\mathrm{Ni(III)} + H_2O_2 \rightarrow \mathrm{Ni(II)} + \bullet\,\mathrm{OOH} + \mathrm{OH^-} \quad (6)$$

$$\mathrm{Cu(II)} + H_2O_2 \rightarrow \mathrm{Cu\ (I)} + \bullet\,\mathrm{OH} + \bullet\,\mathrm{O_2^-} \quad (7)$$

$$\mathrm{Cu(I)} + H_2O_2 \rightarrow \mathrm{Cu\ (II)} + \bullet\,\mathrm{OH} \quad (8)$$

$$\bullet\,\mathrm{O_2^-} + H_2\mathrm{O} \rightarrow \bullet\,\mathrm{OOH} + \mathrm{OH^-} \quad (9)$$

$$\bullet\,\mathrm{O_2^-} + \bullet\,\mathrm{OOH} \rightarrow O_2 + \mathrm{OOH^-} \quad (10)$$

$$\mathrm{Ni(III)} + \mathrm{Fe(II)} \rightarrow \mathrm{Ni\ (II)} + \mathrm{Fe(III)} \quad (11)$$

$$\mathrm{Fe(III)} + \mathrm{Cu(I)} \rightarrow \mathrm{Cu\ (II)} + \mathrm{Fe(II)} \quad (12)$$

$$\mathrm{Ni(III)} + \mathrm{Cu(I)} \rightarrow \mathrm{Cu\ (II)} + \mathrm{Ni(II)} \quad (13)$$

$$\bullet\,\mathrm{O_2^-} + \bullet\,\mathrm{OH} + O_2 + \mathrm{MB} \rightarrow H_2\mathrm{O} + CO_2 + \ \mathrm{Byproducts} \quad (14)$$

4 Conclusion

In this study, magnetic $NiFe_2O_4$-CuO nanoparticles with low cost and environmental friendliness were produced by the hydrothermal method and then utilized as a Fenton-like catalyst to activate H_2O_2 to degrade MB. The prepared $NiFe_2O_4$-CuO nanoparticles demonstrated a good aptitude for MB degradation. Under the ideal circumstances (200 g/L catalyst, 130 mM H_2O_2, and 200 mg/L MB), 80% removal efficiency was achieved within 300 minutes. According to multiple experiment evaluations, $\bullet O^{2-}/\bullet OH/O_2$ was created in the $NiFe_2O_4$-CuO/H_2O_2 system.

5 Reference

[1] R. Dhinesh Kumar, R. Thangappan, and R. Jayavel, "Facile preparation of LaFeO3/rGO nanocomposites with enhanced visible light photocatalytic activity," *J. Inorg. Organomet. Polym. Mater.*, vol. 27, no. 4, pp. 892–900, 2017.

[2] O. A. Fouad, R. M. Mohamed, M. S. Hassan, and I. A. Ibrahim, "Effect of template type and template/silica mole ratio on the crystallinity of synthesized nanosized ZSM-5," *Catal. today*, vol. 116, no. 1, pp. 82–87, 2006.

[3] R. M. Mohamed and M. M. Mohamed, "Copper (II) phthalocyanines immobilized on alumina and encapsulated inside zeolite-X and their applications in photocatalytic degradation of cyanide: a comparative study," *Appl. Catal. A Gen.*, vol. 340, no. 1, pp. 16–24, 2008.

[4] M. K. Guediri, D. Chebli, A. Bouguettoucha, R. Bourzami, and A. Amrane, "Novel Fe2TiO5/reduced graphene oxide heterojunction photocatalyst with improved adsorption capacity and visible light photoactivity: experimental and DFT approach," *Environ. Sci. Pollut. Res.*, vol. 28, no. 7, pp. 8507–8519, 2021.

[5] J. Feng, R. Liu, P. Chen, S. Yuan, D. Zhao, J. Zhang, and Z. Zheng, "Degradation of aqueous 3,4-dichloroaniline by a novel dielectric barrier discharge plasma reactor," *Environ. Sci. Pollut. Res.*, vol. 22, no. 6, pp. 4447–4459, Oct. 2015.

[6] J. Xu, W. Wang, E. Gao, J. Ren, and L. Wang, "Bi2WO6/Cu0: a novel coupled system with enhanced photocatalytic activity by Fenton-like synergistic effect," *Catal. Commun.*, vol. 12, no. 9, pp. 834–838, 2011.

[7] A. Babuponnusami and K. Muthukumar, "A review on Fenton and improvements to the Fenton process for wastewater treatment," *J. Environ. Chem. Eng.*, vol. 2, no. 1, pp. 557–572, 2014.

[8] J. J. Pignatello, E. Oliveros, and A. MacKay, "Advanced oxidation processes for organic contaminant destruction based on the Fenton reaction and related chemistry," *Crit. Rev. Environ. Sci. Technol.*, vol. 36, no. 1, pp. 1–84, 2006.

[9] C. Tan, N. Gao, Y. Deng, Y. Zhang, M. Sui, J. Deng, and S. Zhou, "Degradation of antipyrine by UV, UV/H2O2 and UV/PS," *J. Hazard. Mater.*, vol. 260, pp. 1008–1016, 2013.

[10] M. H. Dehghani, E. Nikfar, A. Zarei, and N. M. Esfahani, "The effects of US/H2O2 processes on bisphenol-A toxicity in aqueous solutions using Daphnia magna.," *Desalin. Water Treat.*, vol. 68, pp. 183–189, 2017.

[11] Y. Pang and H. Lei, "Degradation of p-nitrophenol through microwave-assisted heterogeneous activation of peroxymonosulfate by manganese ferrite," *Chem. Eng. J.*, vol. 287, pp. 585–592, 2016.

[12] U. Kurtan, M. Amir, A. Yıldız, and A. Baykal, "Synthesis of magnetically recyclable MnFe2O4@ SiO2@ Ag nanocatalyst: its high catalytic performances for azo dyes and nitro compounds reduction," *Appl. Surf. Sci.*, vol. 376, pp. 16–25, 2016.

[13] L. Yang, Y. Zhang, X. Liu, X. Jiang, Z. Zhang, T. Zhang, and L. Zhang, "The investigation of synergistic and competitive interaction between dye Congo red and methyl blue on magnetic MnFe2O4," *Chem. Eng. J.*, vol. 246, pp. 88–96, 2014.

[14] X. Peng, J. Qu, S. Tian, Y. Ding, X. Hai, B. Jiang, M. Wu, and J. Qiu, "Green fabrication of magnetic recoverable graphene/MnFe 2 O 4 hybrids for efficient decomposition of methylene blue and the Mn/Fe redox synergetic mechanism," *RSC Adv.*, vol. 6, no. 106, pp. 104549–104555, 2016.

[15] M. Kumari and M. C. Bhatnagar, "Synthesis of nickel ferrite nanorods and nano-octahedrons by hydrothermal method," in *AIP Conference Proceedings*, 2020, vol. 2220, no. 1.

General conclusion and prospects

General conclusion and prospects

The key objective of this work was to synthesize new materials using simple and inexpensive methods and to emphasize the potential of the materials synthesized for the depollution of wastewater effluents. To examine this potential, numerous experiments (such as material characterization, parameter effects, kinetics, and equilibrium studies) were done. Three major ingredients were created and used in two separate processing procedures. Acorus calamus, with the acronym PACK, and Cynara scolymus, with the abbreviation Cs, are used as precursor powders for the treatment of methylene blue via adsorption methods. The NiFe2O4-CuO spinel-oxide complex is employed in the treatment of methylene blue via Fenton heterogeneous processes.

The methylene blue adsorption was carried out on a natural material powder of *Acorus calamus* treated firstly with H_2SO_4 and then activated by $KMnO_4$ in the first chapter. Fourier transform infrared (FT-IR) spectroscopy, pHpzc analysis, and SEM micrograph were carried out to characterize the material. The results obtained related to adsorption kinetics, adsorption isotherms, thermodynamics, and ionic strength were analyzed to explain the adsorption mode of MB onto PACK. This result shows that sorption kinetics followed a pseudo-nth-order model. Among the tested isotherm models, the R-P isotherm was considered to be the most relevant to describe MB sorption onto PACK. From the Advanced statistical physics models data, and based on the R^2 values obtained, the mono-layer two-energy model was found to be the most suitable to describe the MB adsorption onto the PACK material. From this, the adsorption of MB was assumed on two different sites of PACK with two different energies, E_1 for the first site and E_2 for the second site. These two different receptor sites can interact with a variable number of MB molecules (n), n_1 with the first type of sites and n_2 with the second type of sites. The sorption capacity of this material was about 1500 mg/g at 30 °C. The potential of PACK, a readily available material to use as an alternative biosorbent material to eliminate the MB color from aqueous solutions, was therefore confirmed.

In the third chapter, methylene blue (MB) adsorption was performed on a natural material powder of *Cynara scolymus* as a new inexpensive adsorbent. The maximum experimental adsorption capacity of the Cs material was 203.333, 192.187, and 179.380 $mg \bullet g^{-1}$ at 298, 303, and 313 K, respectively. The correlation coefficients (R^2) and average percentage errors APE (%) values for the kinetic and isotherms models indicated that the adsorption kinetics followed a pseudo-nth order model and that the traditional isotherm model Redlich–Peterson (R–P) correctly described the experimental data obtained at 298, 303, and 313 K, respectively. The steric,

energetic, and thermodynamic characteristics of the most relevant advanced model (double-energy single-layer model (AM 2)) were analyzed in detail. The number of active sites for the first receptors (n_1) was determined to be 0.129, 0.610, and 6.833, whereas the number of second active sites (n_2) was determined to be 1.444, 1.675, and 2.036 at 298, 303, and 313 K, respectively. This indicated the presence of both multi–docking and multimolecular modes for the first style of MB ions (n_1), while only a multimolecular mode for the second style of MB ions (n_2). Thermodynamic characteristics demonstrated that MB adsorption onto the Cs adsorbent is spontaneous and feasible.

In the fourth chapter, the hydrothermal approach produced low-cost and environmentally friendly NiFe2O4-CuO nanoparticles. They were then utilized as a Fenton-type catalyst to activate H_2O_2 and degrade MB. The produced $NiFe_2O_4$-CuO nanoparticles exhibited their capacity to effectively destroy MB. Under optimum conditions (200 g/L catalyst, 130 mM H2O2, and 200 mg/L MB), a removal efficiency of 80% was obtained in 300 minutes. According to several experimental assessments, the generation of $\bullet O_2^-/\bullet OH/O_2$ was detected in the CuO-MnFe2O4/H2O2 system.

Future applications prospects

To enhance this study, additional work is necessary:

For the adsorption processes

- Encapsulation of the powder product for easy use and regeneration.
- Study concrete solutions about the evolution of contaminants after the adsorption or regeneration stages.
- Find a more efficient method to produce adsorbents in large quantities quickly.

For the Fenton processes

- Study of the mineralization of the polluting molecule (determination of by-products and TOC).
- Determination of metal concentrations in solutions at the end of treatment to prove that the processes are not subject to secondary pollution.
- Tests on real discharges are recommended to study the effects of interferents on the performance of each process.

International publications

1. Djama, C.; Chebli, D.; Bouguettoucha, A.; Doudou, I.; Amrane, A. Statistical physics modeling of azo dyes biosorption onto modified powder of Acorus calamus in batch reactor. Biomass Convers. Biorefinery. (2021) https://doi.org/10.1007/s13399-020-01190-

2. Sarra, A., Chaker, D., Abdallah, B., Derradji, C., & Abdeltif, A. (2022). Adsorption of a Cationic Dye Crystal Violet onto a Binary Mixture of Forest Waste Biopolymer: Advanced Statistical Physics Studies. *Advanced Materials Research*, *1168*, 93–113. (2021) https://doi.org/10.4028/www.scientific.net/AMR.1168.93

3. Djama, C., Bouguettoucha, A., Chebli, D., Amrane, A., Tahraoui, H., Zhang, J., & Mouni, L. (2023). Experimental and Theoretical Study of Methylene Blue Adsorption on a New Raw Material, Cynara scolymus—A Statistical Physics Assessment. *Sustainability*, *15*(13), 10364. (2023) https://doi.org/10.3390/su151310364

International Communications

1. Djama, C., Bouguettoucha, A., Chebli, D. Elimination d'un colorant organique bleu de méthylène par l'adsoption sur un nouveau biosorbant, (IWEE 2019), 16 17 November, Setif 1 University (Algeria).

2. Djama, C., Bouguettoucha, A., Chebli, D., Doudou, I. Adsorption isotherm, Kinetic modeling, mechanism of azo de methylene bleu onto modified Material,(ICMRE'23 2023), 18 November 2023, Setif 1 University (Algeria).

National Communications

1. Djama, C., Bouguettoucha, A., Chebli, D., Doudou, I. ADSORPTION ISOTHERM, KINETIC MODELING, AND MECHANISM OF AZO DYE METHYLENE BLUE ONTO MODIFIED MATERIAL, (ISMSEM 2022), 07-09 February, Kasdi Merbah University (Algeria).

2. Djama, C., Bouguettoucha, A., Chebli, D., Doudou, I. ADSORPTION ISOTHERM, KINETIC MODELING, AND MECHANISM OF AZO DYE METHYLENE BLUE ONTO MODIFIED MATERIAL, (SNGP 2023), 13-14 December. Kasdi Merbah University (Algeria).

Abstract

This thesis focuses on the synthesis of novel materials suitable for water treatment using two distinct methods: adsorption and Fenton. The adsorption treatment was initially tested using two novel absorbents, Acorus calamus and Cynara scolymus. These absorbents were first treated with sulfuric acid and then activated with potassium permanganate in the case of Acorus calamus. For Cynara scolymus, it was used directly in powder form to prepare the adsorbents. The produced materials were thoroughly characterized using several techniques, including XRD, FTIR, TGA, and SEM. In addition, the study focused on applying the acquired materials as adsorbents in a batch system to remove the basic dye, methylene blue (MB). The study investigated the kinetics of adsorption, equilibrium behavior, and the impact of several parameters, including pH, contact time, initial concentration, ionic strength, and temperature. Consequently, we achieved high levels of adsorption capacity. Furthermore, Fenton's processes demonstrate the efficacy of a novel nanomaterial, $NiFe_2O_4$-CuO, in water treatment. Specifically, it is confirmed that this nanomaterial serves as an effective activator for H_2O_2.

Keywords: Adsorption, Acorus calamus, Cynara scolymus, methylene blue (MB), batch system, Fenton, $NiFe_2O_4$-CuO, H_2O_2

Résumé

Cette thèse se concentre sur la synthèse de nouveaux matériaux adaptés au traitement de l'eau en utilisant deux méthodes distinctes : l'adsorption et le Fenton. Le traitement par adsorption a été initialement testé en utilisant deux nouveaux absorbants, Acorus calamus et Cynara scolymus. Ces absorbants ont d'abord été traités à l'acide sulfurique puis activés au permanganate de potassium dans le cas d'Acorus calamus. Pour Cynara scolymus, il a été utilisé directement sous forme de poudre pour préparer les adsorbants. Les matériaux produits ont été soigneusement caractérisés à l'aide de plusieurs techniques, notamment XRD, FTIR, TGA et SEM. De plus, l'étude s'est concentrée sur l'application des matériaux acquis comme adsorbants dans un système discontinu pour éliminer le colorant basique, le bleu de méthylène (MB). L'étude a étudié la cinétique d'adsorption, le comportement à l'équilibre et l'impact de plusieurs paramètres, notamment le pH, le temps de contact, la concentration initiale, la force ionique et la température. Par conséquent, nous avons atteint des niveaux élevés de capacité d'adsorption. De plus, les procédés de Fenton démontrent l'efficacité d'un nouveau nanomatériau, $NiFe_2O_4$-CuO, dans le traitement de l'eau. Plus précisément, il est confirmé que ce nanomatériau agit comme un activateur efficace du H_2O_2.

Mots clés : Adsorption, Acorus calamus, Cynara scolymus, bleu de méthylène (MB), système batch, Fenton, $NiFe_2O_4$-CuO, H_2O_2

ملخص

تركز هذه الأطروحة على تصنيع مواد جديدة مناسبة لمعالجة المياه باستخدام طريقتين متميزتين: الامتزاز والفنتون. تم اختبار معالجة الامتزاز مبدئيًا باستخدام مادتين ماصتين جديدتين، Acorus calamus وCynara scolymus. تمت معالجة هذه المواد الماصة أولاً بحمض الكبريتيك ثم تم تنشيطها باستخدام برمنجنات البوتاسيوم في حالة Acorus calamus. بالنسبة لـ Cynara scolymus، تم استخدامه مباشرة في شكل مسحوق لتحضير المواد الماصة. تم توصيف المواد المنتجة بعناية باستخدام العديد من التقنيات بما في ذلك XRD، FTIR، TGA وSEM. بالإضافة إلى ذلك، ركزت الدراسة على تطبيق المواد المكتسبة كمواد ماصة في نظام دفعي لإزالة الصبغة الأساسية، الميثيلين الأزرق (MB). بحثت الدراسة في حركية الامتزاز وسلوك التوازن وتأثير العديد من العوامل بما في ذلك الرقم الهيدروجيني وزمن التلامس والتركيز الأولي والقوة الأيونية ودرجة الحرارة. ولذلك، فقد حققنا مستويات عالية من القدرة على الامتزاز. بالإضافة إلى ذلك، تُظهر عمليات فينتون فعالية مادة نانوية جديدة، $NiFe_2O_4$-CuO، في معالجة المياه. وبشكل أكثر تحديدًا، تم التأكد من أن هذه المادة النانوية تعمل كمنشط فعال لـ بيروكسيد الهيدروجين.

الكلمات المفتاحية: الامتزاز، Acorus calamus، Cynara scolymus ، أزرق الميثيلين (MB)، نظام الدفعة، فنتون، $NiFe_2O_4$-CuO، بيروكسيد الهيدروجين